CHEMICAL KINETICS OF BIOMASS AND SORBENT BLENDS FOR GASIFICATION PURPOSES

University of Fort Hare
Together in Excellence

MABUDA AZWIHANGWISI IREN

Thesis Submitted in the fulfillment of the requirement for the degree of

DOCTOR OF PHILOSOPHY

IN

PHYSICS

IN THE FACULTY OF SCIENCE AND AGRICULTURE

UNIVERSITY OF FORT HARE

Supervisor: Dr N.S Mamphweli

Co-supervisor: Prof E.L Meyer

2015

DECLARATION

I, Azwihangwisi Iren Mabuda, hereby declare that the work contained in this dissertation is my own original work and that I have not previously in its entirety or in part submitted it at any other university for a degree.

Signature ---------- Date----------

DEDICATION

This thesis is dedicated to my grandmother, Mrs Nyamukamadi Mabuda

ACKNOWLEGEMENTS

First and for most I would like to thank the Almighty God, He is my helper.

- I would like to express my deep sense of gratitude to my supervisor Professor N.S Mamphweli for all his effort and assistance. He was very supportive and patient with me and always there when I needed him.
- Many thanks to my co-supervisor, Professor E.L Meyer for his contribution, support and guidance.
- Black Researcher Academic Development (BRAD), National Research Foundation (NRF), ESKOM, Goven Mbeki Research and Development Centre (GMRDC), Fort Hare Institute of Technology (FHIT) are acknowledged for their financial support.
- Many thanks to the biomass group people and FHIT staff for their contributions towards this project.
- I would also like to thank my family and friend for their support and believing in me.

ABSTRACT

The main aim of this research was to determine the chemical kinetics of biomass and biomass/sorbent mixtures, which is crucial in assessing parameters including the feasibility, design, and scaling of industrial biomass conversion applications such as pyrolysis and gasification. Many studies have been conducted for co-gasification of coal and biomass, however little has been done for the biomass with sorbent mixtures. Biomass is one of the main renewable energy sources and coupled with carbon dioxide absorbent material such as calcium oxide (CaO) and/or magnesium oxide (MgO) sorbent it increases the biomass conversion efficiency during gasification. The thermogravimetric analyzer (TGA) was conducted in order to establish the material thermal behavior under temperatures for which gasification takes place with specific reference to the pyrolysis stage of gasification. Kinetics of thermal decomposition of biomass with sorbent mixtures of pine wood (wood), CaO and MgO, were investigated using the TGA technique. The different ratios of these materials, which ultimately determines the gasification characteristics of the blends, were investigated. The measurements were carried out in a nitrogen atmosphere at different heating rates of 10, 15 and 20 ºC/min. It was found that the material fully degraded in the devolatilazation zone, which is in the temperature range of 200-800 ºC. At higher temperature some samples were more stable compared to others. The significant mean difference in the rate of degradation between the samples was compared using one way analysis of variance (ANOVA).

The kinetic parameters (activation energy, pre-exponential factor and the reaction order) were obtained from both model free (Kissinger and Flynn-Wall-Ozawa (FWO)) and the regression

models. A computer simulation was performed to establish the ratio that resulted in higher conversion efficiency during gasification.

A mixture of 80% pine wood and 12,5% CaO and 12.5%MgO to make 25%CaO.MgO has resulted in the highest thermal stability compared to other samples. In other words, at higher temperatures these samples degrade at a slower rate compared to others. The activation energy of this sample, 139.63 kJ/mol and the average value of 143.74 kJ/mol was obtained from the Kissinger and FWO method, respectively. The values obtained from the regression models were higher compared to model free methods. Both the model free and model fitting methods were effective in determining the kinetic parameters. However, for accurate results, it is crucial to develop your own model which can fit the data perfectly. Compared to other blends the 25%CaO.MgO sample was found to be suitable to perform better during gasification.

Table of Contents

LIST OF TABLES

LIST OF FIGURES

NOMENCLATURE

A = pre-exponential factor (min^{-1})

ANOVA = analysis of variance

CaO = calcium oxide

c_i = fraction of volatiles produced by the ith component

CV = Gas Caloric Value (MJ/Nm^3)

CV_{H_2} = Caloric Value of Hydrogen by standard

CO_{vol} = Vol concentration of Carbon Monoxide

CV_{co} = Caloric Value of Carbon Monoxide by standard

$CH_{4_{vol}}$ = Volume concentration of Methane

CV_{CH_4} = CV of methane by standard

DEV = deviation between the experimental and calculated DTG curves (%)

df = degree of freedom

DTG = differential weight loss curve (%/min)

E = activation energy (kJ/mol)

Flynn-Wall-Ozawa = FWO

$H_{2_{vol}}$ = Volume concentration of Hydrogen gas

HHV = higher heating value

k = kinetic constant

LHV= lower heating value

M = number of parameters involved in the model

m = mass of samples

m_w = mass of wood sample

MgO = magnesium oxide

MS = means squares

MSE = mean square due to errors

MSG= mean square due to groups

n = reaction order

N = number of individual reactions

R = gas constant (J/mol/ K)

S_p = Pooled sample standard deviation

T = temperature (°C or K)

OF_{DTG} = objective function

t = time (s)

T = temperature (ºC)

TGA = thermogravimetric analyzer

W = experimental sample mass (mg)

W_o = initial dry sample mass at a time (t) (mg)

W_f = final weight parameter (mg)

$\overline{X}$ = mean for the entire data

$\overline{X}_i$ = the mean for group i, i = the number of groups

$\overline{X}_{ij}$ = the value of the individual mean for group j in group i

α = conversion

Z = number of the measured data points

RESEARCH OUTLINE

The following outline has been used in this thesis:

Chapter 1: Introduction

This chapter covers the background of the study, the purpose and objective of the research, motivation, research problem and questions as well as the delineation and limitation of the project.

Chapter 2: Literature review

This chapter presents the theoretical background of the studies, the thermochemical processes, different gasifier designs, the hydrogen production technologies and the background on the kinetics of biomass.

Chapter 3: Research methodology

This chapter presents the sample preparations and the methods used to characterize them. The experimental techniques used and their justification is also discussed in details in this chapter. The procedure of analyzing the data is well explained.

Chapter 4: Proximate, ultimate and thermal analysis

The results obtained from the proximate analysis, such as moisture content, volatile matters and ash content are discussed in this chapter. The elemental composition (ultimate analysis) and thermal analysis results are also discussed here. The statistical test results performed on the samples is also discussed.

Chapter 5: Kinetic modeling of the devolatilization process

This chapter covers the kinetics of the material in the devolitilization zone from both the model free Kissinger and Flyn-Wall-Ozawa methods. The regression model results which include the predicted model values were also discussed in this chapter.

Chapter 6: Computer simulations

The computer simulations of the syngas, such as hydrogen content and the gasification efficiency are discussed in this chapter. The effects of some parameters such as throat angle and throat diameter on the conversion efficiency of a downdraft gasifier were also discussed in this chapter.

Chapter 7: Summary, conclusions and recommendation

The summary of the main findings of this study is made and the conclusions of the results are drawn. The contributions of the study to the knowledge of the field of biomass gasification are explained. The recommendations were made as well.

Referencing style: Harvard method was used for referencing.

CHAPTER 1

INTRODUCTION

1.1. Background

The combustion of fossil fuels has a negative impact on the global climate worldwide. Relying on them as the main energy sources has led to the serious energy crisis and environmental problems [Meng *et al.,* 2006]. Renewable energy is of growing importance in solving these environmental concerns over fossil fuel usage. Some of the main renewable energy resources are wood and other forms of biomass, such as energy crops and agricultural and forestry wastes [Bridgwater, 2003]. The use of biomass plays an important role as one of the replacement for fossil fuels because biomass is an organic matter that is available on a renewable basis through natural resources [Liu *et al.,* 2002]. It is the most abundant renewable resource, formed by fixing carbon dioxide in the atmosphere during the process known as photosynthesis, which makes it a carbon neutral in its life-cycle [Meng *et al.,* 2006].

Gasification is one of the different thermochemical processes for biomass conversion used to generate electricity and other applications such as liquid fuels. This process involves heating the biomass with controlled amount of air, oxygen, steam or various mixtures of these to produce gases such as hydrogen (H_2), carbon monoxide (CO) and methane (CH_4) [Groeneveld *et al.,* 1979]. These gases are known as producer gas or synthesis gas (syngas). Gasification process uses low-value feedstocks and convert them into electricity as well as into transportation fuels [Kumar *et al.,* 2009]. The use of syngas generated from gasification in advanced technologies such as gas turbines and fuel cells results in increased efficiency [Sipilä, 1993]. Most gasification

activities and published data in the world are on gasification with air, which produces a gas with a low heating value (4-7 MJ/m^3n) and low H_2 content (8-14 vol. %) [Delgado *et al.,* 1997].

Interest for hydrogen production is growing worldwide. Currently, hydrogen is largely produced by steam methane reforming and coal gasification, which is from fossil fuels [Florin and Harris, 2007]. Hydrogen can be used in fuel cell technology, which offers nearly zero emissions, flexibility of operation and high conversion efficiency during electricity generation. Hydrogen fuel cells are mainly used for electricity production using hydrogen as a fuel. The fuel cell is an electrochemical device that directly converts chemical energy into electricity. The use of H_2 for fuel cells has gained attention because of its high efficiency (50-65% as compared to the efficiency of IC engines (20–38%) [Dayton *et al.,* 2001, Lester *et al.,* 2007]. In order for a fuel cell to operate, hydrogen and oxygen are required. But hydrogen as a gas (H_2) is not found by itself on earth [Kalinci *et al.,* 2009]. Therefore, it needs to be produced from other energy sources such as carbon-free or carbon-neutral energy or from fossil fuels and oxygen from air.

Biomass syngas contains high concentrations of undesirable tar compounds and particles which must be eliminated from the raw gas before its utilization for most applications [Huang *et al.,* 2011 and Bhattacharya *et al.,* 2005]. Tars can be defined as an organic compounds present in the syngas excluding gaseous hydrocarbons (C1–C6) and benzene [Han *et al.,* 2010]. The tar content in the raw gas (at the gasifier exit) varies from about 1 to 180 g/m^3n from one process to another and should be lowered to only 50-500mg/m^3n, depending on the applications [Delgado *et al.,* 1997, Rensfelt and Ekström, 1989]. The hot raw gas can be purified by the use of catalysts, which, in turn, has different alternatives. A calcined dolomite (CaO.MgO) bed, limestone (CaO),

and/or magnesite (MgO) were used in the downstream of a gasifier for CH_4 and tar cracking which resulted in the increase of hydrogen (H_2) content in the syngas gas [Delgado *et al.,* 1997]. The use of CaO for CO_2 capture from coal combustion flue gas has been investigated [Gupta and Fan, 2002, Iyer *et al.,* 2004]. CaO is one of the most possible sorbent for in situ CO_2 capture in biomass gasifiers and also captures CO_2 based on a gas–solid absorption reaction which is exothermic and provides additional heat to drive the endothermic cracking and reforming reactions [Iyer *et al.,* 2004].

Pyrolysis is one of the processes taking place during biomass gasification. However, pyrolysis is a complex process; in which a series of reactions takes place [Soltes, 1983]. Therefore, it is important to study the fundamentals of biomass pyrolysis. Its kinetics is important for the thermochemical conversion processes aimed at the production of fuel gases, chemicals and energy [Soltes, 1983 and Liu, *et al.,* 2002]. The devolitization of materials in the gasification takes place in the pyrolysis zone, which involves a number of different reactions. The kinetics of lignocellulosic materials involves the knowledge of the reaction mechanisms. However, there are a great number of reactions that occur simultaneously in this process which makes it practically impossible to develop a kinetic model that takes into account all these reactions. Therefore, pyrolysis process is usually studied in terms of pseudo-mechanistic models [Liu, *et al.,* 2002]. Information on chemical kinetics can be obtained from thermogravimetric analysis (TGA) data, which is a method that can be used for measuring the weight loss of materials as a function of time or temperature.

1.2. Problem statement

Currently, the South African electricity is produced mainly from coal fired plants. Apart from the environmental challenges associated with fossil fuels extraction and utilization, these energy sources are being rapidly depleted. About 96% of the hydrogen is also produced by the reactions of natural gas [Ewan and Allen, 2005] which requires fossil fuel as an energy source. In order to have environmentally friendly energy and hydrogen, it must be produced by renewable methods [Mahishi and Goswami, 2007] such as gasification of biomass.

Biomass syngas contains high concentrations of undesirable tar compounds and particles [Huang *et al.,* 2011 and Bhattacharya *et al.,* 2005], which must be eliminated from the raw gas for most applications before its utilization. Again the gas produced has a low heating value (4-7 MJ/m^3n) and 8-14 Vol % H_2 content only [Delgado *et al.,* 1997, Narváez *et al.,* 1996]. The low yield of hydrogen is due to the oxygen content (40%) of biomass [Aznar *et al.,* 2006] which required to fuel the air-blown gasifiers. This makes it, in principle, of not much interest in H_2 production. The net efficiency of electricity generated from the biomass gasification process is usually low (20% to 40%) [Caputo *et al.,* 2005]. There is a need of improving this efficiency. The air-blown biomass gasifiers also suffer the dilution of the combustible constituents of the gas by the presence of nitrogen. This study will help in minimizing CO_2 emissions by using sorbents as well as to enhance the conversion efficiency of the air-blown downdraft gasifier.

Pyrolysis and other thermochemical conversion processes represent an important option for the utilization of biomass and waste. Pyrolysis, as one of the promising thermochemical conversion

routes, plays a vital role in biomass conversion. Knowledge of the pyrolysis characteristics is the basis and thus essentially important for a better understanding of biomass thermal chemical conversion and the reactor design. Biomass gasification involves pyrolysis as one of the stages that the biomass materials go through.

1.3. Aims and objectives

The study aimed at determining the kinetic parameters such as activation energy, pre-exponential factor and the reaction order of biomass and sorbent blends in the pyrolysis zone and to decide on the suitable material for the gasification purposes. This project also sought to develop models from the current data and compares the parameters with the already established models. MATLAB software and a computer simulation program developed by Jaya *et al.,* [2003] were employed for modeling and estimation of the conversion efficiency, respectively. To achieve this goal, the following objectives were investigated:

i. Physical and chemical compositions of biomass and biomass/sorbent blends.
ii. Thermal stability of biomass and biomass/sorbent blends.
iii. The kinetic parameters, such as the activation energy, pre-exponential factor and reaction order of the materials will be evaluated.
iv. To develop a computer model from the current study data and compared them with already established models.
v. The conversion efficiency achieved during simulation of the gasification of the blends.

1.4. Research questions

The following research questions will be answered in this study:

i. What are the physical and chemical compositions of biomass and biomass/sorbent blends and their significance in gasification?
ii. How do the biomass and biomass/sorbent blends behave in terms of thermal stability during gasification during pyrolysis in a downdraft gasifier?
iii. How do the kinetic parameters of the biomass compare to the biomass/sorbent blends and what is their importance in scaling and designing any thermochemical conversion system?
iv. How do the results from the predicted models compare to the already established models?
v. Which blend result in high conversion efficiency and how is it compared to pure material and all other selected blends?

1.5. Motivation of the study

There is a need for producing electricity from non-fossil fuels such as biomass. Biomass is one of the renewable sources of energy and it is carbon neutral. It is readily available as waste in many sawmills in South Africa and elsewhere around the world, including Melani village where the biomass (pine-wood) for this study was collected. The energy generated from biomass such as wood avoids the environmental concerns associated with the extraction and use of the fossil

fuels. Biomass is one of the major potential energy sources, because of its renewability [Demirbes and Balat, 2006, Wang *et al.,* 2007]. This study will assist in establishing a blend which will result in higher conversion efficiency than already achievable during biomass conversion.

In designing and scaling any kind of technology requires chemical kinetic information which is important for in thermal decomposition. Kinetics is basically related to the decomposition mechanisms. The knowledge of the mechanisms allows postulating kinetic equations or vicing versa. Kinetics is the starting point of assuming the mechanisms of the thermal decomposition [Jose´ and Juan, 2005].

On the other hand hydrogen is an energy carrier rather than an energy source. Hence, hydrogen needs to be produced from other sources of energy. The production of hydrogen from biomass also holds the greatest promise, since biomass can be made available everywhere in the world [Bridgwater *et al.,* 2003]. The energy generated from hydrogen is clean with no pollution; therefore this avoids the risk from fossil fuels. Hydrogen from biomass can be used in many applications such as fuel cells.

If the energy is produced from the biomass/sorbent mixtures, it means the cost of electricity produced from this system will be much cheaper compared to what is currently provided by Eskom (South African major electricity supplier) grid. The study will also assist in developing a less polluting and more efficient power system than the ones available, by using an air blown gasifier (i.e. gasification using air as gasifying agent) with cheap organic materials such as waste

wood. Table 1.1 compares the Eskom tariff and the cost of gas power from a downdraft biomass gasifier.

The work will also contribute to the development of the investigation on the kinetic models of biomass and sorbents from the TGA, which is a relatively simple and low priced technique and it provides reliable quantitative information on the pyrolysis processes.

1.6. Delineation and limitations

This study aims to investigate the kinetic parameters such as activation energy, pre-exponential factor and reaction model through modeling, the syngas/producer gas as well as the conversion efficiency of biomass and biomass/sorbent blends through computer simulation. The actual gasification of the material was not conducted. The produced hydrogen needs further purification and separation from the syngas before the end use. Separation and purification did not form part of this study since the method for hydrogen isolation and purification needs a thorough investigation, which the current study will not consider.

Table 1.1: Example of 2MW power station

ESKOM TARIFF	R 1.05
Proposed Increases @ 8%/Annum:	Current: R 1.05
	1st Year: 8% R 1.13
	2nd Year: 8% R 1.22
	3rd Year: 8% R 1.32
	4th Year: 8% R 1.43
	5th Year: 8% R 1.54

Assumptions:	
Annual Expenditure Inflation	6%
Finance Borrowing Rate:	13.50%
Fuel Cost	R 0.40

Notes:
1. Using Eskom's Tariff (kWhrs only) Average
2. Assume Network Demand Charge will fall away
3. Eskom's Services Charges etc assumed to be a continuing expense
5. After 5 years assume an increase relative to Inflation - 6%/Annum
6. Assume they can sell all they produce, via Wheeling
7. Assume farmers sell feedstock for R0.40/KG

Payback - Years 5.04

Gas Producer	0	1	2	3	4	5	6	7	8	9	10	11
Opening Cash		R 100,000	R 8,388,000	R 17,523,560	R 27,604,607	R 38,719,659	R 50,965,087	R 64,445,792	R 78,735,340	R 93,882,260	R 109,937,995	R 126,957,075
Total Sales using Eskom's Tariff Rates		R 18,396,000	R 19,867,680	R 21,457,094	R 23,173,662	R 25,027,555	R 27,029,759	R 28,651,545	R 30,370,638	R 32,192,876	R 34,124,448	R 36,171,915
Total Expenditure		R 10,108,000	R 10,732,120	R 11,376,047	R 12,058,610	R 12,782,127	R 13,549,054	R 14,361,997	R 15,223,717	R 16,137,140	R 17,105,369	R 18,131,691
Cumalative Cash on Hand		R 8,388,000	R 17,523,560	R 27,604,607	R 38,719,659	R 50,965,087	R 64,445,792	R 78,735,340	R 93,882,260	R 109,937,995	R 126,957,075	R 144,997,299
PBITA	-R 51,379,650.00	R 8,288,000	R 9,135,560	R 10,081,047	R 11,115,052	R 12,245,428	R 13,480,705	R 14,289,547	R 15,146,920	R 16,055,735	R 17,019,080	R 18,040,224
Cumulative Cash Flow	-R 51,379,650.00	-R 43,091,650.00	R -33,956,090	R -23,875,043	R -12,759,991	R -514,563	R 12,966,142	R 27,255,690	R 42,402,610	R 58,458,345	R 75,477,425	R 93,517,649
If Amortized over 15 years - Annual Payment		R 8,156,890	R 8,493,511	R 8,493,511	R 8,493,511	R 8,493,511	R 8,493,511	R 8,493,511	R 8,493,511	R 8,493,511	R 8,493,511	R 8,493,511
Loan Balance		R 50,159,012.54	R 48,773,589.02	R 47,201,133.33	R 45,416,396.12	R 43,390,719.39	R 41,091,576.29	R 38,482,048.88	R 35,520,235.27	R 32,158,576.82	R 28,343,094.48	R 24,012,522.03
PBITA including Capex		R 131,110	R 642,049	R 1,587,536	R 2,621,541	R 3,751,917	R 4,987,194	R 5,796,036	R 6,653,409	R 7,562,224	R 8,525,569	R 9,546,713

Cost / kWhr - Gas Power	R 0.58	R 0.61	R 0.65	R 0.69	R 0.73	R 0.77	R 0.82	R 0.87	R 0.92	R 0.98	R 1.03	
Cost / kWhr - Eskom Tariffs	R 1.05	R 1.13	R 1.22	R 1.32	R 1.43	R 1.54	R 1.64	R 1.73	R 1.84	R 1.95	R 2.06	
Cost / kWhr - Eskom Tariffs + Capex	R 1.04	R 1.10	R 1.13	R 1.17	R 1.21	R 1.26	R 1.30	R 1.35	R 1.41	R 1.46	R 1.52	

NPV	R 81,745,161.47
IRR (Pre Tax)	22%

Expenditure												
Fixed Costs	R/kWhr											
Salaries and Wages	R 0.0459	R 804,000.00	R 852,240.00	R 903,374.40	R 957,576.86	R 1,015,031.48	R 1,075,933.36	R 1,140,489.37	R 1,208,918.73	R 1,281,453.85	R 1,358,341.08	R 1,439,841.55	R 1,526,232.04
Eskom Service Charges- Assume will remain	R 0.0151	R 264,000.00	R 279,840.00	R 296,630.40	R 314,428.22	R 333,293.92	R 353,291.55	R 374,489.05	R 396,958.39	R 420,775.89	R 446,022.45	R 472,783.79	R 501,150.82
Spares, Maintenance & Support	R 0.0298	R 522,000.00	R 553,320.00	R 586,519.20	R 621,710.35	R 659,012.97	R 698,553.75	R 740,466.98	R 784,895.00	R 831,988.69	R 881,908.02	R 934,822.50	R 990,911.85
Genset Overhauls (Provision)	R 0.0366	R 642,000.00	R 693,360.00	R 734,961.60	R 779,059.30	R 825,802.85	R 875,351.02	R 927,872.09	R 983,544.41	R 1,042,557.08	R 1,105,110.50	R 1,171,417.13	R 1,241,702.16
Insurance	R 0.0137	R 240,000.00	R 259,200.00	R 274,752.00	R 291,237.12	R 308,711.35	R 327,234.03	R 346,868.07	R 367,680.15	R 389,740.96	R 413,125.42	R 437,912.95	R 464,187.72
Total Fixed Costs	R 0.1411	R 2,472,000.00	R 2,637,960.00	R 2,796,237.60	R 2,964,011.86	R 3,141,852.57	R 3,330,363.72	R 3,530,185.54	R 3,741,996.68	R 3,966,516.48	R 4,204,507.47	R 4,456,777.91	R 4,724,184.59
Variable Costs												
Stores & General	R 0.0219	R 384,000.00	R 407,040.00	R 431,462.40	R 457,350.14	R 484,791.15	R 513,878.62	R 544,711.34	R 577,394.02	R 612,037.66	R 648,759.92	R 687,685.52	R 728,946.65
Vehicle Lease, Fuel and Maintenance	R 0.0082	R 144,000.00	R 152,640.00	R 161,798.40	R 171,506.30	R 181,796.68	R 192,704.48	R 204,266.75	R 216,522.76	R 229,514.12	R 243,284.97	R 257,882.07	R 273,354.99
Contingencies	R 0.0057	R 100,000.00	R 106,000.00	R 112,360.00	R 119,101.60	R 126,247.70	R 133,822.56	R 141,851.91	R 150,363.03	R 159,384.81	R 168,947.90	R 179,084.77	R 189,829.86
Fuel R/KG	R 0.4000	R 7,008,000.00	R 7,428,480.00	R 7,874,188.80	R 8,346,640.13	R 8,847,438.54	R 9,378,284.85	R 9,940,981.94	R 10,537,440.86	R 11,169,687.31	R 11,839,868.54	R 12,550,260.66	R 13,303,276.30
Total Variable Costs	R 0.4358	R 7,636,000.00	R 8,094,160.00	R 8,579,809.60	R 9,094,598.18	R 9,640,274.07	R 10,218,690.51	R 10,831,811.94	R 11,481,720.66	R 12,170,623.90	R 12,900,861.33	R 13,674,913.01	R 14,495,407.79
Total Expenditure	R 0.5769	R 10,108,000.00	R 10,732,120.00	R 11,376,047.20	R 12,058,610.03	R 12,782,126.63	R 13,549,054.23	R 14,361,997.49	R 15,223,717.34	R 16,137,140.38	R 17,105,368.80	R 18,131,690.93	R 19,219,592.38

CAPEX	
Chippers (3Ton/HR)	R 2,000,000.00
Briquette Plant (500Kg/hr) Need 720kgs/hr (Assuming 25% of feed stock needs Brique	R 4,000,000.00
Gasifiers 450Nm3 x 9 (255kW ea)	R 14,400,000.00
Gas Gensets 9 x 255kw ea	R 18,000,000.00
Civils & Structurals (Building etc)	R 3,236,000.00
Conveyors, Elevators, Screw Conveyors and Rotary Valves	R 3,635,000.00
Design & Development Fees	R 1,162,000.00
Transport	R 500,000.00
Electrics	R 2,000,000.00
Contingencies - 5% of Capex	R 2,446,650.00
	R 51,379,650.00

CHAPTER 2
LITERATURE REVIEW

2.1. Introduction

Environmental concerns have led an interest in biomass as an energy source and in the development of new technologies for power generation [Olsson *et al.,* 1997]. Biomass gasification process is an energy conversion technology in which the feedstock is partially oxidized with oxygen and or steam to produce gas (syngas) [Kalinci *et al.,* 2009]. The syngas is a mixture of carbon monoxide (CO), hydrogen (H_2) and methane (CH_4), carbon dioxide (CO_2) and nitrogen (N_2) [Demirbas, 2004]. More detailed models have been applied to study the pyrolysis of mixtures of municipal solid wastes [Sørum *et al.,* 2001], coal and biomass [Aboyade *et al,* 2013] but little has been done on biomass with sorbents. This chapter presents a synthesis of the literature about the conversion of biomass resources into useful energy with specific reference to pyrolysis and gasification.

2.2. Thermochemical processes

The main thermochemical conversion processes are combustion, pyrolysis and gasification. The gasification process converts the feedstock into a mixture of gases by means of different heterogeneous reactions [Di Blasi, 2000, Baykara and Bilgen, 1981]. These mixtures of gases include CO_2, CO, H_2, CH_4, H_2O, trace amounts of higher hydrocarbons, various contaminants such as small char, ash and tar particles [Bridgwater, 1994]. Pyrolysis and gasification are certainly not the most important options for the future; because on the other hand combustion is responsible for over 97% of the world bio-energy production. In order to obtain the energy

content from biomass, thermochemical and biological processes have widely been applied [Demirbas, 2004]. There is still a need of making the thermochemical conversion processes (such as gasification and pyrolysis) the future energy sources. Figure 2.1 shows the types and classification of biomass conversion processes.

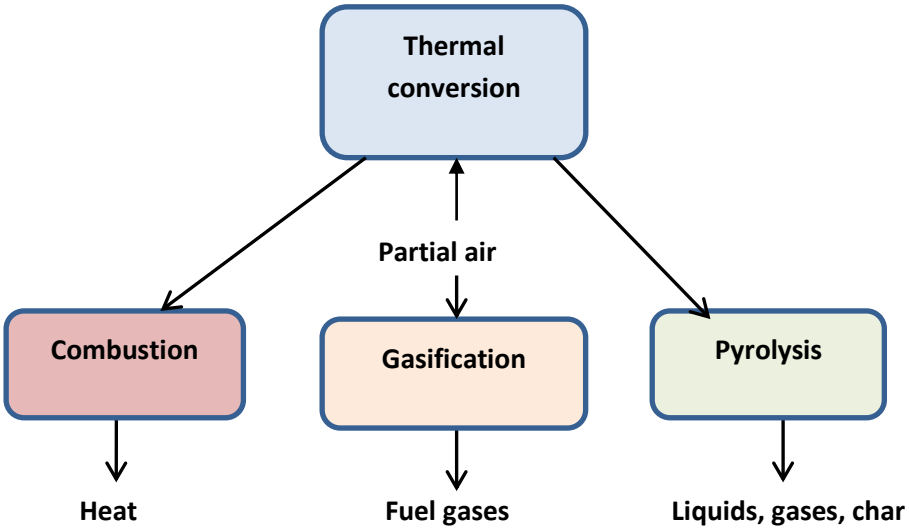

Figure 2. 1: Thermo conversion processes of biomass.

2.2.1. Combustion

Combustion is a process where biomass is burnt in excess air. It produces only heat, to generate steam for the production of electricity using a steam turbine [Jenkins *et al.*, 1998]. Unlike some other thermochemical conversion strategies, combustion uses any type of biomass, and converts the whole fuel to simple products [Jenkins *et al.*, 1998]. The combustion of biomass produces gases at high temperatures of about 800–1000 ºC [McKendry, 2002] which is higher than the temperature inside the reactor.

2.2.2. Pyrolysis

Pyrolysis is the heating of biomass without air and convert it into liquids such as bio-oils, solid charcoal and gaseous compounds [Meng *et al.*, 2006]. The pyrolysis products are shown in Figure 2.2.

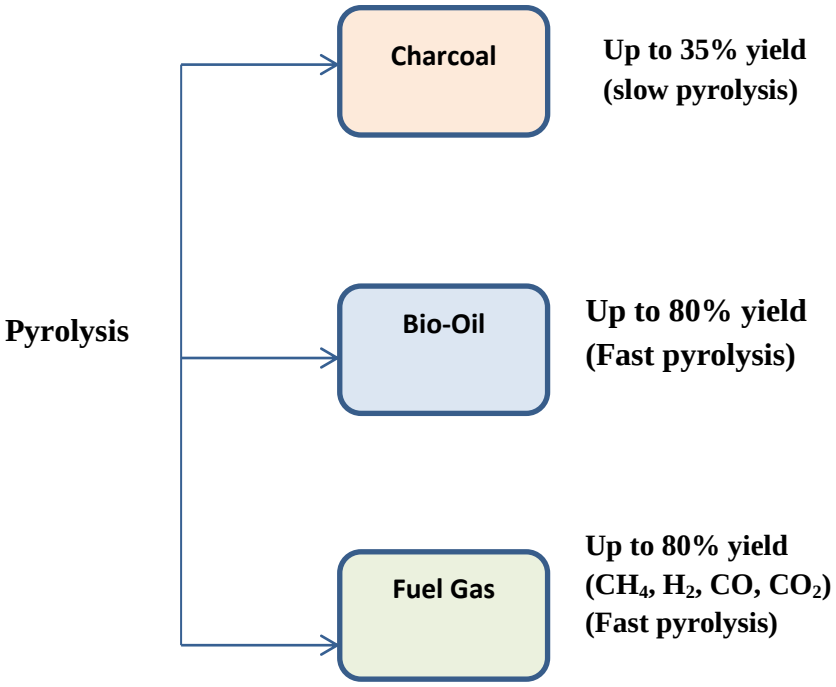

***Figure 2. 2*:** Energy products from pyrolysis.

Pyrolysis is also classified as slow pyrolysis and fast pyrolysis [Meng *et al.*, 2006]. Fast pyrolysis is a high temperature process, in which the biomass feedstock is heated rapidly in the absence of air, to form vapor and subsequently condensed to a dark brown mobile bio-liquid. Fast pyrolysis products can be found in all gas, liquid and solid phases [Meng *et al.*, 2006]. Pyrolysis is also an initial step of gasification and combustion processes. Therefore, the kinetics of the biomass pyrolysis is of relevant importance. To develop a more efficient system, it

requires a fundamental understanding of the thermal properties and reaction kinetics for the thermochemical processes for converting biomass to energy [Kastanaki and Vamvuka, 2006]. During biomass decomposition high amounts of heavy volatiles ('tars') are released which deposit in the various parts of the equipment [Várhegyi *et al.*, 1997]. The knowledge of it for the thermal decomposition of lignocellulosic materials is needed for the design and optimization conditions of gasifiers and pyrolysis reactors [Manyá *et al.*, 2003 Caballero *et al.*, 2005]. The kinetic parameters determination gives us information on the processes taking place durin pyrolysis as well as the structure and composition of the materials [Conesa and Domene, 2011].

2.2.3. Gasification

Gasification process is an energy conversion technology in which the biomass material is partially oxidized with oxygen and/or steam to produce gases (syngas) which can be used either for conversion into different valuable compounds (e.g. Hydrogen, methanol, ammonia, liquid fuels etc.) or to generate heat and power. [Kalinci *et al.*, 2009, Cormos, 2009]. The gasification is a technology in which biomass is heated at high temperatures and disengage to combustible gas. It is also a form of pyrolysis, carried out at high temperatures in order to optimize the gas production. Th gas produc dis also known as producer gas and is a mixture of carbon monoxide (CO), hydrogen (H_2), carbon dioxide (CO_2), nitrogen (N_2) and the traces of methane (CH_4) [Demirbas, 2004]. These gases are possible alternate sources of energy. The gas produced from air-based gasifiers contain a relatively high concentration of nitrogen (50%) with a lower heating value (4 and 6 MJ/Nm^3), whereas, the product gas produced from oxygen and steam-based

gasifiers contains a high concentration of H_2 and CO with a higher heating value (10 and 20 MJ/Nm^3) compared to air-blown gasifiers [McKendry, 2002].

Gasification is an established commercial technology for coal, but it is little used, except where oil and natural gas is expensive such as in South Africa and China [Padró and Putsche, 1999]. Biomass can be considered as the negative carbon dioxide emitted if carbon dioxide produced during gasification is captured during the process [Bishnu *et al.*, 2010]. Therefore, other producer gases will ultimately increase, thereby increasing the conversion efficiency.

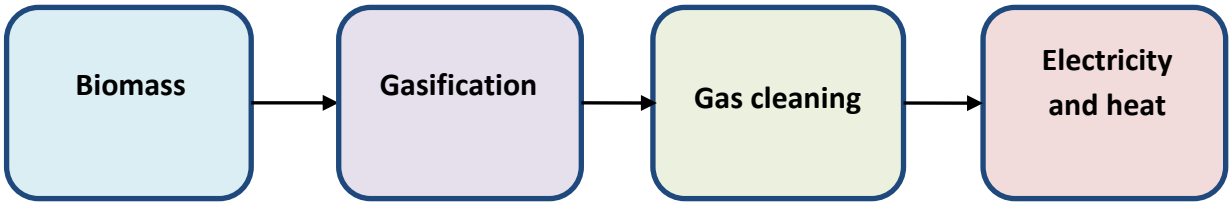

Figure 2. 3: Schematic of gasification process.

The thermochemical biomass gasification is mostly used because its products obtained are more versatile compared to paralysis.

2.3. Basic chemistry of gasification

The following equilibrium reactions take place in the gasifier [McKendry, 2002] :

Partial oxidation: $C + 1/2O_2 \leftrightarrow CO$ $\Delta H = -268$ MJ/mol (2.1)

Complete oxidation: $C + O_2 \leftrightarrow CO_2$ $\Delta H = -406$ MJ/mol (2.2)

Water-gas reaction: $C + H_2O \leftrightarrow CO + H_2$ $\Delta H = +118$ MJ/mol (2.3)

The heats of reaction for the three processes show that the greatest energy release is derived from combustion, which is the complete oxidation of carbon to carbon dioxide, while the partial oxidation of carbon to carbon monoxide accounts for about 65% of the energy released during complete oxidation [McKendry, 2002]. And water-gas shift reaction consumes heat.

Carbon monoxide, hydrogen and steam can undergo further reactions during gasification as follows:

Water-gas shift reaction: $CO + H_2O \leftrightarrow CO_2 + H_2$ $\Delta H = -42$ MJ/kg mol (2.4)

Methane formation: $CO + 3H_2 \leftrightarrow CH_4 + H_2O$ $\Delta H = -88$ MJ/kg mol (2.5)

The qualities of these producer gases can be produced from gasification by varying certain parameters such as the gasifying agent and the method of operation as well as the process operating conditions. Air act as the main gasifying agent, but oxygen/steam as well as hydrogen and CO_2 can also used.

The air is normally used for processes up to about 50 MW_{th} since the use of oxygen for gasification is expensive. The gasifying agent considered in this study is air. The limitation is that the nitrogen introduced by the air dilutes the syngas, giving gas with a net calorific value (CV) of 4–6 MJ/Nm^3 (compared with natural gas at 36 MJ/ Nm^3) [McKendry, 2002].

2.4. Feedstock properties

The following properties of the biomass feedstock have significant impact on the performance of the gasifier:

2.4.1. Lignocellusosic biomass

Lignocellulose is a major component of biomass [Perez and Dorado, 2002]. The cellulose, hemicellulose and lignin are the major constituents of lignocellulosic biomass. Cellulose is a major constituent of lignocellulose and has a linear polymer of D-glucose, which is linked with β-1,4; hemicellulose is a heterogeneous polymer that is linked with both 5 and 6 carbon sugars, and lignin is a randomly constructed, three dimensional polymer with three diferent precurser monomers and also a highly aromatic cross-linked macromolecule. Lignocellulostic biomass contain 60–80% cellulose and hemicellulose, and 10–25% lignin [Baxter, 2005]. The products composition are affected by these polymers in the biomass. It is important to know the behavior of these components, in order to understand more on biomass pyrolysis [Osorio *et al*, 2006].

2.4.1.1. Hemicellulose

Hemicellulose is a branched polysaccharide consisting of D-glucose and other sugars such as mannose, xylose, arabinose, methylglucuronic and galaturonic acids [Sinha *et al.,* 2000]. Its molecular weight is less than 30,000 and accounts about 20% - 40% of the biomass material by weight [McKendry 2002]. Figure 2.4 shows the chemical structure of hemicelluloses.

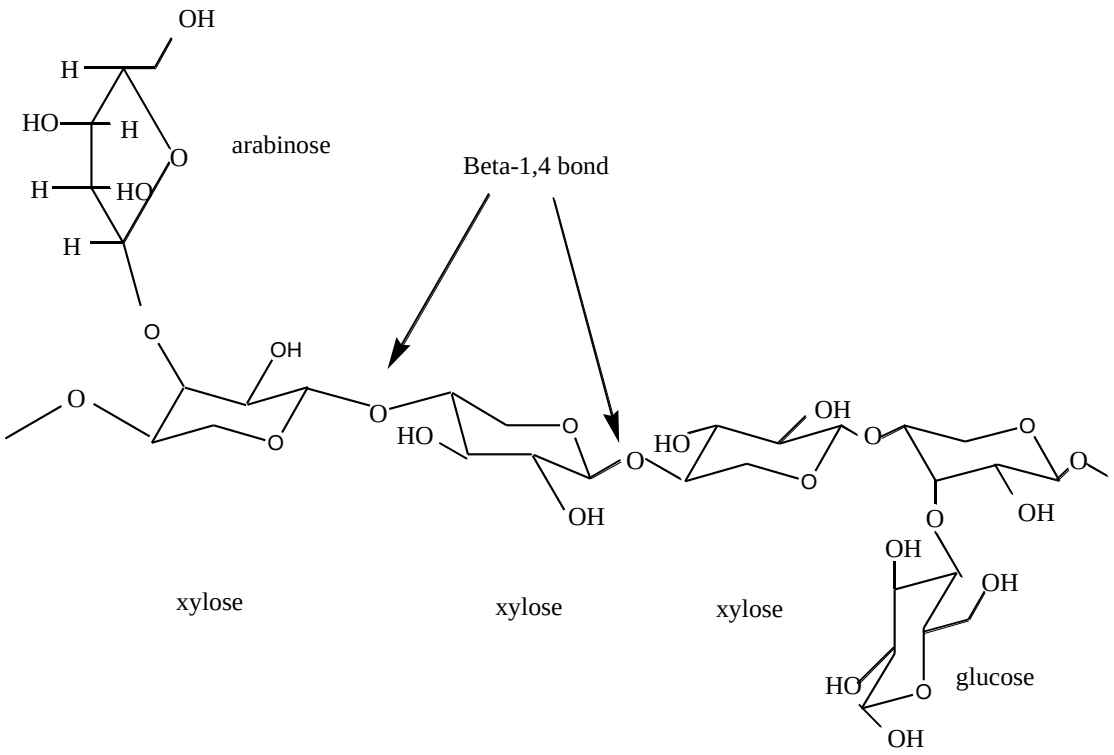

Figure 2. 4: Chemical structure of hemicelluloses [SMRI, 2011].

Hemicellulose is the most sensitive component and decomposes between the temperature range 200 ºC and 260 ºC. This may take place in two steps, namely: the degradation of polymer into soluble fragments and/or conversion into monomer units that further degrades into volatile products [Soltes and Elder, 1981]. It also results to more volatiles and less tar as well as reduced char compared to cellulose [Sinha *et al.*, 2000].

2.4.1.2. Cellulose

Cellulose is the main polysaccharide in wood [Kumar *et al.*, 2009], which makes up to 45% of the dry weight of wood [Perez and Dorado, 2002]. It is a major constituent of lignocellulose and

has a linear polymer of D-glucose, which is linked with β-1,4 [Sjöström, 1993]. Figure 2.5 present the chemical structure of cellulose.

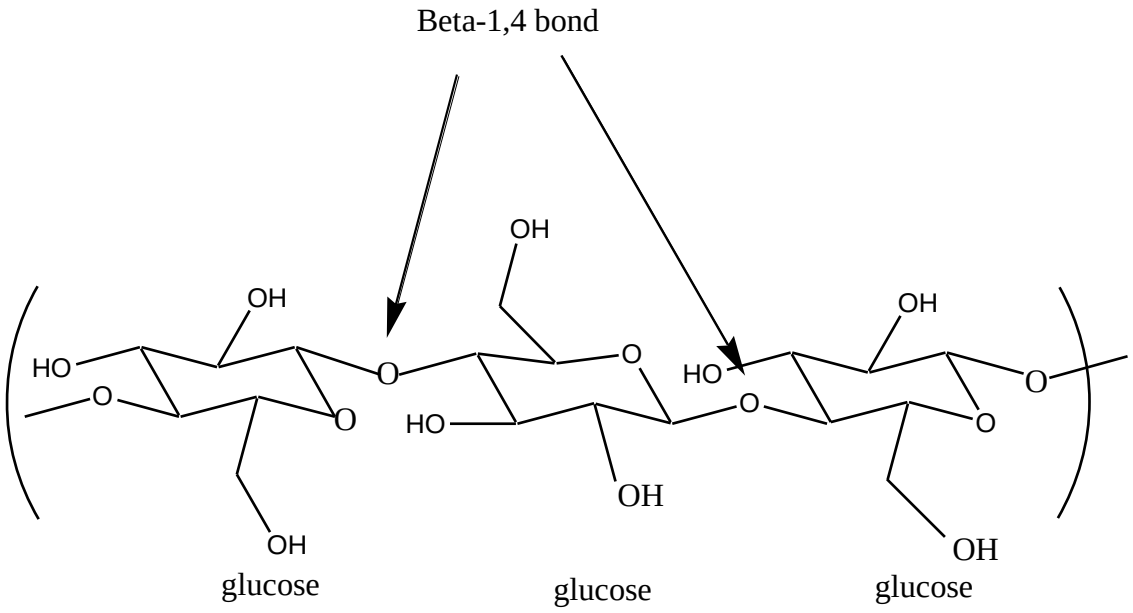

Figure 2. 5: Chemical structure of cellulose [SMRI, 2011].

The molecules are completely linear with a strong tendency to form intra- and intermolecular hydrogen bonds which leads to bundling of cellulose molecules into microfibrils, and in turn form fibrils and cellulose fibers [Kumar *et al.,* 2009]. Cellulose being the highest in proportion of lignocellulose possesses about 40% - 50% of the biomass by weight. It consists of a long chain of glucose units that are polymerized together with a molecular weight of around 100,000 [McKendry 2002]. The study by Shafizadeh shows that at temperatures below 300 ºC, the reduction process dominant in the degree of polymerization, whereas formation of char, tar and gaseous products takes place at temperatures above 300 ºC, which is the second step.

Laevoglucosan being the major component of tar which vaporizes and decomposes when the temperature increases [Shafizadeh, 1982].

The influence of the lignin and cellulose components on the air-steam gasification of different biomass species have been studied by Hanaoka *et al.*, [2005a]. They used an atmospheric fluidized bed during their experiments, which has an internal diameter of 150 mm. They observed that it is possible to predict product gas composition from different type of biomass fuels of the constituent quantities of cellulose and lignin.

2.4.1.3. Lignin

Lignin is a high molecular weight compound that binds the cellulosic fibers together. The proportion of lignin and cellulose determines the suitability of a biomass material for energy applications [McKendry 2002]. It is also a polymer which consists of phenylpropane units [Pasangulapati *et al*, 2012]. The lignin component in biomass varies between 17 and 30% [Sinha *et al.*, 2000]. It decomposes when heated between 280 ºC and 500 ºC [Soltes and Elder, 1981]. Char is the most dominant constituent (55%) in the products of lignin pyrolysis. A pyroligneous acid, which is a liquid product consists of 20% aqueous components, which is composed of methanol, acetic acid and acetone as well as water. It also consists of 15% tar residue, which consists mainly of homologous phenolic compound of lignin on a dry basis. The gaseous products (10%) of the lignin are methane, ethane and carbon monoxide [Sinha *et al.*, 2000]. The chemical structure of lignin is shown in Figure 2.6.

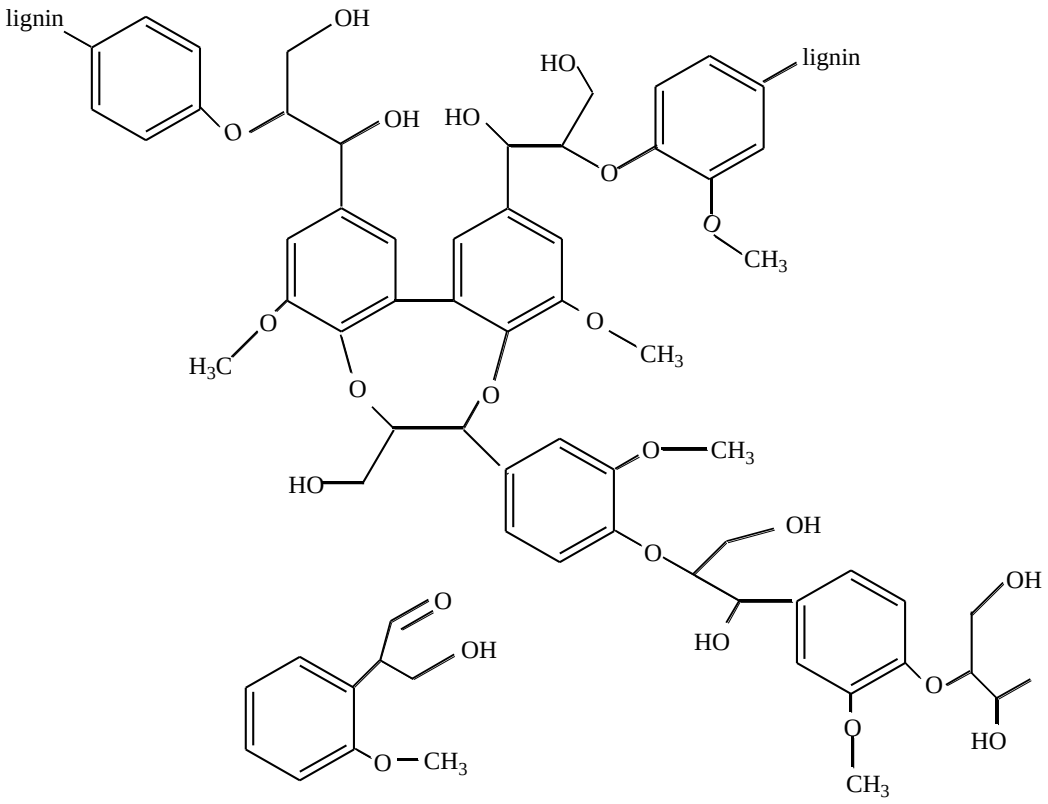

Figure 2. 6: Chemical structure of lignin [SMRI, 2011].

The influence of the biomass chemical composition has been examined by Walawender *et al.,* [1985] in the gasification process. The authors found that the gas production from different biomass species could be correlated with the cellulose content if gasified under similar conditions.

2.4.2. Moisture content

To obtain a high calorific value (CV) gas the feed should have the moisture content of less than 15–20%, pre-drying of the biomass feedstock is usually performed [Lettner *et al.,* 2007] to ensure that the remaining moisture content is suitable for gasification. Fuel with high moisture

content usually more than 30% makes ignition difficult and then reduces the CV of the product gas because it is necessary to evaporate the additional moisture before combustion or gasification [McKendry, 2002]. If the moisture content is high it reduces the temperature achieved in the oxidation zone, which results in the incomplete cracking of the hydrocarbons that are released from the pyrolysis zone. A high level of moisture together with CO produce H_2 by the water gas shift reaction and this result in the increased H_2 content of the gas and also produces more CH_4 by direct hydrogenation. The increased H_2 and CH_4 of the product gas does not compensate for the loss of energy due to the reduced CO content of the gas. Therefore, the product gas will results in a low CV [McKendry, 2002].

2.4.3. Ash content

The resultant ashes from gasification of the biomass should be removed from the gasifier by using a movable grate in the bottom of the equipment. Therefore the charcoal bed in the reduction zone can be easily stirred to help with prevention of blockages which can obstruct the gas flow. The temperature in the oxidation zone is often above the melting point of the biomass ash which can lead to clinkering or slagging problems in the hearth and block the subsequent feed. If the ash is high in alkali oxides and salts it results in clinkering problem for ash contents (above 5%) [McKendry, 2002].

2.4.4. Particle size

The size of the fuel particles is crucial in determining the difficulty and fuel delivery, as well as the behavior of fuel in the gasifier. The influence of feed particle size on the product gas yield

was observed by Herguido *et al.*, [1992]. The size of the fuel also determines the thickness of the gasification zone. The typical feed particle sizes are in the range of 20–80 mm. The larger particles should be avoided since they form bridges which prevent the feed from moving down; on the other hand smaller particles tend to clog the available air voidage, which can lead to a high pressure drop and subsequent shutdown of the gasifier [McKendry, 2002].

2.4.5. Heating value

The heating value is also one of the most important properties of biomass fuels that can assist in designing calculations or numerical simulations of the thermal conversion systems for biomass [Sheng and Azevedo, 2005]. The heating value of a fuel is generally reported on the higher heating value (HHV) as well as the lower heating value (LHV). The HHV is the heat that is released from the fuel combustion with the original and generated water in a condensed state, whereas the LHV is based on gaseous water as the product [Sheng and Azevedo, 2005]. The heat value (kJ/kg), is one of the important characteristics of a fuel which indicates the total amount of energy available in the fuel. The heat value in a given fuel type is a function chemical composition of the fuel [McKendry, 2002].

2.4.6. Conversion efficiency

The efficiency of gasification is the percentage energy of biomass that is converted into a cold producer gas. The average energy conversion efficiency of the gasifiers of wood is defined as:

$$\eta_{Gas} = \left(\frac{Calorific\ value\ of \frac{gas}{kg} of\ fuel}{Avr.calorific\ value\ of\ 1\ kg\ of\ fuel} \right) \times 100\% \quad (2.6)$$

The value of the conversion efficiency of biomass ranges between 60-70% [Bhoi *et al.,* 2006].

2.5. The gasification processes

Four different processes can be distinguished in gasification are drying, devolatilization, oxidation and reduction:

2.5.1. Drying zone

The drying zone lies at the top of the reactor and at this point, fuel wood is fed into the gasifier. Wood then descends through the gasifier as a result of the consumption of wood particles in the gasification zone and there is no air movement through this region. The main purpose in this zone is drying of wood. The wood fuel entering the gasifier usually has a moisture content of 10-30% [Rajvanshi, 1986]. Drying occurs below 120 ºC and the necessary heat is transferred by conduction through wood particles. The water vapour will flow downwards and add to the water vapour formed in the oxidation zone. Part of it may be reduced to hydrogen and the rest will end up as moisture in the gas [Jayah, 2002].

2.5.2. Devolatilization

Devolatilization or pyrolysis zone is where biomass feedstock decomposes by heat in the absence of air. This step produces 75 to 90% volatile materials in the form of gaseous and liquid

hydrocarbons. It is also an endothermic process. When drying process is complete, the particle temperature rises to 200-300 ºC and this is when devolatilization starts to take place. The release of volatiles begins at 250 ºC [Reed & Das 1988] and this process is known as primary pyrolysis. In some wood species, devolatilization starts from 200 ºC till 500 ºC [Sinha *et al.,* 2000]. The char is the remaining nonvolatile material which contains high carbon content [Bridgwater and Evans, 1993].

This is an important process in the gasification of coal and biomass gasification [Xu and Qiao, 2012]. The gasification rate of various coals and biomasses with different chemical composition is affected primarily through this process. It also has a strong effect on char reactivity [Khan and Hshieh, 1989]. Therefore, it is critical to include the devolatilization process when modeling biomass gasification [Xu and Qiao, 2012] and most of volatiles are emitted during this process.

2.5.3. Oxidation zone

Below the pyrolysis region lies the oxidation (combustion) zone through which air is fed into the gasifier. Oxygen in the input air reacts with char produced in the pyrolysis zone and produces combustion gas (CO_2) and water vapour. The reaction is highly exothermic in the combustion zone, which results in high temperature. The reactor has the highest temperature which is greater than 1200 °C [Belgiorno *et al.,* 2003]. The hot combustion gas and water vapour produced in the combustion zone are next drawn into the reduction zone.

2.5.4. Reduction zone

The reduction zone lies at the bottom of the downdraft gasifier. The reaction products of the devolatilization zone move downward into this zone. The surrounding gases such as carbon dioxide and water vapour initially react with the char particles at their outer surface. These reactions are endothermic and they cause the temperature to decline from 1200 ºC to 600 ºC in the gasification zone [Jayah, 2002]. The combustible gas is usually the end product of the chemical reactions takes place in this zone. This combustible gas is used as a fuel gas in burners and is suitable for internal combustion engines after dust removal and cooling.

Table 2.1 presents a series of chemical reactions that occur during the conversion of biomass into useful products in a gasification system [Ruiz *et al*, 2013].

Table 2.1: Gasification reactions.

Reaction type	**Heat of reaction**	**Equation**
Oxidation reactions		
$C + O_2 \rightarrow CO_2$	-394 kJ/mol	(2.7)
$C + ½O_2 \rightarrow CO$	-284 kJ/mol	(2.8)
$H_2 + ½O_2 \rightarrow H_2O$	-242 kJ/mol	(2.9)
$CH_4 + 2O_2 \leftrightarrow CO_2 + 2H_2O$	+803 kJ/mol	(2.10)
Reduction reactions		
$C + CO_2 \leftrightarrow 2CO$	+172 kJ/mol	(2.11)
$C + H_2O \leftrightarrow CO + H_2$	+131 kJ/mol	(2.12)
$C + 2H_2 \leftrightarrow CH_4$	+74.8 kJ/mol	(2.13)

$C + ½O_2 \rightarrow CO$	-111 kJ/mol	(2.14)
Shift reaction		
$CO + H_2O \leftrightarrow CO_2 + H_2$	+41.2 kJ/mol	(2.15)
Methanization reaction		
$2CO + 2H_2 \rightarrow CH_4 + CO_2$	-247 kJ/mol	(2.16)
$CO + 3H_2 \leftrightarrow CH_4 + H_2O$	+206 kJ/mol	(2.17)
$CO_2 + 4H_2 \rightarrow CH_4 + 2H_2O$	-165 kJ/mol	(2.18)
Steam reactions		
$CH_4 + H_2O \leftrightarrow CO + 2H_2$	+206 kJ/mol	(2.19)
$CH_4 + ½O_2 \rightarrow CO + 2H_2$	+36 kJ/mol	(2.20)

2.6. Types of gasifiers

The gasifier is the reactor in which feedstock is converted into fuel gas. The two main types of gasifiers are fixed bed and fluidized bed, with variations within each type [Rampling and Gill, 1993]. The third type is the entrained flow gasifier.

2.6.1. Entrained flow gasifier

Entrained flow gasifiers are less tolerant of particle size as a result, they are commonly used for coal gasification. The diagram of an entrained flow gasifier is shown in Figure 2.7.

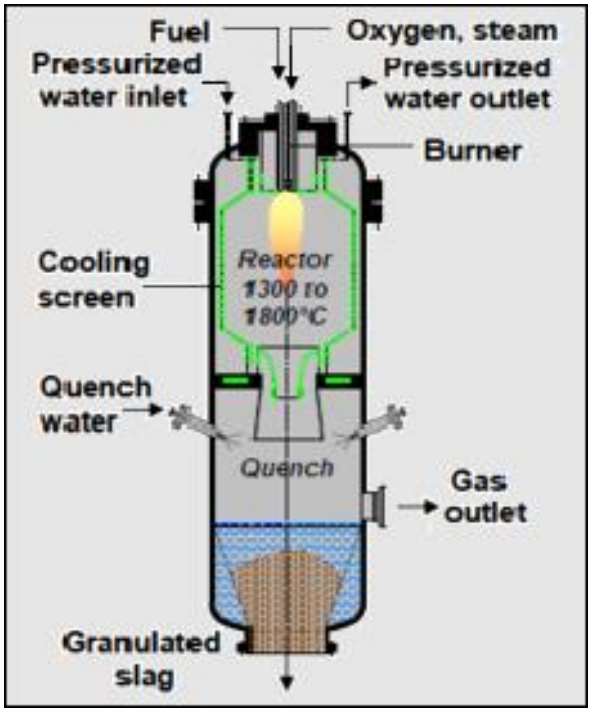

Figure 2. 7: Schematic diagram of an entrained flow gasifier [Skov, 1974].

They operate at high temperature of about 1200-1600ºC and pressure of about 2-8 MPa. This high operating temperature can lead to melting of ash, which results in the formation of a corrosive substance known as slag. This is why the entrained flow is not suitable for gasification of feedstock of high ash content. However, its high operating temperature offers the advantage of tar reduction which causes the equipment blocking and fouling [Damartzis and Zabaniotou, 2011].

Tar is an undesirable product due to its tendency of condensation at low temperature. Entrained flow gasifiers possess some other characteristics which include short residence time, large capacities which results in high throughput and high oxygen demand. This high oxygen demand is what accounts for the high operating temperature due to the exothermic reaction that exists

between the oxygen and the char [Ruiz *et al*, 2013]. In an entrained flow gasifier, oxidizing agents are fed in alongside with finely grinded particles.

2.6.2. Fixed bed gasifier

Fixed bed are gasifiers which uses a reactors of solid fuel particles where air and gas pass either up or down. Fixed-bed, countercurrent (updraft), and concurrent (downdraft) reactors are very simple to construct and operate. They are of high carbon conversion with long solid residence times, and low amount of ash carry-over. On the other hand, the updraft process is more thermally efficient than the downdraft process, but with high tar content of the gas [Di Blasi *et al.,* 1999]. The entrained suspension gasifier is a third type that has been developed for coal gasification, but there it still require a finely divided feed material (<0.1–0.4 mm). These types can be operated at ambient or increased pressure and are thermochemical conversion of solid biomass into a secondary fuel in a gaseous state (producer gas). Fixed-bed gasifiers generally have the advantage of having a simple design and their drawback is of producing a low calorific value gas with high tar content. The produser gas composes of typically N_2 (40–50%), H_2 (15–20%), CO (10–15%), CO_2 (10–15%) and CH_4 (3–5%) with a net calorific value of 4–6 MJ/Nm^3 [McKendry, 2002].

2.6.2.1. Downdraft gasifier

The feedstock material in a downdraft reactor is fed in from the top and the air gasifying agent is introduced at the sides above the grate of the reactor. The combustible gas is often withdrawn under the grate [Quaak *et al*, 1999, Hauserman *et al.*, 1997, Bridgwater, 1994]. The fuel and the

gas flowing downwards through the reactor enables the pyrolysis gases to pass through a throated hot bed of char which is supported by a grate [Sivakumar *et al.*, 2006]. The layer of unreacted charcoal above the ash grate is usually discharged with the ash [Lettner *et al.*, 2007]. The schematic view of the downdraft is shown in the Figure 2.8. Most of the early research and development of this gasifier type occurred around the period of the II World War and was aimed at a light, small reactor fuelling wood blocks for 20-100kW car and lorry engines [Groeneveld and Van Swaaij, 1979].

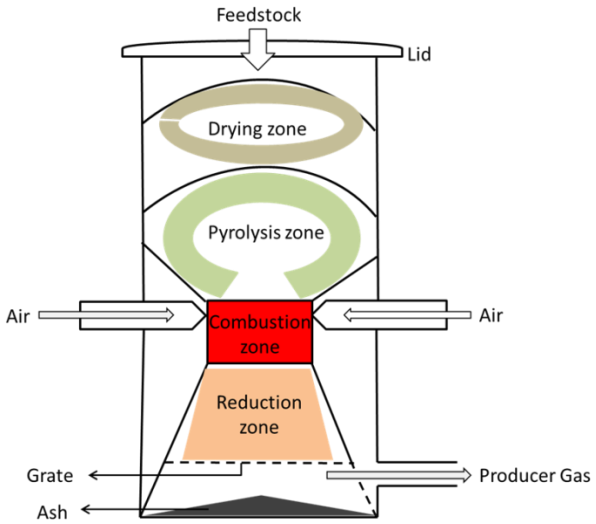

Figure 2. 8: Schematic diagram of a downdraft gasifier [Skov, 1974].

The downdraft gasifiers are of advantageous because there is less tar production compared to the updraft gasifiers since the tars prom the pyrolysis zone are forced to pass through the combustion zone [Stoppiello 2010 in Lettner *et al.*, 2007], after which they can be transformed into stable and non-condensable gases. The final product gas consists of small concentrations of tar compounds. This type of a gasifier is usually preferred for small scale power generation from

biomass. It should also be realized that the tar from down-draft gasifiers is more stable than from up-draft gasifiers, which may still provide problems in tar removal [Beenakers, 1999]. It requires a feedstock moisture content below 20 % and blocky (small block pieces) fuel to allow easy gravity feeding through the constricted hearth [Groeneveld and van Swaaij, 1979]. Further, the classical downdraft gasifier with its typical throat is not possible to scale it up to large sizes because the air which enters at the sides of the reactor and is not capable of penetrating a large diameter fuel bed unless size is proportionally increased. Its maximum size is limited to about 1 MWe even with special designs, such as a rotating cone in the throat which increases its efficiency [Groeneveld and Van Swaaji, 1979].

There are two types of downdraft gasifiers: (1) the throat type gasifiers which are used for biomass fuels which have a low ash and uniform size and (2) the open core gasifiers which can tolerate more variation in fuel properties such as fuel moisture, size and ash content. The gasifiers with the smaller throat diameter produce gas with high velocities at the oxidation and reduction zones. Hence the tars will be reduced, but increases dust loading [Sivakumar *et al.*, 2006 in Sivakumar *et al.*, 2013]. The throat type downdraft gasifier is considered for this study over open core design for its crucial role in reducing the tar content in a well-designed down-draft [Groeneveld and Van Swaaij, 1979].

2.6.2.2. Updraft gasifier

The simplest gasifier design is the updraft reactor (Figure 2.9), named according to the direction of air flow through a packed-bed of reacting biomass. Updraft (counter-current) gasifier is a

gasifier in which the feedstock material is loaded from the top and air gasifying agent is introduced from the bottom of the reactor [Belgiorno *et al.,* 2003].

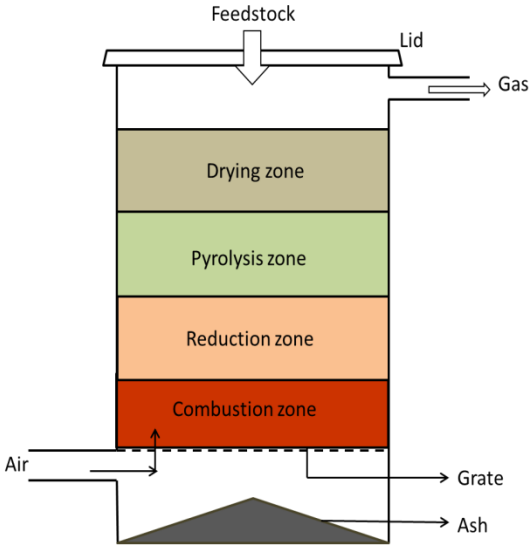

***Figure 2. 9*:** Schematic diagram of an updraft gasifier [Skov, 1974]

In general the feedstock is treated in the following sequence, drying (on the top), pyrolysis, reduction and lastly, combustion [Juniper, 2000; Quaak *et al.,* 1999]. The combustion releases heat and carbon dioxide that drive gasification and pyrolysis as the combustion products, travel up through the bed [Larson, 1998].

The gasification medium and the produced wood gas flow in the updraft gasifier are in the opposite direction of the fuel bed. Meaning that if the reactor is fed from the top, the gasification media (air, oxygen, steam) enter the reactor in the area of the grate [Lettner *et al.,* 2007]. The disadvantage of this type of gasifier is higher tar content compared to the downdraft type [Di Blasi *et al.,* 1999].

2.6.3. Fluidized bed

Fluidized-bed reactors use a fluidized mix of bed material and biomass. The gasification medium of this type flows in through the nozzle at the bottom and fluidizes the bed material [Lettner *et al.,* 2007]. It was originally developed to solve the operational problems of fixed bed gasification which are related to feedstocks with high ash content as well as to increase the heat and mass transfers in the reactor [Quaak *et al.,* 1999]. However, due to their high degree of solids mixing as well as particle entrainment, a single fluidized bed cannot achieve high solids conversion. The efficiency of a fluidised bed gasifier is higher than that of the fixed bed (about five times) [Quaak *et al.,* 1999]. These reactors do not consist of different reaction zones. The Figure 2.10 shows a schematic view of a fluidized bed.

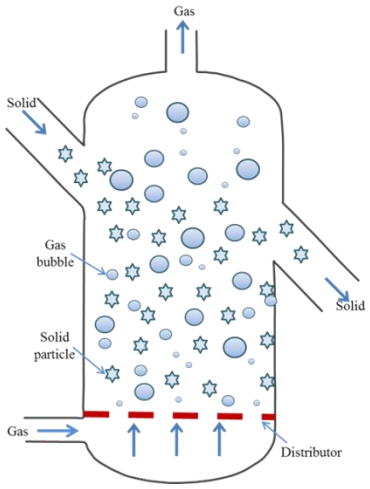

***Figure 2. 10*:** Schematic diagram of fluidized bed gasifier [Skov, 1974]

Their isothermal bed usually operate at temperatures usually between 700 ºC and 900 ºC which is less than maximum temperatures of a fixed bed gasifiers [Belgiorno *et al.,* 2003]. Fundamental

and pilot studies are required for scale-up, as well as to fill in the gaps in understanding the underlying principles of this type [Li *et al.,* 2004].

Table 2.2: Advantages and disadvantages of fixed bed gasifiers [Rajvanshi, 1986]

Gasifier type	Advantages	Disadvantages
Updraft	• Small pressure drop • Good thermal efficiency • Little tendency towards slag formation	• Great sensitivity to tar and moisture and moisture content of fuel • Relatively long time required for startup of IC engines • Poor reaction capability with heavy gas load
Downdraft	• Flexible adaptation of gas production to load • Low sensitivity to charcoal dust and tar content of fuel	• Design tends to be tall • Not feasible for very small particle size of fuel
Crossdraft	• Short design height • Very fast response time to load • -Flexible gas production	• Very high sensitivity to slag formation • High pressure drop

2.7. Hydrogen production

Hydrogen is currently being widely examined as a possible energy carrier to reduce carbon emissions from electricity production and transportation. It can be produced from any hydrocarbon, water and some industrial by-products. The choice of production method is likely to vary depending on local source availability and cost [Shoko *et al.,* 2006]. It is one of the simplest elements in the world and also the most plentiful gas in the universe. Hydrogen gas rises

in the atmosphere because it is lighter than air. Hence, hydrogen as a gas (H_2) is not found on earth by itself [Kalinci *et al.,* 2009], it is found only in compound formed with other elements. When it is combined with carbon, it forms different compounds such as methane (CH_4), coal, and petroleum. Hydrogen is a carrier not an energy source and can be produced from fossil fuels as well as biomass and water [Kalinci *et al.,* 2009].

There are several possible routes for producing hydrogen which involves conventional, commercial or advanced technologies and are under development. The commercial processes for hydrogen production, which are presently used include steam reforming of natural gas [Pena *et al.,* 1996)], partial oxidation of heavy oil residues (followed by water–gas shift (WGS) conversion) and electrolysis of water. Currently, H_2 produced via steam methane reforming (SMR), coal gasification, oil reforming, and electrolysis is about 48%, 18%, 30%, and 3.9% of total, respectively. The total H_2 production from fossil fuel sources amount to 96% [Ewan *et al.,* 2005]. These methods mainly consume fossil fuel as an energy source, which is not only full with emission problems, but also fossil fuels are being depleted at an alarming rate. Development of new methods for hydrogen production, especially from renewable sources, such as biomass [Athanasios *et al.,* 2002] is necessary.

Hydrogen can be used in fuel cell systems without any carbon emissions and minimal emissions of other pollutant gases [Bose and Maji, 2009]. When hydrogen is burned, hydrogen combustion does not produce toxic products such as hydrocarbons, carbon monoxide, oxide of sulfur, organic acids or carbon dioxide, instead its main by-product is water. Hydrogen gas has a great potential in the future as an energy carrier, but is not widely used currently [Bose and Maji, 2009]. It is

mainly used as feedstock for the chemical industry and as liquid fuel for space applications. However, developments in the area of fuel cells dictate that, in the future, hydrogen will be used as a secondary energy carrier for the electricity production for mobile and small-to-medium scale stationary applications [Athanasios *et al.,* 2002]. H_2 is also used in the petroleum and chemical sectors for upgradrading crude oil and synthesize methanol and ammonia [Florin and Harris, 2008].

2.7.1. Hydrogen from biomass gasification

Hydrogen is currently produced mainly by catalytic steam reforming of natural gas [Pena *et al.,* 1996]. However, in order to have environmentally friendly hydrogen, it should be produced from renewable methods such as biomass gasification [Mahishi and Goswami, 2007]. Biomass gasification as one of the thermochemical process has been identified as a potential technology for producing hydrogen [Turn *et al.,* 1998, Asadullah *et al.,* 2002]. But there are major challenges in moving towards a H_2 energy economy which is to produce enough H_2 to meet future demand as well as the hydrogen storage, transportation and cost [Florin and Harris, 2008].

There are still many subjects that need to be investigated further, such as proper facility design and suitable operating conditions for maximum hydrogen yield [Lv *et al.,* 2004]. Biomass gasification with air as a gasifying agent produces a gas with low hydrogen content (8-14 vol %) [Narváez *et al.,* 1996].

2.7.2. Use of catalyst

Catalysts (indigenous or added) are needed for the efficient gasification of carbonaceous materials including coals and biomass [Devi and Kannan, 1998]. They can also be used in higher temperature in an entrained flow gasifier where the fine catalyst is mixed intensively with the producer gas after which is separated and the recycled to the gasifier. In recent years, Lin and co-authors proposed a novel gasification method for hydrogen production from carbonaceous materials using a CO_2 sorbent. This method has been applied to various carbonaceous materials such as coal, oil, biomass, and plastic [Lin *et al.,* 2002].

Florin and Harris investigate the steam gasification of biomass, in the presence of a calcium oxide (CaO) sorbent to capture carbon dioxide (CO_2) which is a promising pathway for renewable and sustainable hydrogen (H_2) production. The experimental H_2 concentrations were reported for the steam gasification of biomass, without CO_2 capture and was ranging between 40 and 50% vol, but when CaO was used to capture CO_2 from the product gas, it then increased to 40–80% vol (dry basis) [Florin and Harris, 2008].

This method for hydrogen production is a new technique integrating steam gasification of carbonaceous materials, water-gas shift reaction and CO_2 absorption using calcium oxide as a CO_2 sorbent in a single reactor [Hanaoka *et al.,* 2005b]. The conventional method consists of three processes (reaction (2.21)–(2.23)). However, in this method, hydrogen can be obtained in a single reactor (reaction (2.24)) [Hanaoka *et al.,* 2005b].

$$C\ (\text{Carbonaceous materials}) + H_2O \rightarrow CO + H_2; \qquad \Delta H = 112.7\ \text{kJ/mol} \qquad (2.21)$$

$$CO + H_2O \rightarrow CO_2 + H_2; \qquad \Delta H = -41.5\ \text{kJ/mol} \qquad (2.22)$$

$$CaO + CO_2 \rightarrow CaCO_3; \qquad \Delta H = -178\ \text{kJ/mol} \qquad (2.23)$$

$$C\ (\text{Carbonaceous materials}) + CaO + 2H_2O \rightarrow 2H_2 + CaCO_3 \qquad \Delta H = -88\ \text{kJ/mol} \qquad (2.24)$$

The CaO loaded in the gasifier plays it absorbs the released CO_2 to enhance the water-gas shift (Eq. (2.21)) and water-gas shift (Eq. (2.22)) reactions towards hydrogen production and it also provide the necessary energy needed for the endothermic gasification through the carbonation reaction (Eq. (2.23)) [Han *et al.* 2010 in Hanaoka *et al.*, 2005b].

Mahishi and Goswami steam gasified the Southern pine bark in the presence of calcium oxide sorbent at various temperatures ranging from 500 ºC to 700 °C. The authors observed that the total gas yield with the presence of sorbent was more than doubled at a gasification temperature of about 500 °C while at temperature of 600 °C the gas yield was almost 62% higher than the base case [Mahishi and Goswami, 2007]. The hydrogen yield at a temperature of 600 °C, and carbon conversion efficiency was increased by 48.6% and 83.5%, respectively, for the sorbent enhanced case. It was also observed that the hydrogen produced for the sorbent case at a temperature of 500 ºC and 600 ºC was more than the conventional hydrogen produced at 700 °C. Therefore, it is possible to operate the gasifier at a lower temperature when using the sorbent and still get the same hydrogen yield or higher [Mahishi and Goswami, 2007].

The CO_2 being absorbed by calcium oxide usually depends on the equilibrium temperature which correspond to the partial pressure of CO_2 [Madhukar *et al.,* 2007]. The dominant experimental parameters, reaction temperature and steam-to-biomass ratio has been reported to be the ones that influences both the concentration of H_2 in the product gas and the total gas yield.

Corella *et al.,* [1998 and 1999] had performed a study of biomass air gasification with the direct use of dolomite in the gasifier and demonstrated that calcined dolomite has nearly the same influence on biomass gasification either in the gasifier or in the downstream fixed bed reactor. Therefore calcined dolomite can be used directly in the fluidized bed gasifier, and a downstream or second bed of dolomite would be unnecessary [Lv *et al.,* 2004]. Until now, not so much literature has been found involving hydrogen production from biomass catalytic gasification [Rapagna` *et al.,* 1998, Turn *et al.,* 1998]. The syngas, which has increased hydrogen also contains other gases such as CO, CH_4, CO and some hydrocarbons [Madhukar *et al.,* 2007]. This approach has been used in this study for air blown gasification without any additional steam to test whether the hydrogen produced will be enhanced from this gasifier type.

2.7.2.1. Calcium oxide sorbent

Calcium oxide (CaO), also known as limestone, is a white crystalline solid. CaO is a sorbent material that can be used to adsorb CO_2 during gasification. It has the possibility to reduce tars in the syngas by catalysis of the CaO additives. Among various tars reduction methods, catalyst thermal cracking using cheap natural minerals such as CaO and dolomite (CaO.MgO) (or their calcined forms) has been of interest. It is widely reported that both primary (loading the minerals

directly inside the gasifier) [Gil *et al.*, 1999] and secondary (downstream hot gas cleaning) [Simell *et al.*, 1992] methods are efficient to eliminate tar species. Tars elimination during biomass gasification is of significance to prevent the decrease of system efficiency and blocking problem of downstream units [Han *et al.*, 2010]. CaO plays the role not only of a CO_2 sorbent, but also that of a catalyst for the gasification of biomass [Hanaoka *et al.*, 2005a and Madhukar *et al.*, 2007]. This type of catalyst was chosen because it is cheaper compared to others, such as nickel and activated carbon. It is also not harmful to the environment [Choi *et al.*, 2009].

A. Calcium oxide CO_2 adsorption capacities

The adsorption of CO_2 on calcium oxide is mainly based on the stoichiometry carbonation reaction and the maximum theoretical amount of CO_2 adsorbed is 17.8 $mmolg^{-1}$ [Choi *et al.*, 2009]. The large adsorption capacity and capability at high operating temperatures makes the Ca-based material a potential CO_2 sorbent. The disadvantage is that the adsorption capacity for CaO-based sorbents decays with respect to the number of cycles [Abanades *et al.*, 2003]. Recently, many methods have been proposed which can be used to improve the uptake capacity and the life cycle performance of a CaO-based sorbent, including reactivation by steam hydration, incorporation of inert materials as well as modification of the pore structure. The sorbent must maintain its activity through many cycles in the process to be economically viable [Christina *et al.*, 2010]. A possibility of enhancing the stability of sorbents under cyclic runs is usually achieved by the incorporation of inert materials. MgO is commonly seen in the incorporation of CaO-based sorbents for it is inert under the conditions where CO_2 is adsorbed onto CaO [Huang *et al.*, 2010]. For this reason MgO was also used together with CaO.

B. Calcium oxide kinetics

The rate of the carbonation process governs the kinetics of CO_2 adsorption on calcium oxide adsorbents which can be limited by the rate of the chemical reaction and sometimes is limited by the rate of the CO_2 transport to the unreacted adsorption sites of the metal oxide [Choi *et al.,* 2009]. This kinetics of CO_2 on calcium oxide adsorbents is much slower than on zeolites and activated carbons, sometimes it requires several hours of adsorption to achieve 70% of the total capacity. The carbonation reaction rate consists of a fast stage of carbonate layer growth followed by a typically slow stage that continues until a conversion plateau. In the first, rapid stage the adsorption rate is influenced by the temperature and pressure of CO_2 and becomes faster as the temperature or pressure increases. In contrast, in the second stage the rate of the carbonation reaction is barely affected by the CO_2 pressure and it decreases gradually due to filling of pore during the course of the carbonation reaction [Choi *et al.,* 2009].

C. Calcium oxide regenerability

In the regenerator, the CaO is regenerated from $CaCO_3$ with the release of the CO_2 [Lin *et al.,* 2004].

$$CaO + CO_2 \rightarrow CaCO_3 \qquad (2.25)$$

The regeneration step requires high temperature (up to 950^{o}C) which leads to sintering of the material and consequently in rapid capacity decay up on multiple cycles. This is the main drawback of CaO. The regenerability of calcium oxide adsorbents are also strongly influenced by

their physical characteristics which includes the particle size, porosity, surface area, and others [Choi *et al.,* 2009].

D. Uses of calcium oxide

CaO is usually used as tar cracking catalyst in gasification [Wang *et al.,* 2010] as discussed earlier. It is a strong base which reacts with acids and also neutralizes it. It is being used in treating wastewater, drinking water and other industrial acid streams. Calcium oxide has been used widely to desulfurize stack emissions from coal- and oil-fired power plants. It is also used effectively in removing phosphorus, sulfur, and silica as well as to a lesser extent, manganese. CaO also has significant uses in the secondary refining of steel and where the steel products are manufactured. Lime has been widely used in the manufacture of precipitated calcium carbonate. If CO_2 gas is introduced into lime slurry then calcium carbonate ($CaCO_3$) is precipitated out of solution. The precipitated calcium carbonates are produced are usually in large quantities and can be used for paper, plastics, sealants, food and pharmaceuticals [European commission, 2010].

2.7.2.2. Magnesium oxide sorbent

Magnesium oxide (MgO) is an alkaline earth metal oxide. The majority of produced magnesium oxide today is achieved from the calcination of naturally occurring minerals such as magnesite, $MgCO_3$, which is the most common. The seawater, underground deposits of brine and deep salt beds from which magnesium hydroxide [$Mg(OH)_2$] are the important sources of MgO. Magnesium is the eighth most abundant element which constitute of about 2% of the earth's crust and typically 0.12% of seawater. $MgCO_3$ and $Mg(OH)_2$ are both converted into MgO by means

of calcination. It is the most important industrial magnesium compound and is mostly applied in the steel and refractory industry. Magnesium oxide is largely used in many foods and animal feed industries. It has a number of refractory and is fast-hardening and as well as general repair applications. It is also used as a curing agent room temperature for phosphate cements [European commission, 2010].

I. Magnesium oxide regenerability

Magnesium oxide (MgO) compared to calcium oxides has been studied as a possible CO_2 for their lower energy requirement for the regeneration [Feng *et al.,* 2007]. It has been observed that CO_2 adsorbed by magnesium oxides can be recovered by 1 hour of regeneration under vacuum at a temperature of 700 ºC, on the other hand 4 hours of heating are required to remove CO_2 from calcium oxides under similar experimental conditions [Beruto *et al.,* 1987].

II. Magnesium oxide CO_2 adsorption capacities

The difference between the adsorption of CO_2 by magnesium oxides by calcium oxides is that this material hardly reacts with CO_2 after 20 h at 350 ºC even though the CO_2 pressure is high compared to the equilibrium pressure for $MgCO_3$ formation [Beruto *et al.,* 1987]. This low adsorption capacities of magnesium oxide adsorbents, compared to calcium oxide-based adsorbents, implies that these materials are not likely to be strong options for CO_2 capture from producer gases that have low concentrations of CO_2 [Choi *et al.,* 2009].

2.8. Background on kinetics of biomass

The knowledge of kinetics provides necessary information on kinetic mechanisms which can be used to describe the conversion during biomass gasification, which is important in designing, evaluating and to improve the performance of gasifiers [Puig-Arnavat *et al.*, 2010]. Kinetic determination of lignocellulosic materials involves the knowledge of the reaction mechanisms. But, the number of reactions that occur simultaneously in the pyrolysis process is so huge that it is practically not possible to develop a kinetic model that can take into account all the reactions taking place. Therfore, the pyrolysis process is usually studied in terms of pseudo-mechanistic models [Conesa and Domene, 2011].

Thermogravimetric analysis (TGA) is a technique which provides an insight into the kinetics of heterogeneous reactions [Vyazovkin *et al.*, 1998]. This technique was used for its advantages such as the use of the relatively small set of data to be treated, continuous recording of weight loss as a function of temperature, which ensures equal weightage to examine over the whole range of study as well and the use of a single sample is analyzed over the whole range of temperature, the variation in the value of the kinetic parameters, if any, can be indicated [Science J. (1995)]. The disadvantages of TGA method are the limited range of samples, time consuming and usually not qualitative. The method that is employed for the kinetics is usually classified as either ‘model free’methods or ‘model fitting’methods [Aboyade *et al.*, 2013]. The model fitting approach allows to choose an appropriate model for your data and estimate the reaction order, while for the model free (isoconversional) method you do not need to choose any model or estimate any reaction order [White *et al.*, 2011].

2.8.1. Model free (isoconversional)

Model free (isiconversional) methods do not require the assumption of reaction models, and yield kinetic parameters as a function of either conversion or temperature [Vyazovkin *et al.,* 2000]. This method is of advantageous since it does not require any previous knowledge of the reaction mechanism for thermal decomposition of biomass [White *et al.,* 2011]. Another advantage it can eliminate the systematic error resulted from the kinetic analysis during the estimation of the Arrhenius parameters [Brown *et al.,* 2000]. Various isoconversional methods have been employed by many authors in the analysis of the non-isothermal decomposition of biomass and/or its components [Biagini *et al.,* 2008, Cai *et al.,* 2009, Leroy *et al.,* 2010].

2.8.2. Model fitting

Model fitting methods are the estimation of kinetic parameters that are associated with a particular reaction model and then assumed to represent the dependence conversion of the reaction rate [Vyazovkin *et al.,* 2011]. The estimation of kinetic parameters from TGA data using model fitting approach involves assuming a certain reaction order and then manipulating the differential or integral form of the ensuing rate equation until a straight line plot can be obtained after which the remaining unknown parameters (kinetic parameters, E and A) can be obtained by linear regression [Aboyade *et al.,* 2013]. However, these approaches suffer from two main deficiencies, especially in cases where data from only a single heating rate is used [Kemmler *et al.,* 2000]:

(a) The use of the model fitting approach to single heating-rate data generally fail to obtain a clean separation between the reaction model and the temperature dependence [Vyazovkin, 2000]. For this reason, the application of the model fitting methods to single heating rate data produces kinetic parameters that are highly not certain and, therefore, cannot be meaningfully as compared with the isothermal values [Chen *et al.,* 2006, Gonzalez-Perez *et al.,* 2004].

(b) It also tends to produce one set of kinetic parameters for every range of conversion, and not taking into account the complexity of mechanisms that are involved during pyrolysis of biomass [Vyazovkin *et al.,* 1999].

The model fitting methods can as well be reliable as the model-free methods as long as different models are fitted simultaneously to multiple data sets which are obtained under different temperature programs [Brown *et al,* 2000].

2.8.3. Chemical kinetics modeling

The thermal decomposition of cellulosic materials such as wood proceeds through a complex series of chemical reactions, coupled with heat and mass transfer processes [Sinha *et al.,* 2000]. The actual reaction scheme of pyrolysis of biomass is extremely complex because of there are over a hundred intermediate products that are formed [Babu and Chaurasia, 2003, Roberts, 1971]. Babu and Chaurasia, 2003 reported the basic phenomena that take place during pyrolysis of materials as follows:

(1) There is a heat transfer from a heat source that can lead to an increase in temperature inside the biomass;

(2) There is also an initiation of pyrolysis reactions that are due to the increased temperature which lead to the release of volatiles and the char formation;

(3) The outflow of volatiles which results in heat transfer between the hot volatiles and cooler unpyrolysed biomass fuel;

(4) The condensation of some of the volatiles matters in the cooler parts of the fuel which lead to the production of tar;

(5) And finally the autocatalytic secondary pyrolysis reactions which are due to the interactions discussed earlier.

Biomass pyrolysis is then generally modeled on the basis of apparent kinetics. Preferable, the chemical kinetics model should account for both the primary decomposition and the secondary reactions [Babu and Chaurasia, 2003].

The following two step mechanism scheme was developed to describe the kinetics of the biomass pyrolysis [Koufopanos *et al.*, 1991]:

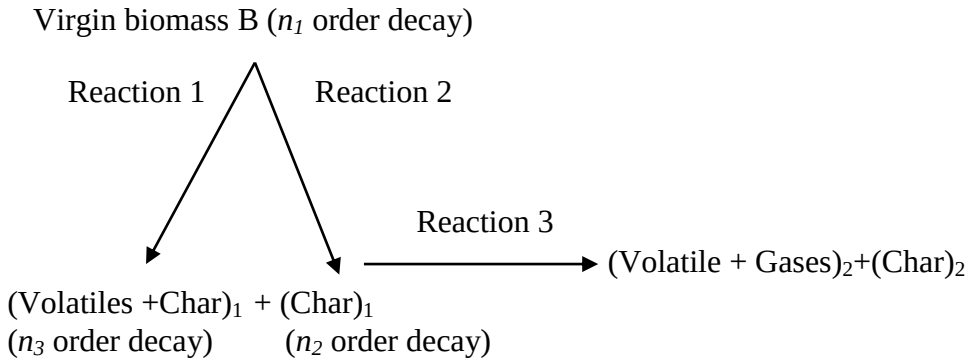

The latter reaction scheme shows that the biomass decomposes to volatile, gases and char (reactions 1 and 2), which is a primary pyrolysis. The volatiles and gases also further react with char, in a secondary pyrolysis (reaction 3) to produce the different types of volatile gases and char in which the compositions are different [Babu and Chaurasia, 2004]. The later scheme can be represented by the following reaction mechanism [Sinha *et al.*, 2000]:

$$\frac{dm}{dt} = -k_1 {m_w}^{n1} - k_2 {m_w}^{n1} \tag{2.26}$$

$$\frac{dm_{G1}}{dt} = -k_1 {m_w}^{n1} - k_2 {m_{G1}}^{n2} {m_{C1}}^{n3} \tag{2.27}$$

$$\frac{dm_{C1}}{dt} = -k_2 {m_w}^{n1} - k_3 {m_{G1}}^{n2} {m_{C1}}^{n3} \tag{2.28}$$

$$\frac{dm_{G2}}{dt} = -k_3 {m_{G1}}^{n2} {m_{C1}}^{n3} \tag{2.29}$$

$$\frac{dm_{C2}}{dt} = \delta k_3 {m_{G1}}^{n2} {m_{C1}}^{n3} \tag{2.30}$$

where m_w, m_{G1}, m_{G2}, m_{C1} and m_{C2} are the masses of wood, primary and secondary gas and primary and secondary char respectively, n_1, n_2 and n_3 are orders of the three reactions; k_1, k_2 and k_3 are the rate constants of the three reactions, δ is the yield ratio of the secondary char to gas. The reaction rates for the reactions of 1, 2 and 3 were determined from Eq. (2.31):

$$k_i = A_i \exp\left(\frac{D_i}{T} + \frac{L_i}{T^2}\right) \quad (2.31)$$

where A_i is a pre-exponential factor, D_i and L_i are constants defined by expression k_i, and their values are given in Table 2.1 [Koufopanos *et al.*, 1991]:

Table 2.3: Kinetic data for wood from Koufopanos *et al.*, [1991]

i	Reaction	A_i (s^{-1})	D_i (K)	L_i (K^2)
1	Biomass→ (Volatile gases)$_1$	$9.973x10^{-5}$	17254.4	-9061227
2	Biomass→ (Char) $_1$	$1.068x10^{-3}$	10224.4	-6123081
3	(Vol gases) $_1$ + (Char) $_1$→ (Vol gases) $_2$+ (Char)$_2$	$5.7x10^5$	-9742.6	0

In a mechanism in which the volatiles and tar formed by primary pyrolysis, they undergo secondary pyrolysis [Chan 1983]. Again other primary reactions where char and gas are formed from wood are parallel and competing with the formation of tar reaction. Evolution of moisture in wood in the form of water vapour was also considered as one of the pyrolysis reactions as shown in the following scheme:

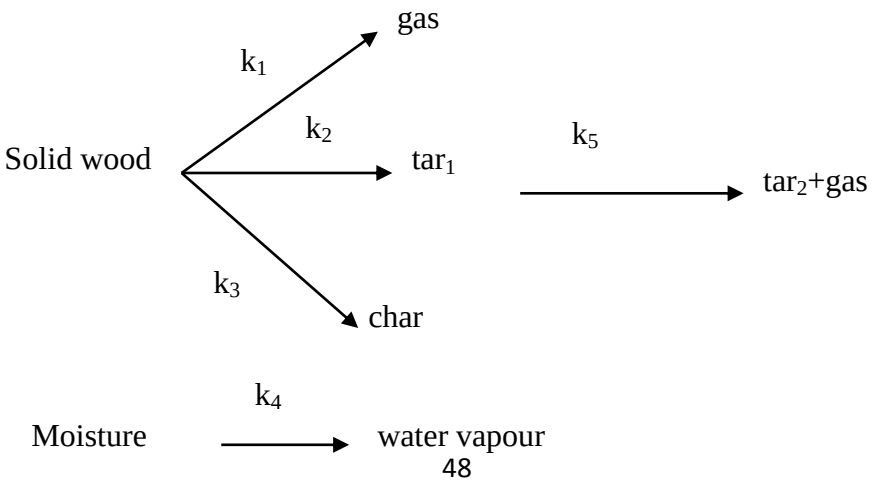

The rate constant of each reaction is written as $k_i=A_i \exp(-E_i/RT)$, where E_i is the activation energy, R is the universal gas constant and the temperature is represented by T. The values of A and E_i are tabulated in Table 2.3.

Table 2.4: Kinetic constants used by Chan [1983].

i	Reaction	A_i (s^{-1})	E_i (kJ/mol)
1	Wood → Gas	$1.3x10^8$	140
2	Wood → $(Tar)_1$	$2x10^8$	133
3	Wood → Char	$1.08x10^7$	121
4	Moisture → Water Vapour	$5.13x10^6$	87.9
5	$(Tar)_1$ → $(Tar)_2$+Gas	$1.48x10^6$	144

Many author have studied cellulose pyrolysis in order to understand the mechanism of pyrolysis of wood since cellulose is the major constituent of lignocellulostic wood and pyrolyses at the temperature range of 280-380 ºC [Shafizadeh, 1982, Bradbury *et al.*, 1979]. The scheme below shows the general set of reactions for cellulose [Shafizadeh, 1982]:

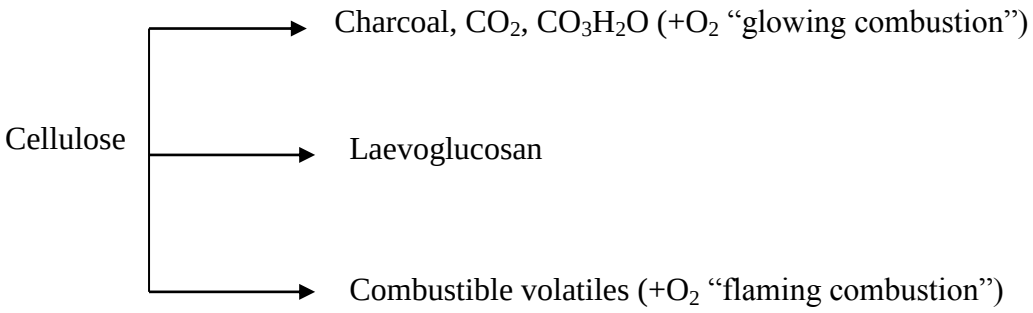

A more detailed description of possible pathways that may contribute to weight loss during pyrolysis is shown below [Lewellen *et al.*, 1969]:

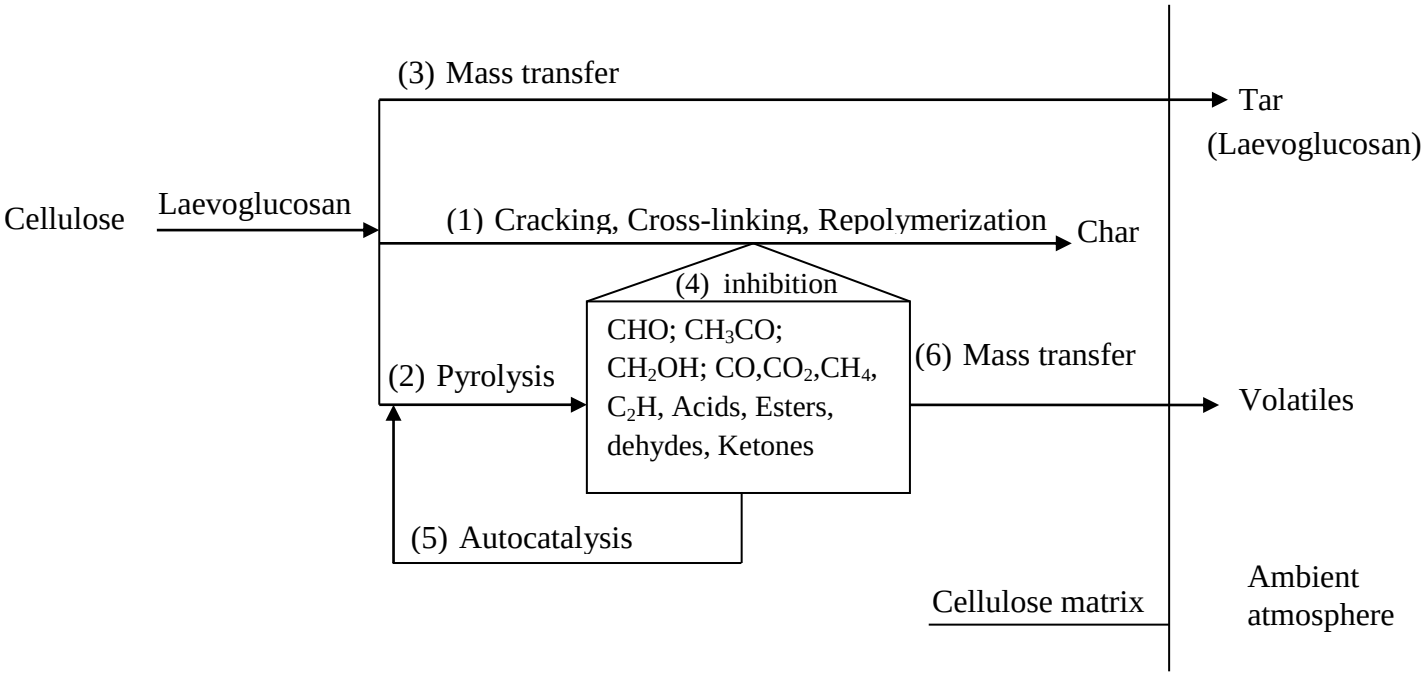

The latter scheme shows that cellulose decomposes rapidly to laevoglucose which is an intermediate product. It may as well be transformed from the cellulose matrix using path 1 to produce tar, or may repolymerize, crack, or it can cross linked to give path 2 (Pyrolysis) which the mass transfer, or be polymerized through path 3 (inhibition) to lighter volatile products which include CO, CO_2, fixed gases, organic acids, ketones, esters, aldehydes and free radicals, some of which could inhibit char formation through autocatalyst (path 4), or autocatalyze step 3 (Mass transfer) through path 5. Stable products which are lighter would escape the matrix through path 6 to produce volatiles. Hence, there are a number of possible pathways for the pyrolysis of cellulose alone, which then reflects the complexity of pyrolysis mechanism of wood as a whole [Sinha *et al.*, 2000].

CHAPTER 3

RESEARCH METHODOLOGY

3.1. Introduction

This chapter presents the methods employed in data collection as well as justification for the data collected. The Carbon Hydrogen Nitrogen and Sulphur (CHNS) analyzer, Thermogravimetric analysis (TGA), analysis of variance (ANOVA) and bomb calorimeter methods were used in the characterization of the samples. The simulation software developed by Jayah *et al.,* [2003] was used for the simulation of the syngas/produce gas production and the gasification conversion efficiency. MATLAB software was used to develop the kinetic models for this study.

3.2. Sample preparation

The samples were mixtures of biomass (pine wood), calcium oxide (CaO) and/or magnesium oxide (MgO) and their ratios are listed in Table 3.1. Pine wood was used as the organic material while calcium oxide (CaO) and/or magnesium oxide (MgO) were used as the sorbent materials for CO_2 capture. The sorbent materials were used without any further preparations. Pine wood was coarsely ground to 250 μm and mixed with CaO and/or MgO. The pestle and mortar were used to mix the materials in different percentages. To ensure that the materials are homogeneously mixed, the mixing was repeatedly made and the samples were continuously shaken in a bottle. The mixtures were in different percentages as listed in Table 3.1.

Table 3.1: The mixture of wood, CaO and MgO materials.

Samples	Wood (%)	CaO (%)	MgO (%)	CaO.MgO (%)	Blend
1.	100	-	-	-	Wood
2.	95	5	-	-	5%CaO
3.	95	-	5	-	5%MgO
4.	90	10	-	-	10%CaO
5.	90	-	10	-	10%MgO
6.	90	5	5	10	10%CaO.MgO
7.	85	15	-	-	15%CaO
8	85	-	15	-	15%MgO
9.	85	7.5	7.5	15	15%CaO.MgO
10.	80	20	-	-	20%CaO
11.	80	-	20	-	20%MgO
12.	80	10	10	20	20%CaO.MgO
13.	75	25	-	-	25%CaO
14.	75	-	25	-	25%MgO
15.	75	12.5	12.5	25	25%CaO.MgO

Note the remaining percent (after adding CaO and/or MgO) is for the pine wood.

3.3. Characterization and Analysis methods

The materials discussed above were characterized and analyzed using the following methods:

3.3.1. CHNS Analyzer

The ultimate analysis was conducted using Carbon, Hydrogen, Nitrogen and Sulphur (CHNS) Analyzer. This equipment only evaluates the carbon, hydrogen, nitrogen, and sulphur composition of the material. The composition of oxygen is calculated using the difference

method [Harun *et al.*, 2008]. The elemental composition of biomass and biomass/sorbents for this study were determined using this technique. This device can handle different types of sample, such as solids, liquids, volatile as well as viscous samples, in the fields of polymers, pharmaceuticals, environment, chemicals, energy and food [Thompson, 2008]. In order to avoid confusion and to give a good representation of the fuel itself, an ultimate analysis is performed and reported on a dry basis, because otherwise moisture is indicated as additional hydrogen and oxygen [Stahl *et al.*, 2003]. This technique was used because it determines the lighter elements (C, H, N and O) which are necessary for the current study, unlike Energy-dispersive X-ray spectroscopy (EDX) which does not detect some lighter elements such as hydrogen and it only measure the composition on a few micrometer (μm) depth from the surface. The schematic view of CHNS analyzer is shown in Figure 3.1.

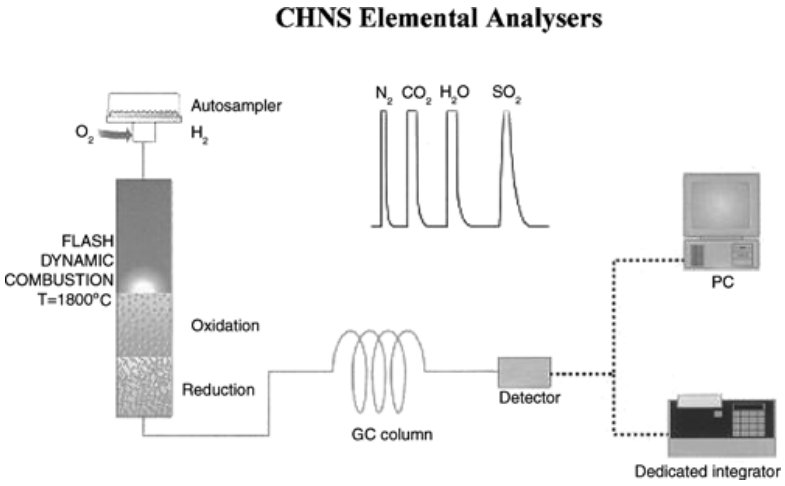

Figure 3. 1: A schematic view of a CHNS analyzer [Greenfield *et al.*, 2006]

3.3.2. Bomb calorimeter

Bomb calorimeter is a technique which can be used to determine the heating value or calorific value of solid and liquid materials which can be burned as fuels [Cal2k, 2013]. They are usually presented as a lower heating value (LHV) or a higher heating (HHV). It is defined as the measurements of the enthalpy change between reactants and products [Sheng *et al.,* 2005]. The calorimeter determines the higher heating value as it includes the latent heat of vaporization. The energy values of the samples considered in this study were determined using this technique. Figure 3.2 shows a bomb calorimeter employed in determining the calorific value of the materials.

Figure 3. 2: A schematic view of a bomb calorimeter [Cal2k, 2013].

The gas heating value or caloric value (CV) (MJ/Nm^3) can be calculated in terms of percentage composition of the combustible gases as follows [Mamphweli, 2009]:

$$CV_{gas} = \left[\frac{\left[\left(H_{2_{vol}} \times CV_{H_2}\right) + \left(CO_{vol} \times CV_{CO}\right) + \left(CH_{4_{vol}} \times CV_{CH_4}\right)\right]}{100}\right] \quad (3.1)$$

where:

CV_{gas} = Gas Caloric Value (MJ/Nm^3)

$H_{2_{vol}}$ = Volume concentration of Hydrogen gas (%)

CV_{H_2} = Caloric Value of Hydrogen from the standard gas table (MJ/Nm^3)

CO_{vol} = Volume concentration of Carbon Monoxide (%)

CV_{co} = Caloric Value of Carbon Monoxide from the standard gas table (MJ/Nm^3)

$CH_{4_{vol}}$ = Volume concentration of Methane

CV_{CH_4} =Calorific value of methane from the standard gas table (MJ/Nm^3)

3.3.3. Computer simulation software

A DOS based computer program was used to simulate the conversion efficiency of a biomass and biomass/sorbent blends downdraft gasifier. The program was developed by Chen and Gunkel, [1987] then modified by Jayah *et al.*, [2003]. It is basically used to simulate the performance of a downdraft gasifier. It was performed to identify the optimum design parameters and desirable operating parameters for enhanced conversion efficiency. Basically the model was developed for the downdraft wood gasifiers to study the effects of operating and design parameters on reactor performance [Chen, 1987]. The model development consists of two sub-models: (1) flaming pyrolysis zone sub-model which is used to estimate the product concentration and temperature of gas leaving the flaming pyrolysis zone and (2) the gasification zone sub-models zone sub-model which is used to predict the output of the producer gas and the

length of the gasification zone at any given time step [Jayah, 2002]. The model develops the concepts of equilibrium in chemical reactions with mass and energy balance principles. For the present study the software was used to predict the producer gas concentration with specific reference to H_2 achieved with various mixtures of pine-wood and sorbents and the conversion efficiency.

3.3.3.1. Flaming pyrolysis zone sub model

In the flaming pyrolysis zone the general equation of reaction of wood can be expressed by equation 3.2:

$$CH_aO_b + wH_2O + m(0.21O_2 + 0.79N_2) \rightarrow x_{char}Char + x_{tar}Tar + x_1CO + x_2H_2 + x_3CO_2 + x_5CH_4 + x_6N_2 \quad (3.2)$$

where char was taken as carbon and ultimate analysis of tar as $CH_{1.03}O_{0.03}$ [Adams, 1980]. From equation 3.3 and 3.4 we can obtain the equilibrium equation and the corresponding equilibrium constant respectively.

$$CO + H_2O \leftrightarrow CO_2 + H_2 \quad (3.3)$$

$$K_3 = \frac{x_3 \times x_2}{x_1 \times x_4} \quad (3.4)$$

The correlation between the temperature and equilibrium constants for the above is given by equation 3.5 [Gumz, 1950].

$$Log(K_3) = -36.72508 + \frac{3994.704}{T} - 4.46241 \times 10^{-3}T + 6.71814 \times 10^{-7}T^2 + 12.2228\log(T) \quad (3.5)$$

where T is the temperature (K). By mass balance the Eq. (3.6-3.9) can be obtained:

Carbon: $$1 = x_{char} + x_{tar} + x_1 + x_3 + x_5 \quad (3.6)$$

Hydrogen: $$a + 2w = 1.03x_{tar} + 2x_2 + x_1 + 2x_4 + 4x_5 \quad (3.7)$$

Oxygen: $$b + w + 0.42m = 0.03x_{tar} + x_1 + 2x_3 + x_4 \quad (3.8)$$

Nitrogen: $$0.79m = x_6 \quad (3.9)$$

The energy balance in flaming pyrolysis zone is given by Eq. (3.10):

$$H_c wood = H_c Char + H_c Tar + H_c Gas + H_s Char + H_s Tar + H_s Gas + Heatloss \quad (3.10)$$

where *w* is the number of moles of water, including fuel moisture, air moisture, and water or steam addition [Chen, 1987] and can be calculated by the following equation:

Moisture in fuel wood = dry matter in fuel wood × moisture content on dry basis

$$w = (12 \times 1 + 1 \times a + 16 \times b) \times mc_{db} kg \quad (3.11)$$

where mc_{db} is the moisture content in wood, a and b are given, heat loss and m (number of moles of oxygen input) are obtained from the experiment, x_5, x_{char} and x_{tar} are assumed, x_1, x_2, x_3, x_4, x_6 and T are solved by using the successive approximation method with a Fortran programme. The higher heating value (kJ/g) of wood, char and tar are calculated from the equation as follows [Channiwala, 1992].

$$H_C Wood = 0.3491 f_C + 0.1783 f_H - 0.1034 f_O \text{ (N_2 and ash content are neglected)} \quad (3.12)$$

$$H_C Char = 0.3491 \times f_{C,char} \quad (3.13)$$

$$H_C Tar = 0.3491 \times f_{C,tar} + 0.1783 f_{H,tar} - 0.1034 f_{O,tar} \quad (3.14)$$

The chemical energy content of output gas, and sensible energy of char, tar and output gases are calculated as follows:

$$H_C Gas = 241000 x_1 + 283000 x_2 - 802300 x_5 \quad (3.15)$$

$$H_S Char = 12.15 x_{char} \times (T - 300) \quad (3.16)$$

$$H_S Tar = 21.95 x_{tar} \times (T - 300) \quad (3.17)$$

$$H_S Gas = x_1 H_{CO} + x_2 H_{H2} + x_3 H_{CO2} + x_4 H_{CO2} + x_4 H_{H2O} + x_5 H_{CH4} + x_6 H_{N2} \quad (3.18)$$

3.3.3.2. Gasification zone sub-model

The gasification zone is modelled by following a particle along the axis of the reactor. The computer program has been formulated using FORTRAN language to calculate the characteristic profiles along the reactor axis. The profile includes temperature, concentrations, efficiency and distance the particle travelled. The length co-ordinate is coupled with a time variable through the solid phase velocity. A small time increment approach is used in calculating the product composition of the zone. It involves the use of a step procedure starting from the gasification zone and marches axially through the reactor in appropriate time increments. The output values of the flaming pyrolysis zone are used as inputs for modeling the gasification zone [Jayah, 2002].

3.3.4. MATLAB software

MATLAB is a powerful and sophisticated software which can be used for computation, visualization, and programming. It can be used for data analysis, for developing algorithms, and creating models and applications. It is a high level language tool as well as a built-in math functions which allows one to explore multiple approaches which can enable one to reach a solution faster than using spreadsheets or traditional programming languages, like C/C++ or Java™ [Mathworks, 2013]. Statistical analysis and model fitting kinetics were performed using this software.

3.3.5. The analysis of variance (ANOVA)

ANOVA was developed by Ronald Fisher in 1918 and is the extension of the T-test [Fisher, 1925]. It can be used to compare the mean of two or more samples, simultaneously [Segurola *et al.,* 1999]. ANOVA can be found in most statistical packages, which makes it accessible to researchers in many fields of studies [Larson, 2008]. The T-test was commonly used before the use of ANOVA but its disadvantage is that it cannot be applied to more than two groups. Several tests have been developed to test the statistical significance between two or more groups of the mean values of some characteristics, but so far ANOVA is the most powerful, because it is not limited to determining mean of only two groups [Miller & Brewer, 2003]. ANOVA is normally used to test the equality among several means when comparing variance among groups and the variance within groups which is the random error [Larson, 2008].

There are two types of ANOVA tests: one way ANOVA test which is a method that is used to compare means of two or more samples (basically, using the F distribution) and two way ANOVA test, which is the extension of one way test. The one way ANOVA test was employed in this study to determine the significance in the mean difference of the samples.

3.3.5.1. One way ANOVA test

A one-way ANOVA test is basically used when the data are divided into groups according to only one factor. Usually the following two questions are of interest:

(a) If there a significant difference between groups?

(b) And if there is, which groups have significantly mean different from the other?

It is a method that can be used only for numerical data [Howell, 2002]. The following assumptions can be made [Larson, 2008] when performing one way ANOVA test:

(1) Individual observations are equally independent;

(2) The random errors are distributed normally;

(3) The random errors are homogeneously varied.

ANOVA test basically measures two sources of differentiation in the data and compares their relative sizes [Lazić, 2004]**:**

(1) The variation between groups: looking at the difference between its group mean and the overall mean for each data value.

$$(\overline{X}_\iota - \bar{X})^2 \tag{3.19}$$

Where $\overline{X}$= mean for the entire data and *i* is the number of groups.

(2) The variation within groups: looking at the difference between the value and the mean of its group for each group data value.

$$(\overline{X}_{ij} - \overline{X}_i)^2 \tag{3.20}$$

where $\overline{X}_i$ is the mean for group *i*, $\overline{X}_{ij}$ is the value of the individual mean for group j in group *i.* The ANOVA F-statistics is a ratio of the variation between groups/variation within groups, i.e,

F = MSG/MSE. Where, MSG and MSE are the mean square between groups and within groups, respectively. A large value of F indicates that there are more differences between the groups than within the groups.

The standard deviation of the entire data set can be calculated from the following equation:

$$S^2 = \frac{\sum(\overline{X}_{ij}-\overline{\overline{X}})^2}{n-1} = \frac{SST}{DFT} = MST \quad (3.21)$$

where $SST=(n-1)s^2$, is the total sum of squares, $MST=S^2$ and is the total mean squares, i.e *SST* and *MST* measure the variation in the data set.

$$S_i^{\,2} = \frac{\sum(X_{ij}-\overline{X_i})^2}{n_i-1} = \frac{SST}{DFT} = \frac{SS(within\ group\ i)}{df_i} \quad (3.22)$$

where n_i = number of individual for *j* in group *i*, therefore, *SS* (within group *i*) = (s_i^2) x (df_i). The *SSE* (sum of squares within groups*)* can be then determined from the standard deviations and *df* (degree of freedom) of each group:

$$SSE = \sum s_i^{\,2}(n_i - 1) = \sum s_i^{\,2}(df_i) \quad (3.23)$$

It is assumed that all groups have the same standard deviation and can be estimated with a weighted average as follows:

$$S_p{}^2 = \frac{\sum(n_1-1){S_1}^2+(n_2-1){S_2}^2+\cdots+(n_1-1){S_1}^2}{n-1} \quad (3.24)$$

$$S_p{}^2 = \frac{\sum(df_1){S_1}^2+(df_2){S_2}^2+\cdots+(df_2){S_1}^2}{n-1} \quad (3.25$$

$$S_p{}^2 = \frac{SSE}{DFE} = MSE \quad (3.26)$$

3.3.6. Thermogravimetric Analysis

Thermogravimetric analyzer (TGA) is one of the major thermal analytical techniques that are used to study the thermal behavior of carbonaceous material as a function of time or temperature [Çulcuoğlu *et al.*, 2001]. TGA provides a semiquantitative understanding of thermal degradation processes occurring during thermochemical conversion under various atmospheres [Mansaray and Ghaly, 1999]. When the materials are heated, they lose weight from a simple process of drying, or from chemical reactions that release gases. During the heating, materials gain weight by reacting with the atmosphere in the testing environment. The knowledge of the magnitude and the temperature range of those reactions are necessary because the weight loss and gain are disruptive processes to the sample material or batch. This is done in order to design an adequate thermal ramp and which can holds during those critical reaction periods. TGA is one of the most techniques that have been used because of its rapidity and requires a lesser necessity of sample manipulation compared to other methods in conventional analysis [Fern´andez-Berridi *et al.*, 2006]. The proximate analysis and kinetics of biomass and biomass/sorbent samples was

conducted using this method. It also provides insight regarding the kinetics of heterogeneous reactions of the materials [Vyazovkin and Wight, 1998].

3.3.6.1. Proximate analysis

Proximate analysis basically covers the estimation of moisture content, volatile matter (VM), fixed carbon (FC) and ash content in the carbonaceous material [Mayoral *et al.*, 2001]. The following equations are used in proximate analysis:

3.3.6.2. Kinetic study

Kinetics of solid state decompositions are usually based on equation 3.27 [Vyazovkin *et al.*, 2011]:

$$\frac{d\alpha}{dt} = k(T)f(\alpha) \tag{3.27}$$

The rate constant, k (T), and the dependence on the extent of conversion of the reaction model, f (α) represent the dependence of the process rate on temperature. The rate of a single-step process is usually described by Equation (3.27). The conversion (α) is determined experimentally as a fraction of the overall change in a physical property that accompanies a process. The α values is evaluated as a fraction of the total mass loss in the process if a process is accompanied by mass loss, as shown in Eq. (3.28):

$$\alpha = \frac{W_0 - W}{W_0 - W_f} \tag{3.28}$$

where w is the mass of substrate present at any time t, w_0 is the initial substrate mass and w_f is the residue of solids or unreacted substrate remaining after the reaction is complete. Almost every kinetic model uses a rate law which obeys the Arrhenius rate expression fundamentals, Eq. (3.29) [Vyazovkin and Wight, 1999]:

$$\frac{d\alpha}{dt} = Aexp\left(-\frac{E}{RT}\right) \tag{3.29}$$

where T is the absolute temperature in kelvin (K), R (J/K/mol) is the universal gas constant, A (min^{-1}) is the frequency factor or pre-exponential, and E (kJ/mo1) is the activation energy of the reaction. The Arrhenius parameters (E and A) and the reaction model (f (α)), are usually called the kinetic triplet [Vyazovkin *et al.*, 1999].

The physical significance of the Arrhenius parameters (i.e., E and A) for homogeneous reactions which involves gases, is basically interpreted in terms of molecular collision theory. The activation energy, E, is regarded as the energy threshold that must be overcome before molecules can get close enough to react and form products. Those molecules with an adequate kinetic energy to surmount this energy barrier are the only once that will react [White *et al.*, 2011]. The materials can be analyzed using a model fitting or the model free (isoconversional) approach. For the model fitting, an appropriate model is chosen for the data and estimates the reaction order. For the model free method there is no need to choose any model or estimate any reaction order [White *et al.*, 2011].

3.3.6.3. Model fitting method

Model fitting methods are the estimation of kinetic parameters that are associated with a particular reaction model and then assumed to represent the dependence conversion of the reaction rate [Vyazovkin *et al.*, 2011]. They involve the fitting of different models to the data so that a model which gives the best statistical fit can be chosen as the model from which the kinetic parameters are estimated [Slopiecka *et al.*, 2011]. The reaction model takes a different form, some of which are in Table 3.2. It can be accomplished by minimizing the difference between the experimental measured thermogravimetric (DTG) data and calculated DTG data.

The experimental data can be either isothermal, constant heating rate data, or a mixture of the two. Minimization of the experimental data can be accomplished by using linear or nonlinear regression methods. The key difference between linear and nonlinear methods is that linear methods do not need an initial estimate of A and E, while nonlinear methods do. Although non-linear methods are superior in many ways, they also benefit from initial estimates from linear methods [Vyazovkin *et al.*, 2011].

***Table 3.2**:* Some of kinetic models that are used in the solid state kinetics [Vyazovkin *et al.*, 2011].

	Reaction model	f(α)	g(α)
1	Power law	$4\alpha^{3/4}$	$\alpha^{1/4}$
2	Power law	$3\alpha^{2/3}$	$\alpha^{1/3}$
3	Power law	$2\alpha^{1/2}$	$\alpha^{1/2}$
4	Power law	$2/3\alpha^{-1/2}$	$\alpha^{3/2}$
5	One-dimensional diffusion	$1/2\alpha^{-1}$	α^{2}
6	Mampel (first order)	$1-\alpha$	$-\ln(1-\alpha)$
7	Avrami–Erofeev	$4(1-\alpha)[-\ln(1-\alpha)]^{3/4}$	$[-\ln(1-\alpha)]^{1/4}$
8	Avrami–Erofeev	$3(1-\alpha)[-\ln(1-\alpha)]^{2/3}$	$[-\ln(1-\alpha)]^{1/3}$
9	Avrami–Erofeev	$2(1-\alpha)[-\ln(1-\alpha)]^{1/2}$	$[-\ln(1-\alpha)]^{1/2}$
10	Three-dimensional diffusion	$3/2(1-\alpha)^{2/3}[1-(1-\alpha)^{1/3}]^{-1}$	$[1-(1-\alpha)^{1/3}]^{2}$
11	Contracting sphere	$3(1-\alpha)^{2/3}$	$1-(1-\alpha)^{1/3}$
12	Contracting cylinder	$2(1-\alpha)^{1/2}$	$1-(1-\alpha)^{1/2}$
13	Two-dimensional diffusion	$[-\ln(1-\alpha)]^{-1}$	$(1-\alpha)\ln(1-\alpha)+\alpha$

Rearranging and integrating Eq. (3.29) for isothermal condition gives:

$$g_j(\alpha) = k_j(T)t \tag{3.30}$$

where $g(\alpha) = \int_0^{\alpha}[f(\alpha)]^{-1}\,d\alpha$ is the integral form of the reaction model that are in Table 3.2. The subscript j emphasizes that when substituting a particular reaction model into Equation (3.31) the corresponding rate constant can be evaluated from the slope of a plot of g_j (α) versus t.

The rate constants are evaluated at several temperatures, T_i, from each reaction model that has been selected and the Arrhenius parameters (E and A) are determined by using the Arrhenius equation in its logarithmic form, Equation (3.31),

$$lnk_j(T_i) = lnA_j - \frac{E_j}{RT_i} \tag{3.31}$$

In order to select an appropriate reaction model which can suit the data, a plot of α versus a reduced time variable t/t_α, where t_α is the time that is required to reach a specified conversion (e.g., $\alpha = 0.9$).

For non-isothermal data obtained at a constant heating rate β. dT/dt, $d\alpha/dt$ in the Eq. (3.29) is replaced with $\beta\, d\alpha/dT$. Therefore Eq. 3.29 can be rewritten as follow:

$$\frac{d\alpha}{dT} = \frac{A}{\beta}\exp\left(\frac{-E}{RT}\right) f(\alpha) \tag{3.32}$$

Equation (3.32) is a first order separable differential equation, hence, integral method is used to solve the equation.

Integrating Eq. (3.32) with respect to variables α and T we get:

$$g(\alpha) = \int_0^\alpha \frac{d\alpha}{f(\alpha)} = \frac{A}{\beta}\int_0^{T_\alpha} \exp\left(-\frac{E}{RT}\right) dT \tag{3.33}$$

where T_α is the temperature at conversion α. If we define $x = E/RT$, Eq. (3.33) becomes

$$g(\alpha) = \frac{AE}{\beta R}\int_0^\alpha \frac{exp^{-x}}{x^2} = \frac{AE}{\beta R}P(x) \tag{3.34}$$

where $P(x)$ is called the temperature integral and it represents the rightmost integral in Eq. (3.34).

The Coats and Redfern (CR) integral equation [Coats and Redfern, 1964 and 1965] is a non-isothermal model-fitting method that requires an assumption regarding the reaction order for $g(\alpha)$ value. CR method approximates $P(x)$ in Eq. (3.34) by using a Taylor series expansion resulting in the following expression [White *et al.*, 2011]:

$$\ln\left(\frac{-\ln(1-\alpha)}{T^2}\right) = \ln\left[\frac{AR}{\beta E}\left(1-\frac{2RT'}{E}\right)\right] - \frac{E}{RT} \tag{3.35}$$

where T' is a mean value temperature [Coats, 1964]. Equation (3.35) can be simplified by knowing that for customary values of E, the term $2RT'/E << 1$, as depicted from experimental results:

$$ln\left(\frac{g(\alpha)}{T^2}\right) = ln(\frac{AR}{\beta E}) - \frac{E}{RT} \tag{3.36}$$

The slope ($-E/R$) of a straight line ($\ln[g(\alpha)/T^2]$ versus T^{-1}) graph allows the determination of the activation energy E and the pre-exponential factor A from its intercept $\ln(AR/\beta E)$. The CR method was chosen for its ability to determine A and E from a single heating rate plot. Its

drawback is the same arguments that have been presented against all of the model-fitting methods [White *et al.,* 2011]. The model fitting approach application to single heating-rate data generally fail to obtain a clean separation between the temperature dependence, and the reaction model, [Vyazovkin, 2000]. The application of this method to single heating rate data results in Arrhenius parameters that are highly uncertain and, therefore, they are not meaningfully as compared to the isothermal values [Chen *et al.,* 2006, Gonzalez-Perez *et al.,* 2004].

For this study Eq. (3.35) will be used without any assumption and the results for the pre-exponential values will be compared with Eq. (3.36) model.

The evaluation of the best fit kinetic parameters achieved was accomplished by the nonlinear regression which involves minimizing the difference between the experimental measured DTG and calculated DTG data on the reaction rate. The overall conversion rate is described Eq. (3.37):

$$-\frac{dm}{dt} = \sum_i c_i \frac{d\alpha_i}{dt} \qquad i=1,\ldots\ldots N \tag{3.37}$$

where the coefficient c_i is the involvement of each partial process to the whole weight loss which essentially represents the fraction of volatiles that are produced by the *i*th component and is given by Eq. (3.38):

$$c_i = m_{o,i} - m_{char,i} \tag{3.38}$$

The optimum kinetic parameters can be identified by means of the minimization of the objective function (QF_{DTG}), as shown in Equation (3.39) [Kastanaki and Vamvuka, 2006]:

$$QF_{DTG} = \sum_{i=1}^{N} \left[\left(\frac{dm}{dt}\right)_i^{exp} - \left(\frac{dm}{dt}\right)_i^{cal} \right]^2 \quad (3.39)$$

where $\left(\frac{dm}{dt}\right)_i^{exp}$ and $\left(\frac{dm}{dt}\right)_i^{cal}$ is the experimental and the calculated DTG curve, respectively.

The minimization of the objective function was used as follows:

$$DEV(\%) = \frac{\sqrt{QF_{DTG}/(Z-M)}}{\max\left[(dm/dt)_{cal}\right]} \times 100 \quad (3.40)$$

where M and Z represent the number of the parameters of the model (A_i, E_i, and c_i) and the number of the measured data points, respectively.

Unlike linear or polynomial regression, a nonlinear regression cannot be performed in one step. Instead the problem must be solved iteratively. The first guess, which is an initial estimate of the value of each parameter, must be provided, usually from linear regression. The procedure of the nonlinear regression, then adjusts the estimated values so that the fit of the curve to the data can be improved. The new values can then be adjusted so that the fit can be improved again. These iterations proceed until they are negligible, hence, improvement can occur. Nonlinear regression is a powerful tool that can be used to fit data to an equation in order to determine the values of

one or more parameters [Motulsky *et al.*, 1987]. The goal of this analysis is to minimize the squared residuals for the actual function (Eq. 3.39) and the estimated values of the parameters [Manyá *et al.*, 2003]. It also determines how well the model fits the data. As with linear regression, nonlinear regression method determines the values of the parameters (i.e., *E* and *A*) that minimize the sum of the squares of the distances of the data points on the TGA or DTG curve.

The combined kinetic analysis is one of the ways that can be used to perform linear model-fitting [Vyazovkin *et al.*, 2011 in Vyazovkin *et al.*, 1999 and Perez-Maqueda *et al.*, 2006]. This method can be used to determine the whole kinetic triplet (*E*, *A*, and $f(\alpha)$) by simultaneously plotting several kinetic curves that are measured under different arbitrary temperature programs. It is not limited to the list of kinetic models such as shown Table 3.2 to determine the reaction model, but from Eq. (3.41):

$$f(\alpha) = c\alpha^m(1-\alpha)^n \tag{3.41}$$

3.3.6.4. Model free approach

Generally the methods for estimating Arrhenius parameters based on a single heating rate parameter began in the 1960s. The "model free" methods are also known as isoconversional methods [White *et al.*, 2011 in Brown *et al.*, 2000]. Isoconversional methods can either be a differential or an integral to the treatment of the TGA data. The Kissinger and the Flyn-Wall-Ozawa model free methods have been used in this study.

I. Kissinger method

The Kissinger approach is a model free method, which allows obtaining the kinetic parameters (*E* and *A*) without the knowledge the reaction mechanism. A model-free non-isothermal method developed by Kissinger [1956] does not need to calculate *E* for each conversion (α) value in order to determine the kinetic parameters. A plot of ln (β/T_m^2) against $1000/T_m^2$ (Equation (3.42)) allows the determination of the value of the activation energy (*E*) for a series of experiments performed at different heating rates, β (ºC/min), where T_m represent the temperature of the maximum DTG curve peak. The equation is as follows:

$$\ln\left(\frac{\beta}{T_m{}^2}\right) = ln\left(\frac{AR}{E}\right) - \frac{E}{RTm} \qquad (3.42)$$

From the slope of the plot ($-E/R$), *E* can be calculated, and from the intercept of the plot, (ln (AR/E)) the pre-exponential factor (*A*) can be calculated. The drawback of this method is that it produces a single value of the activation energy for any of process regardless of its actual kinetic complexity. Therefore, the activation energy estimated can adequately represent only a single-step kinetics (Eq. (3.42)) [Galwey and Brow, 2002].

II. Flynn-Wall and Ozawa method

The Flynn-Wall-Ozawa method (FWO) [Ozawa, 1965, Liu *et al.*, 2002] is also a model free method that allows obtaining apparent activation energy (E_α) from a plot of ln (β_i), versus $1000/T_{\alpha i}$, from Equation (3.43) which represents the linear relation with a given value of conversion (α) at different heating rates.

$$\ln(\beta_i) = \ln\left(\frac{A_\alpha E_\alpha}{Rg(\alpha)}\right) - 5.331 - 1.052\frac{E_\alpha}{RT_{\alpha i}} \quad (3.43)$$

where $g(\alpha)$ is a constant at a given value of the α. The subscripts β_i and α_i denote the given value of the heating rate (β) and the given value of α, respectively. From the slope -1.052E_α/R, E can be calculated. The results between the two methods discussed will be compared. According to the model free method, the pre-exponential factor and the activation energy are not constant for the entire decomposition process, but they depend on conversion (α) [Šimon, 2004]. The results of the mathematical description of a process of the model free method are A and E that are dependent on the conversion which is related to the mechanism of reactions [Gašparovič *et al*, 2010].

CHAPTER 4

PROXIMATE, ULTIMATE AND THERMAL ANALYSIS

4.1. Introduction

This chapter presents the proximate, ultimate and thermal analysis results obtained from the thermogravimetric analyzer (TGA), as well as the elemental compositions from Carbon, Hydrogen, Nitrogen and Sulfur (CHNS) analyser. The importance of this analysis in relation to gasification is well explained and compared to the literature.

4.2. Proximate and Ultimate analysis

Table 4.1 presents the proximate and ultimate results of the biomass and biomass/sorbent mixtures. The pine-wood is higher in carbon content as compared to biomass/Sorbent blends since pine-wood is a carbonaceous material. The hydrogen content, however, remained fairly constant in both pure wood and the blends because sorbents do not contain carbon. This should not be confused with the impact of these blends on hydrogen production during gasification because the production of hydrogen is enhanced by chemical reactions. The nitrogen content is very small in all the samples; however the small quantity does not have a significant impact on gasification. The sulphur content was not detected in all the samples.

Table 4. 1: Proximate and ultimate analysis of biomass and biomass/sorbents blends.

Proximate analysis					**Ultimate analysis**			
Sample	**Moisture content**	**Fixed carbon**	**Volatile matter**	**Ash content**	**Carbon**	**Hydrogen**	**Nitrogen**	**Oxygen**[1]
Wood	8.6	23.8	67.72	0.40	47.51	6.52	0.09	45.87
5%CaO	6.2	9.5	65.5	18.8	42.9	6.2	0.04	51.76
5%MgO	6.1	8.04	64.08	21.8	42.2	5.93	0.05	51.77
10%CaO	5.6	11.45	58.05	24.9	43.78	5.89	0.07	50.26
10%MgO	5.3	14.42	59.08	21.2	43.19	6.19	0.08	50.54
15%CaO	5.9	21.55	62.6	9.95	42.92	5.92	0.05	51.11
15%MgO	6.1	18.7	63.90	11.3	40.45	5.67	0.04	53.84
20%CaO	5.6	22.48	56.42	15.7	38.33	5.99	0.06	55.62
20%MgO	5.9	21.3	58.37	13.9	39.16	5.47	0.06	55.12
25%CaO	4.8	29.88	54.72	10.6	39.37	5.26	0.08	55.29
25%MgO	4.9	21.4	56.4	17.3	38.41	6.02	0.05	55.52
10%CaO.MgO	6.0	29.86	59.28	4.86	43.24	6.28	0.08	50.40
15%CaO.MgO	6.0	32.24	47.10	4.66	43.19	6.23	0.04	50.54
20%CaO.MgO	5.9	18.72	61.5	13.88	41.48	5.99	0.04	52.49
25%CaO.MgO	5.0	26.32	50.42	18.26	45.37	6.50	0.07	48.07

[1]calculated by difference

The moisture content of the samples was between 4 and 9%, due to the fact that the samples underwent processing thereby losing some moisture. This moisture content is within the moisture levels for gasification in a downdraft gasifier. Therefore, the handling of the samples resulted in the lowering of the moisture within the acceptable ranges for gasification in downdraft gasifiers. Hence, the reaction kinetics as observed through TGA analysis would resemble what would happen during gasification. The volatile matter is higher in pine-wood (69%) than in the blends

(47-65.5%). In generally biomass is higher in volatile matter (70-80%) [Sami *et al.*, 2001] than the sorbents. Hence, a weight loss of this order may be expected after devolitilization is complete and all the volatile matter is released. Very low quantity of ash is observed for wood sample (0.4%), and is in agreement with the literature (0.1-5.0%) [Ragland and Aerts, 1991]. However, the biomass/sorbent blends have between 5 and 20% of the remaining carbonates. This is due to high volatility maters in biomass, which implies that the addition of oxides to biomass decreases the volatile content of the blends. The fixed carbon (FC) is high in 25%CaO, 10%CaO.MgO, 15%CaO.MgO and 25%CaO.MgO mixtures (26-32%) compared to wood (23.8%), because at higher temperatures the sorbents crack tar during gasification. This implies that these blends can produce more energy from the remaining carbon (FC).

4.3. Thermal analysis

Thermal behavior of biomass and sorbent blends was determined using thermogravimetric analyzer (TGA). The experiments were carried out in a nitrogen atmosphere with the flow rate maintained at 20 ml/min. The sample's mass was ranging between 5-12g. The Figure 4.1-4.9 shows the TGA (a) and DTG (b) curves of biomass and biomass/sorbent blends at the heating rate of 10, 15 and 20 ºC/min, respectively. The descending TGA thermal curve indicates that a weight loss has occurred. From all the curves the initial weight loss is due to water vaporization up to 120 ºC, followed by devolatilization, which is the major step in all thermo-chemical conversion processes involving biomass. This step is well represented by the second stage of decomposition at temperature between 200 to 580 ºC, where the remarkable slope of the TGA curves is observed. This stage corresponds to a significant drop in weight of samples due to

liberation of volatiles, such as CO_2, CO, H_2O, from slow pyrolysis thermal decomposition of hemicelluloses, cellulose and some part of lignin contained in the wood [Gašparovič *et al.*, 2010]. The Figure 4.1-4.3 represent the TGA (a) and the DTG (b) of 5%CaO, 5%MgO, 10%CaO, 10%MgO samples at 10, 15 and 20 ºC/min, respectively.

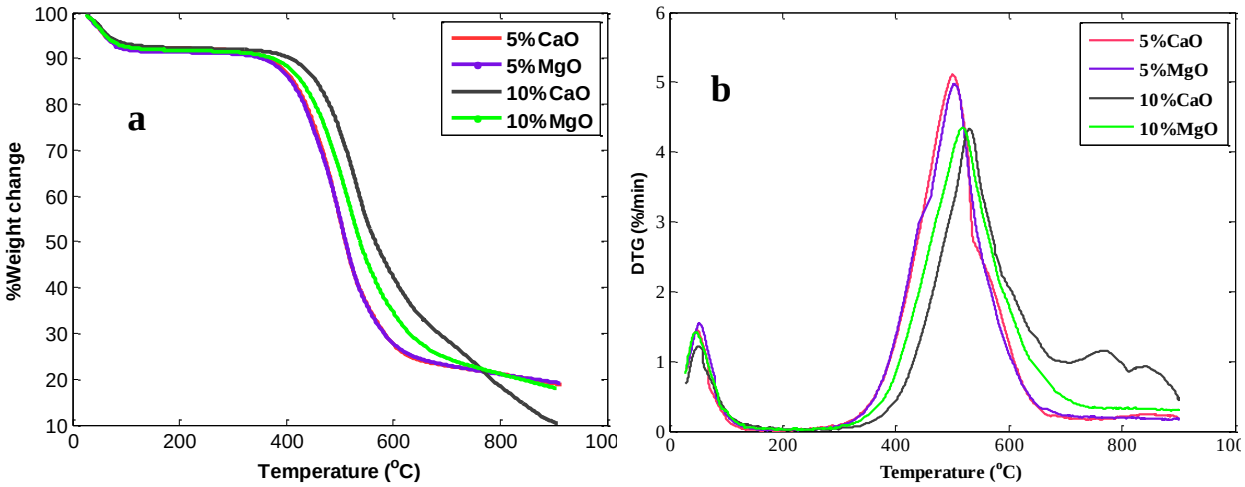

***Figure 4.1**:* TGA (a) and DTG (b) curves of biomass/sorbent blends (5%CaO, 5%MgO, 10%CaO, 10%MgO) at 10 ºC/min.

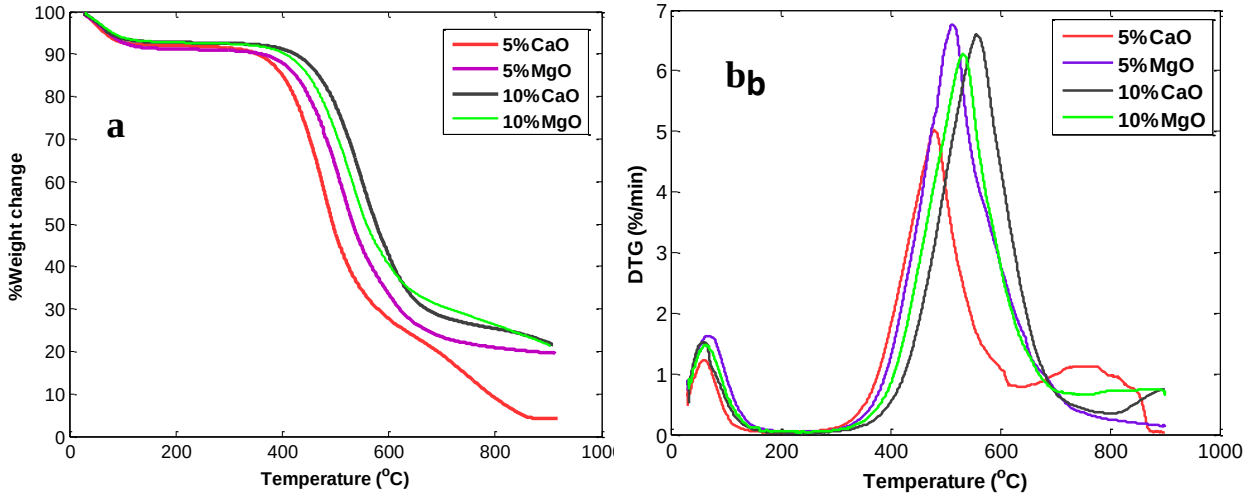

***Figure 4.2**:* TGA (a) and DTG (b) curves of biomass/sorbent blends (5%CaO, 5%MgO, 10%CaO, 10%MgO) at 15 ºC/min.

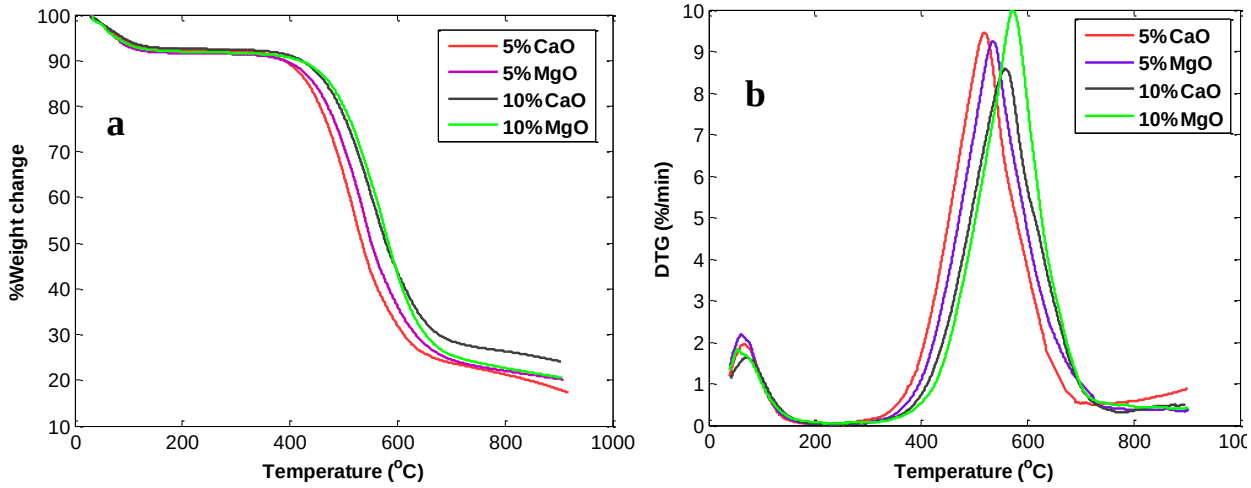

***Figure 4.3**:*TGA (a) and DTG (b) curves of biomass/sorbent blends (5%CaO, 5%MgO, 10%CaO, 10%MgO) at 20 ºC/min.

From both figures, the weight loss (6%) is due to water evaporation. As temperatures increase the second stage of weight loss was observed, which is due to the release of the volatile matters, i.e. devolatilization. This is where about 60% of the degradation of materials takes place at temperatures between 200 ºC and 700 ºC. The DTG curve of 10%CaO at 10 ºC/min shows two peaks after 700 ºC associated with carbonation of calcium carbonate ($CaCO_3$). It is known that the decomposition of calcium carbonates occurs between 650 and 750 ºC [Várhegyi *et al.*, 1996]. The peaks, especially calcium oxide, are mainly in the form of hydroxides and carbonates, which during heating in the TGA apparatus decompose releasing H_2O and CO_2. The percentage difference in the degradation rate is about 28% between the blend of wood with 10%CaO and 5%CaO mixture. However, in Figure 4.2 and 4.3, the same blend is 21% and 14% stable compared to the other mixtures, respectively. For this reason 10%CaO blend was compared with the more stable blends discussed in this section. This is done in order to determine the suitable blend for the syngas enhancement and gasification purposes.

The Figures 4.4-4.6 show the degradation curves of pine wood, 10%CaO.MgO, 15%CaO.MgO, 20%CaO, 20%MgO and 25%CaO.MgO samples at the heating rates discussed earlier.

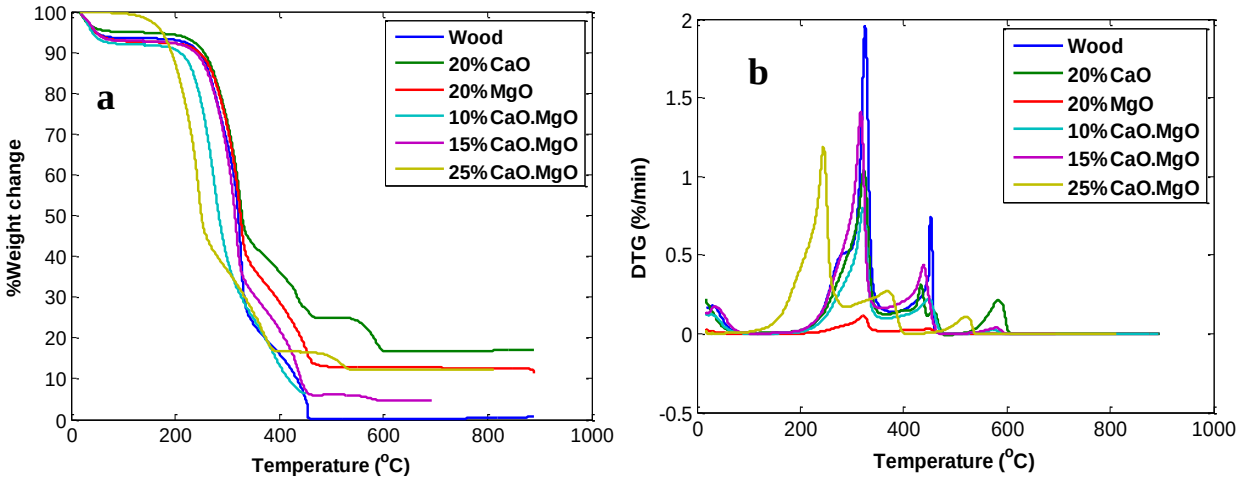

***Figure 4.4**:* TGA (a) and DTG (b) curves of biomass/sorbent blends (wood, 10%CaO.MgO, 15%Ca.MgO, 20%CaO, 20%MgO 25%CaO.MgO) at 10 ºC/min.

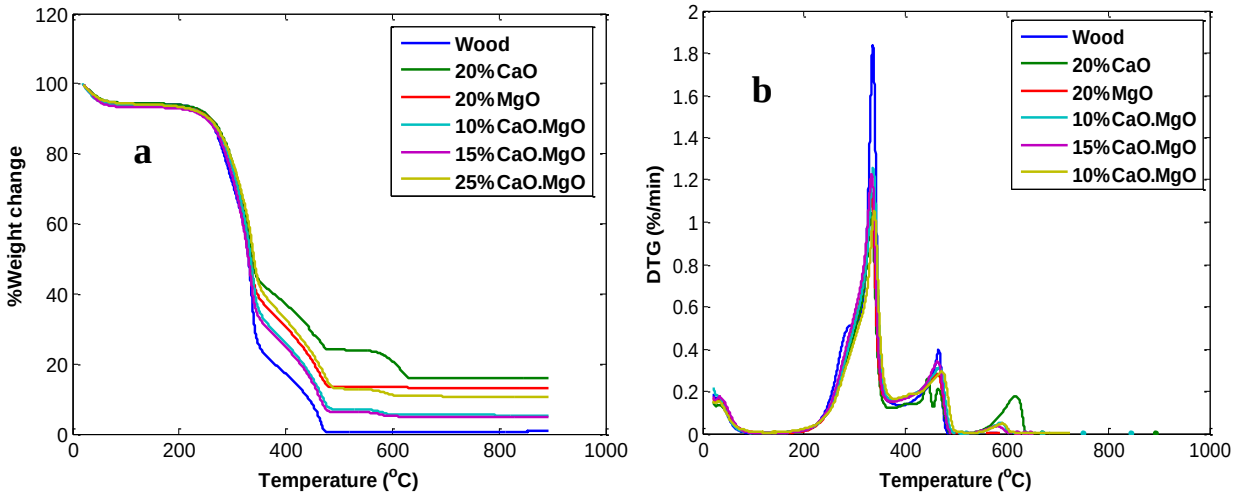

***Figure 4.5**:* TGA (a) and DTG (b) curve of biomass/sorbent blends (wood, 10%CaO.MgO, 15%CaO.MgO, 20%CaO, 20%MgO 25%CaO.MgO) at 15 ºC/min.

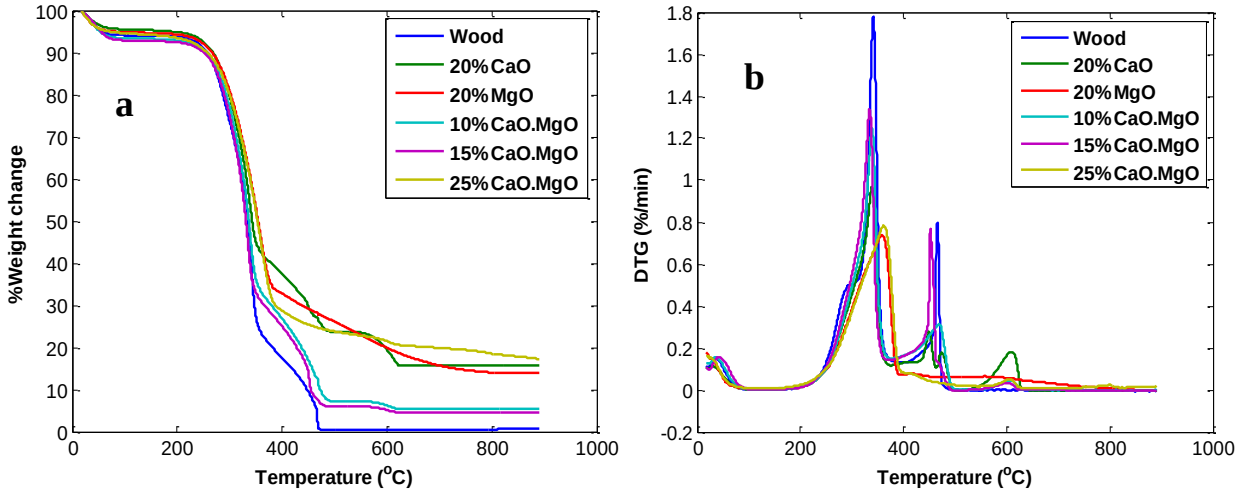

***Figure 4.6**:* TGA (a) and DTG (b) curves of biomass/sorbent blends (wood, 10%CaO.MgO, 15%CaO.MgO, 20%CaO, 20%MgO 25%CaO.MgO) at 20 ºC/min.

The devolatilisation of the wood occurred in a narrow temperature interval (200–470 ºC). The sample weight of wood seemed to be constant after the temperature reach 470 ºC. However, in Figures 4.5 and 4.6 the weights of samples with sorbents are constant after 600 ºC. The trend is due to the high volatile content in biomass as compared to biomass/sorbent blends. This is confirmed by the DTG peaks (b) at about 300 ºC, where the wood shows higher volatile matters compared to the blends. Therefore, addition of oxides to biomass decreases the volatile content of the blends and improves thermal stability. The composition of biomass changes when mixed with the sorbent powder. The properties of the material such as composition can influence the process of thermal decomposition [Gašparovič *et al.*, 2009].

The latter TGA curves (Figures 4.4 and 4.5) show that the blend of 20%CaO is the most thermally stable compared to other samples, except in Figure 4.6 where 25%CaO.MgO shows more stability than the latter. However, the percentage difference between the rates of

degradation for the two blends is not significant. Compared to the wood material, these samples are over 90% thermally stable after 600 ºC. For this reason these blends were compared with other thermally stable materials discussed in this thesis. The third stage of the weight loss between 580 ºC and 800 ºC in the case of CaO mixture can be attributed to the carbonation of $CaCO_3$, through which CaO can absorb the released CO_2 to form $CaCO_3$ product [Villain *et al.*, 2007]. For the MgO and CaO. MgO samples, the decomposition peaks appear at temperatures between 270 ºC and 400 ºC, which indicates an effect of MgO in the mixture as it promotes decarbonation and dehydration at lower temperatures [Alarcón *et al.*, 2004]. Figures 4.7-4.9 shows the TGA (a) and DTG (b) curves of 15%CaO, 15%MgO, 25%CaO, 25%MgO and 20%CaO.MgO samples.

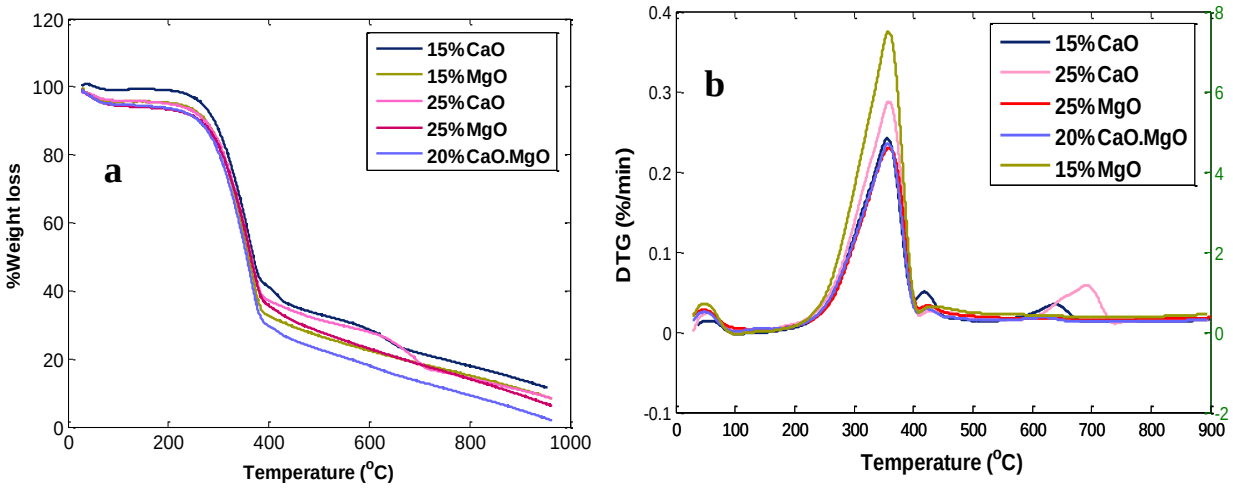

Figure 4.7: TGA (a) and DTG (b) curves of biomass/sorbent blends blends (15%CaO, 15%MgO, 25%CaO, 25%MgO and 20%CaO.MgO) at 10 ºC/min.

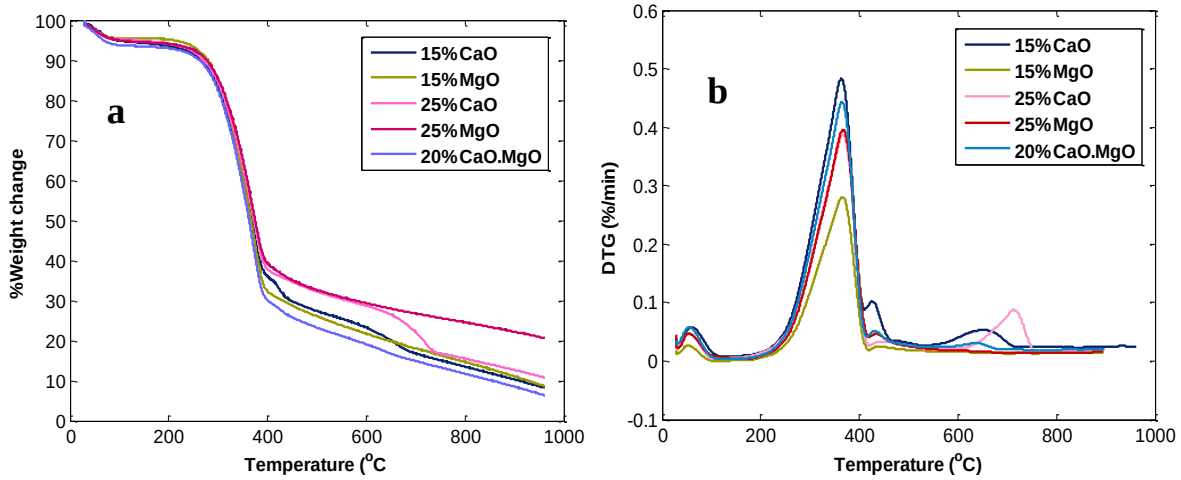

***Figure 4.8**:* TGA (a) and DTG (b) curves of biomass/sorbent blends blends (15%CaO, 15%MgO, 25%CaO, 25%MgO and 20%CaO.MgO) at 15 ºC/min.

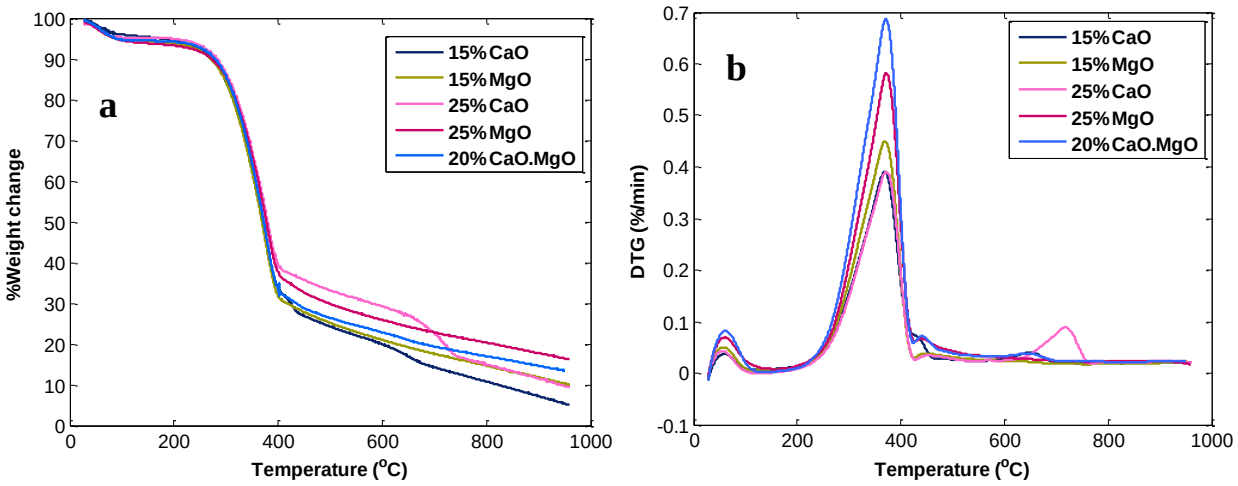

***Figure 4.9**:* TGA (a) and DTG(b) curves of biomass/sorbent blends (15%CaO, 15%MgO, 25%CaO, 25%MgO and 20%CaO.MgO) at 20 ºC/min.

From the TGA graphs it can be observed that 25%MgO sample is 5% stable compared to others, except in Figure 4.7 where the 15%CaO degrade slower than other blends. However, the percent difference between 15%CaO and 25%MgO blend is not significant. Because of this insignificant

difference 25%CaO mixture was compared to the most stable blend, which was 10%CaO, 25%CaO, 20%CaO and 25%CaO.MgO.

Figure 4.10 shows a comparison of the most thermally stable materials discussed in this section. The materials are, 10%CaO, 25%CaO, 20%CaO, 25%CaO.MgO blends and will be compared to wood sample at 20 ºC/min.

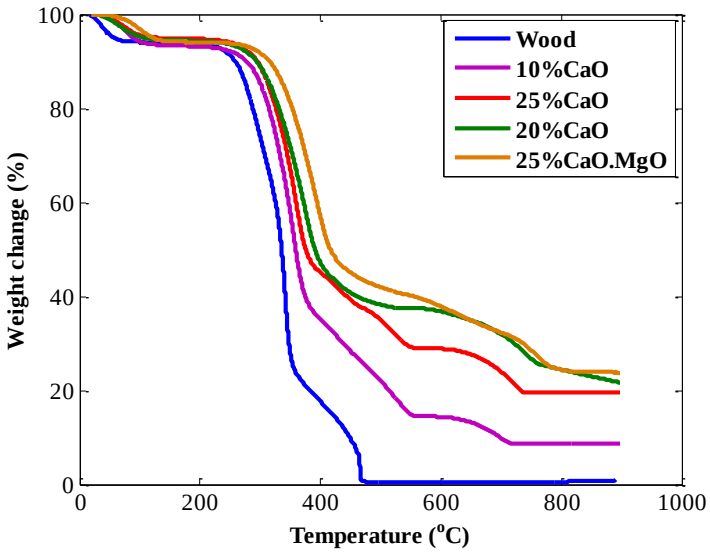

Figure 4. 10*:* TGA graph of wood, 10%CaO, 25%CaO, 20%CaO and 25%CaO.MgO blends at 20 ºC/min.

The main goal of this analysis is to determine the most thermally stable material between wood and wood blended with sorbents and to establish the material thermal behavior under temperatures in which gasification takes place using TGA method. It can be clearly seen that pine-wood degrades rapidly at a lower temperature than the blends. The drop in weight of the wood sample is due to the release of volatile from rapid thermal decomposition of

hemicelluloses (200-360 ºC), cellulose (360-480 ºC) and some part of lignin, which takes place in both regions [Gašparovič *et al,* 2010]. However the weight of this sample is constant after 480 ºC which signifies that the process was already done and what's left is ash. The devolatilization of the blend takes place between 200-700 ºC. The small decomposition peak appears at temperatures between 550-700 ºC can be attributed to the carbonation of $CaCO_3$, through which CaO can absorb the released CO_2 to form $CaCO_3$ product for 10% CaO, 25%CaO and 20%CaO samples, respectively [Biagini *et al.,* 2006]. It can also be observed from the plot that 25%CaO.MgO blend is the most thermally stable compared to others, thereby releasing energy over an extended period. Its rate of thermal degradation is 90% difference than of pure wood. This is due to the addition of CaO in the wood material. Hence, CaO plays the role as a CO_2 sorbent and as a catalyst for biomass gasification [Hanaoka, *et al.,* 2005a, Madhukar *et al.,* 2007].

4.4. Effect of the heating rate

The heating rate is known to affect both the location of the TGA curve and the maximum DTG peaks [Slopiecka *et al.,* 2011]. For each sample three runs were performed at different heating rates. Figures 4.11 and 4.12 shows the TGA (a) and DTG (b) curves of wood and wood with 10% CaO, 25%CaO, 20%CaO and 25% CaO.MgO blends at three different heating rates of 10 ºC/min, 15 ºC/min and 20 ºC/min, respectively. The TGA and DTG for the other samples are presented in the Appendix A.

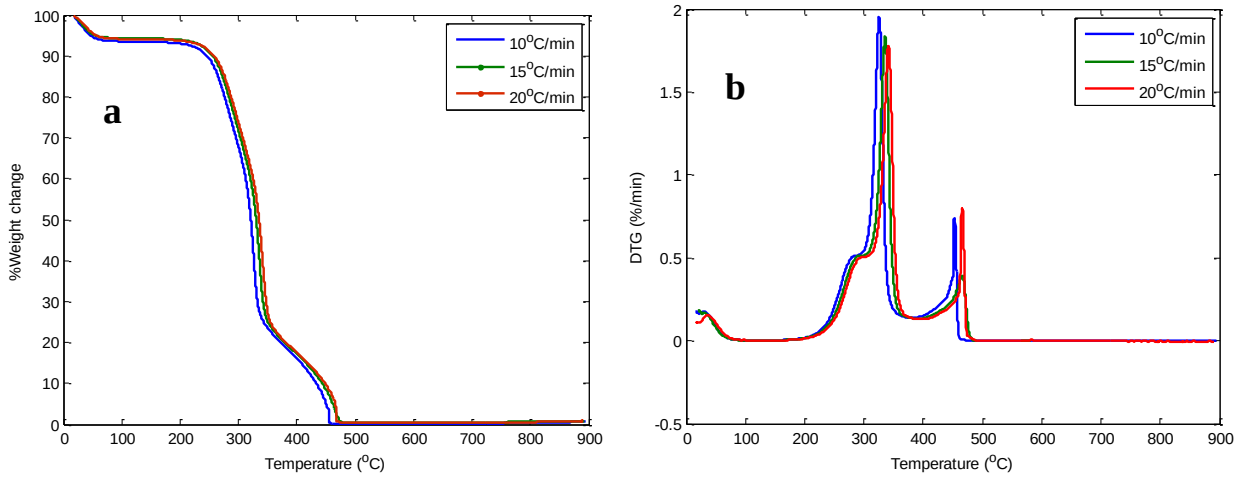

Figure 4.11: TGA (a) and DTG (b) curves of wood at various heating rates of 10, 15 and 20 ºC/min.

The DTG is used to determine the temperature of maximum mass loss rate, the initial decomposition temperature and the final decomposition temperature. It can be observed in Figure 4.11 (a) that there is a shift of 2.9 % and 5.7% difference in the weight loss curves between heating rates of 10 and 15 ºC/min and of 10 and 20 ºC/min, respectively. The sample degrades more quickly at low heating rates. Thus, at a higher heating rate, individual weight loss is reached at higher temperatures. It can also be observed from Figure 4.11 (b) that the height of the DTG peaks decreases with an increase in the heating rate. As discussed earlier, the first peak is due to the evaporation of moisture of the samples just above 100 ºC. The second peak between the temperature of 220-300 ºC is for the hemicellullose peak. The last two clear peaks between 300-390 ºC and 400-500 ºC are cellulose peaks. It is known that lignin is in between both peaks [Gašparovič *et al.*, 2010]. As illustrated by the DTG curves, devolatilization is completed in approximately the same temperature range (200 ºC to 800 ºC) for all heating rates.

Figure 4.12 (a) and (b) shows the TGA and DTG curves of wood with 10%CaO blend at various heating rates of 10, 15 and 20 ºC/min, respectively.

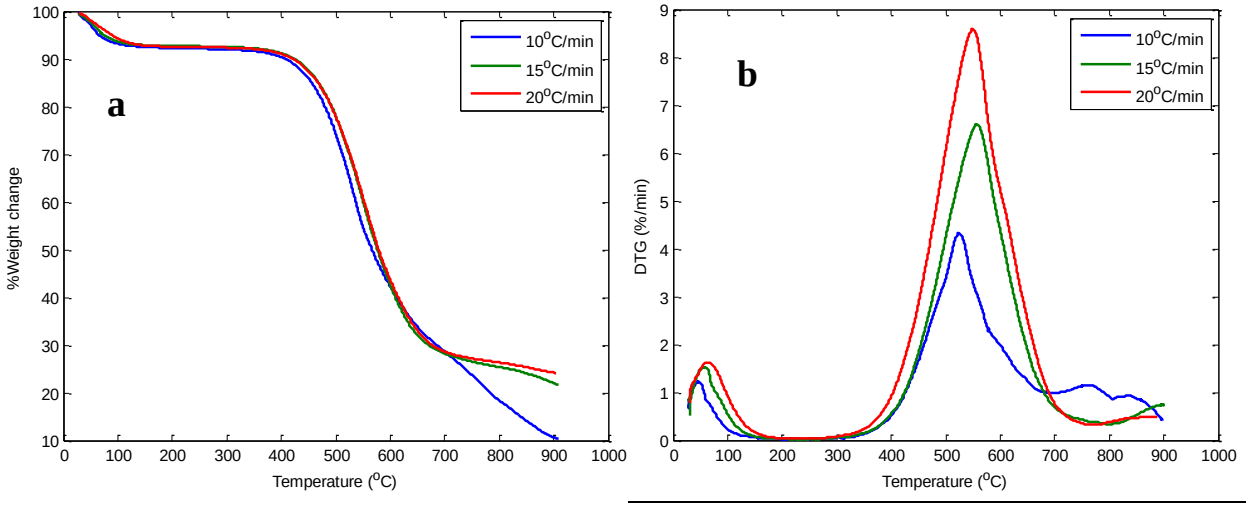

Figure 4.12: TGA (a) and DTG (b) of 10%CaO blend at various heating rates of 10, 15 and 20 ºC/min, respectively.

It can be observed from Figure 4.12 (a) that the TGA curve quickly drops in the rate of 10 ºC/min between 700-900 ºC due to the lower reaction rate associated with the lower heating rate. Thus, quick weight loss is observed at a higher heating rate. The reaction rate increases with the increase in heating rate, resulting in a shift on the 15 ºC/min and 20 ºC/min curves respectively. From the DTG (b) curve, it was observed that the maximum peak is reached at the highest heating rate and the smallest peak at the lowest heating rate. The DTG (b) of the 15 ºC/min heating rate curve shows two degradation peaks between 700-900 ºC. These peaks are associated with the carbonation of calcium carbonate ($CaCO_3$). The DTG peaks increases with an increase in the heating rate except at 700 900 ºC where the higher peak corresponds to the lower heating rate (10 ºC/min). This is associated with heat and mass transfer limitation. For the measurements

at a lower heating rate a larger instantaneous thermal energy is provided in the system which requires a longer time for the purge gas to reach equilibrium with the temperature of the furnace [Gašparovič *et al.,* 2010]. Whereas the higher heating rate has a short reaction time and require low temperature for the sample to decompose [Quan *et al.*, 2009].

4.5. Statistical analysis

Furthermore, the rate of degradation of the samples was compared using one way analysis of variance (ANOVA). This test compares the means of two or more groups. The temperature range of 200 ºC – 800 ºC was considered since it covers the wide range of the devolatilization process. The change in the weight loss of the sample in this range can be clearly observed as discussed earlier. For simplicity the analysis was conducted for the heating rate of 20 ºC/min. This test will be of assistance with the selection of the material that exhibits the best performances in terms of degradation rate compared to the others. The results discussed earlier shows that some samples degrade slower and have higher thermal stability compared to others. Therefore, this test will determine how significant the difference of degradation rate between samples is. Figure 4.13 shows the mean values of weight loss between 200 ºC – 800 ºC of wood with 5%CaO, 5%MgO, 10%CaO and 10%MgO blends.

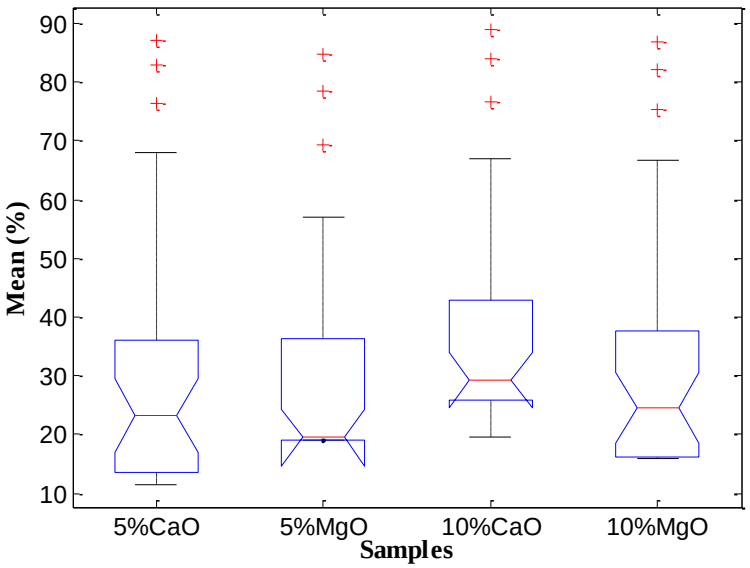

Figure 4.13: The mean value of wood with 5%CaO, 5%MgO, 10%CaO, 10%MgO blends.

The size of the F-statistic and the *p*-value are represented by the box plot. The large differences in center lines of the boxes correspond to the larger values of F and correspondingly smaller values of *p*. The larger the value of F, the more likely it is that the null hypothesis, of no differences among the group means is false [Anderso, 2001]. The *p*-value is used to test this null hypothesis [Scheffé, 1999]. The red crosses show the uncertainties of the results. One of the assumptions of the ANOVA test is that it normalizes the data, which implies that any unnecessary data is eliminated. From Figure 4.13, it can be observed that wood with 10%CaO blend has higher mean value (37%) compared to other samples. The 13% difference can be observed between wood with 10%CaO and 5%MgO samples, which has the least mean value of 30%. As discussed in section 4.3, the wood with 10%CaO blend was found to have higher thermal stability which is consistent with the ANOVA test. The ANOVA test results for these samples are presented in the Table 4.2.

Table 4. 2: ANOVA table for wood with 5%CaO, 5%MgO, 10%CaO, 10%MgO blends

Source	**SS**	**Df**	**MS**	**F**	**Prob>f**
Group	981.8	3	327.274	0.81	0.4925
Error	48679.2	120	405.66		
Total	49661.1	123			

Although a one way ANOVA test does not show which samples has the significant mean difference from the other, the results in Table 4.2 of wood with 5%CaO, 5%MgO, 10%CaO and 10%MgO blends do not differ significantly since $p>0.05$, for $F(3, 120) = 0.81$ $p = 0.4925$. A smaller value of p indicates that differences between the means are highly significant [Scheffé, 1999]. A multiple comparison test was conducted to determine the significant mean difference between the samples with higher mean values.

The mean value of wood and wood with 20%CaO, 20%MgO, 10%CaO.MgO, 25%CaO. MgO blends are shown in figure 4.14 and the ANOVA results are in Table 4.3.

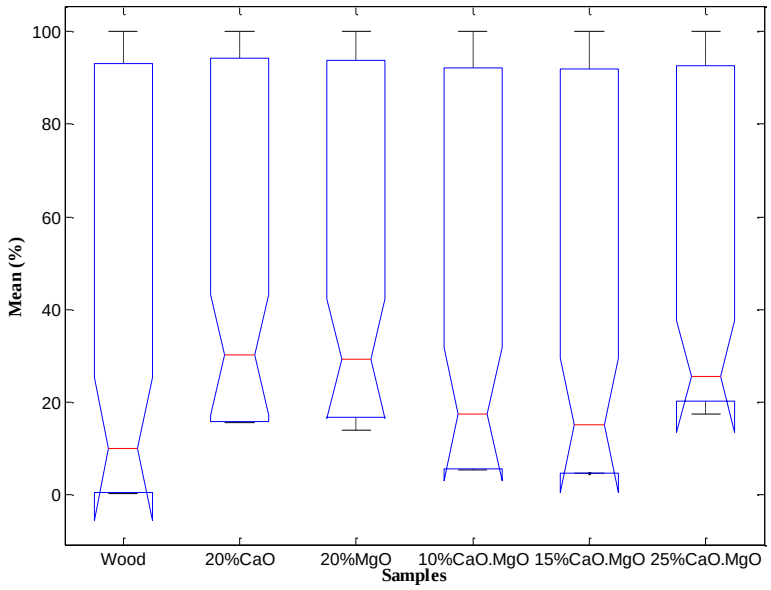

Figure 4.14: The mean value of pure wood, wood with 20%CaO, 20%MgO, 10%CaO.MgO, 25%CaO. MgO blends.

Table 4. 3: ANOVA table for wood and wood with 20%CaO, 20%MgO, 10%CaO.MgO, 25%CaO. MgO blends

Source	**SS**	**df**	**MS**	**F**	**Prob>f**
Group	13743	5	2748.6	1.94	0.0865
Error	749071.6	528	1418.7		
Total	762814.6	533			

The sample of wood with 20%CaO blend shows a high mean value compared to other (51.29%). Again, this table does not show any significant mean difference of the degradation rate between these samples since p = 0. 0865. The significant mean difference of 20%CaO sample was compared with the samples with high mean values. Figure 4.15 shows the mean value of wood with 15%CaO, 15%MgO, 25%CaO, 25%MgO, 20%CaO.MgO blends.

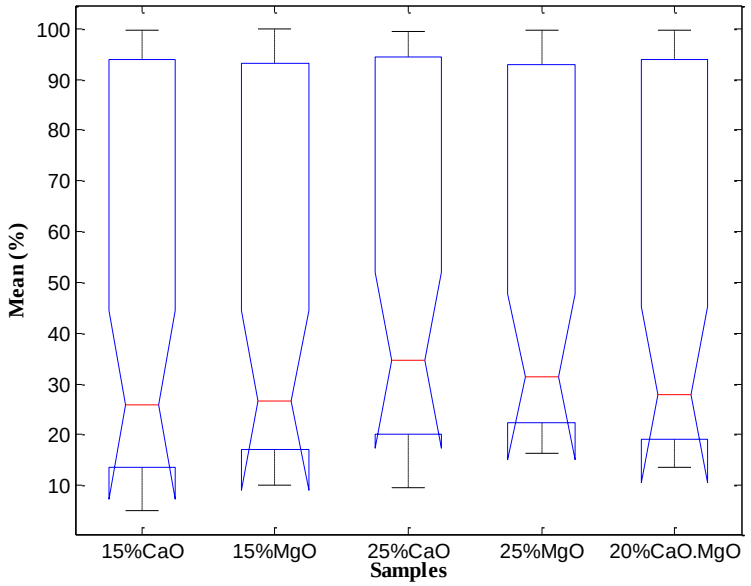

Figure 4.15: The mean value of wood with 15%CaO, 15%MgO, 25%CaO, 25%MgO, 20%CaO.MgO blends

The test was performed at the same temperature range as discussed earlier. The ANOVA results for these samples are presented in Table 4.4. The sample of wood with 20%CaO.MgO blend shows a high mean value (49%) compared to others.

Table 4. 4: ANOVA table for wood with 15%CaO, 15%MgO, 25%CaO, 25%MgO, 20%CaO. MgO blends

Source	**SS**	**df**	**MS**	**F**	**Prob>f**
Group	721	4	180.24	0.14	0.9654
Error	281394.2	226	1250.64		
Total	282115.1	229			

The significance mean difference of the samples (10%CaO, 20%CaO, 25%CaO, and 25%CaO.MgO) which has resulted in higher thermal stability are also compared with pure wood in Figure 4.16.

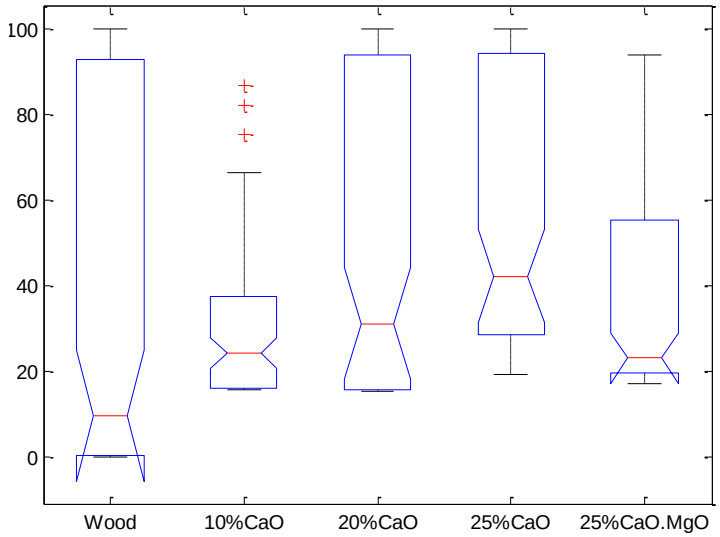

Figure 4. 16: The mean value of wood and wood with 10%CaO, 20%CaO, 25%CaO, and 25%CaO. MgO blends

The test was performed at the same temperature range as discussed earlier. The sample of wood with 25%CaO.MgO blend shows a high mean value compared to other (48.79%). The ANOVA results for these samples are presented in Table 4.5.

Table 4.5: ANOVA table for wood, wood with 10%CaO, 20%CaO, 25%CaO, and 25%CaO. MgO blends

Source	**SS**	**df**	**MS**	**F**	**Prob>f**
Group	20633.8	4	5158.46	4.37	0.0019
Error	382465.1	324	1180.45		
Total	403098.9	328			

From the ANOVA Table (4.5), we can conclude that there is a significant difference between the mean of these samples since *p* is near zero. Although one way ANOVA test shows the significant mean difference between the groups, it does not show which sample has a significant mean difference from the others. Therefore, a multiple comparison test can be conducted to evaluate the significant mean differences. Figure 4.17 shows a multiple comparison test between the samples with higher mean values.

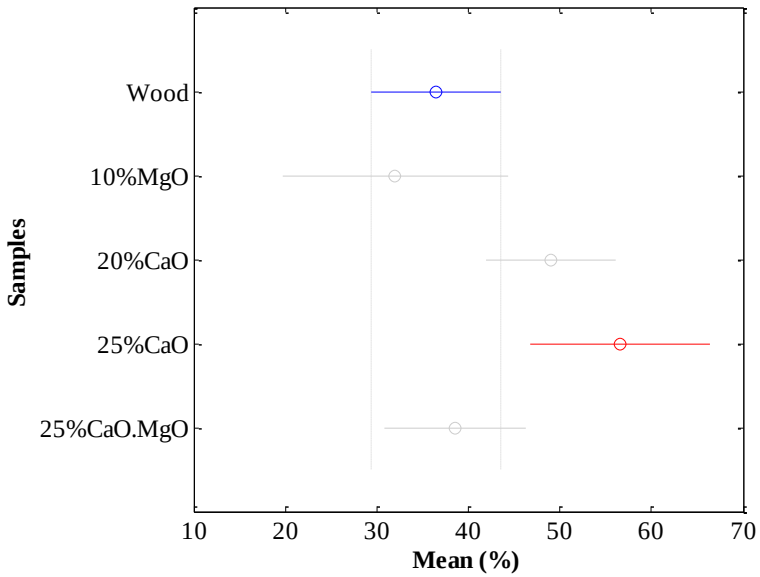

Figure 4.17: The mean value of wood and wood with 10%CaO, 20%CaO, 25%CaO, and 25%CaO. MgO blends.

This test is able to establish which sample has a significant difference in the mean between the groups. The red plot indicates that the mean difference between the samples is significant from the other. By clicking one of the grey plots you can be able to see which group has a mean significant difference from the other. A significant difference in the mean can be observed between wood, 10%CaO, 25%CaO.MgO with 25%CaO sample for F (4, 324) = 4.37 p = 0.0019.

No significant mean difference was observed between 20%CaO and 25%CaO blends and between 20%CaO with other samples. Since there was an insignificant difference between these samples kinetics will be performed for wood, 10%CaO, 25%CaO.MgO, 20%CaO samples.

It can be clearly seen from this table that the sample with a higher mean value is 25%MgO (51.29%) which is not very different from 25%CaO (51.17%). The results discussed earlier shows significant mean difference between 25%CaO with wood, 10%CaO and 25%CaO.MgO sample. Therefore, we can conclude that the mean of 25%MgO can as well differ significantly with these samples and the samples with very low mean values. Figure 4.18 shows the mean values of all the samples from the higher to the lower mean value.

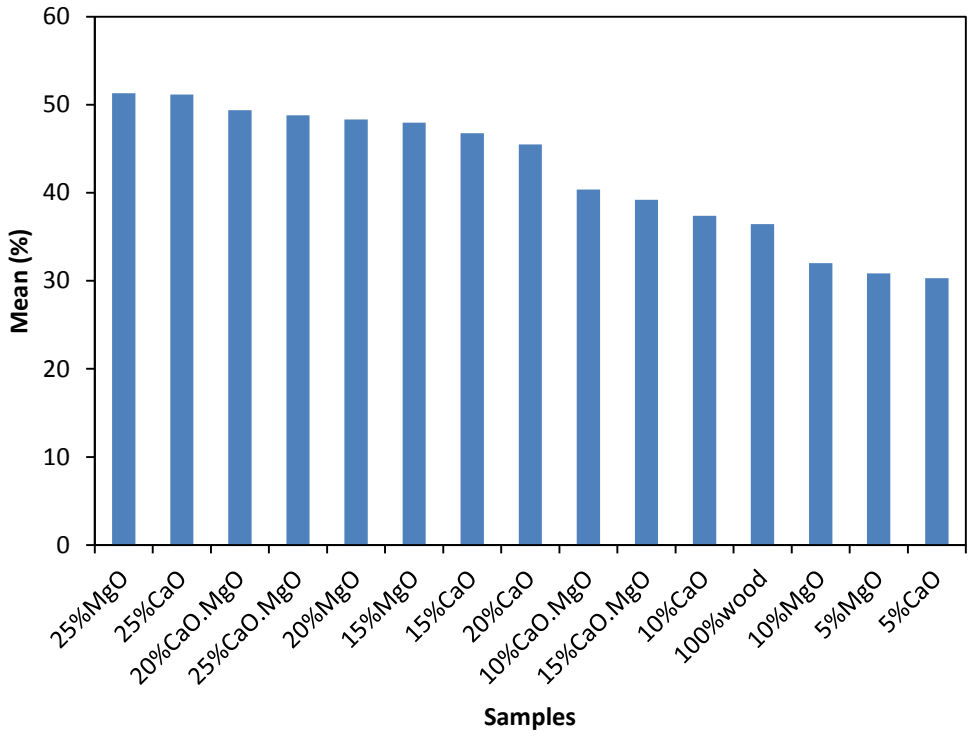

Figure 4. 18: The mean value of all the samples

The percentage difference between the sample with a higher and lower mean value is 40%, which is significant.

CHAPTER 5

KINETICS OF THE DEVOLATILIZATION PROCESS

5.1. Introduction

The devolatilization is the basic step of thermochemical processes and requires a fundamental characterization. The knowledge of the solid devolatilization kinetics may help with the better understanding and planning of important industrial processes because pyrolysis is part of the gasification and combustion processes not only an independent conversion technology [Grønli *et al.,* 2002]. Kinetics in this process were obtained by applying both model free (isoconversional) and regression model fitting methods and their results are discussed in details in this chapter. The data from the thermogravimetric analyzer (TGA) were used to investigate the reaction kinetics of the materials discussed in chapter 3. The temperature-conversion data are elaborated according to the specific method needs for the kinetic analysis. The kinetic parameters such as activation energy (E), pre-exponential factor (A) and the reaction order (n) were investigated. The activation energy is a property of a specific reaction and should not depend on the operating conditions. However, the global value of the activation energy obtained in the case of biomass fuel devolatilization is a complex sum of several reactions, which explains that it usually depends on operating conditions…

5.2. Model-free kinetic analysis

The kinetic parameters such as activation energy (E) and pre-exponential factor (A) mainly in the stage of pyrolysis of the materials were obtained from model free non-isothermal TGA data.

These require a set of experimental tests at different heating rates. The heating rates considered here were 10 ºC/min, 15 ºC/min and 20 ºC/min as indicated earlier. The model-free methods considered are Kissinger and Flyn-Wall-Ozawa (FWO). Figure 5.1 shows the Kissinger plot of $\ln(\beta / T_m^2)$ versus $1000/T_m$ (K^{-1}) of the decomposition process for wood and wood with 10% CaO, 20% CaO and 25% CaO.MgO mixtures.

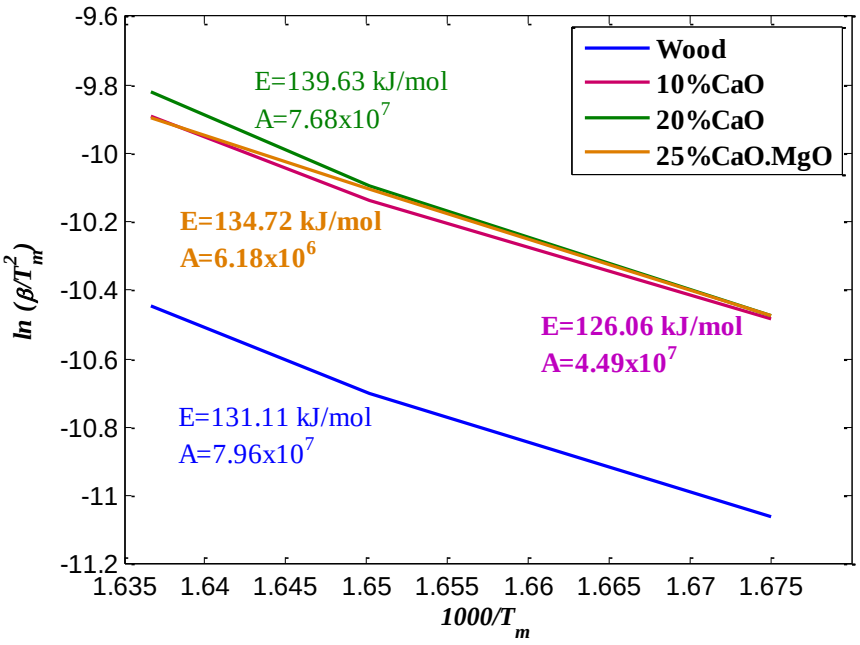

Figure 5.1: Plots of $\ln(\beta/T_m^2)$ versus $1000/T$ of wood sample (blue) and wood with 10% CaO (red) 20% CaO (green) and 25% CaO.MgO (orange) blends for the heating rates of 10 ºC/min, 15 ºC/min and 20 ºC/min.

A linear fit to the data enabled the determination of E and A as per Eq. (3.42). The activation energy (E) and the pre-exponential factor (A) of the samples were calculated from Eq. (3.42) where T_m is a temperature that corresponds to the maximum weight loss peaks calculated from DTG curve. The peak temperatures were corresponding to 10 ºC/min, 15 ºC/min and 20 ºC/min

heating rates, respectively. Table 5.1 presents the results for activation energy and pre-exponential factor obtained from this method.

Table 5.1: Kinetic parameters (*E* and *A*) obtained by Kissinger method.

	***E* (kJ/mol)**	**ΔE (%)**	***A* (min^{-1})**
Wood	131.54	–	7.96×10^{7}
10%CaO	126.06	–	4.49×10^{7}
20%CaO	139.63	6.15	7.68×10^{8}
25%CaO.MgO	134.72	2.36	6.18×10^{6}

The calculated squares of the correlation coefficient (R^2), were in the range between 99.3% to 99.5% for all the samples. The results obtained from this method present the actual values of kinetic parameters. These values are the same for the whole pyrolysis process [Slopiecka *et al.*, 2011]. However, the blend of wood with 20%CaO needs higher activation energy to start reacting compared to others. Hence, the reaction mechanism is not the same (6.10% difference) for the decomposition process. Gašparovič *et al.* [2010] reported that the heating rate, the type of biomass tested and the atmosphere in which thermal degradation takes place have significant effects on the thermal degradation rates and, therefore, on the activation energies. The physical significance of parameters *E* and *A* can be interpreted using molecular collision theory [White *et al.*, 2011]. According to the collision theory of chemical reactions, molecules collide before they can react and to effectively initiate a reaction the collision must be sufficiently energetic (kinetic energy) to bring about bond disruption. These energetic collisions between reactant molecules cause interatomic bonds to stretch and bend, temporarily weakening them so as to make them

susceptible to cleavage. The pre-exponential factor (A) represents the frequency of collision between reactant molecules which depend on the concentration of each reactant. Therefore, the value obtained for A represents the frequency of collision between reactant molecules during gasification. However, most molecular collisions do not necessarily result in a chemical change. Before any change can take place on collision, as mentioned earlier, the colliding molecules must have a minimum kinetic energy called the activation energy. Therefore, the value of E obtained for this study represents the minimum amount of energy required to ignite particles in the gasifier so as to bring about bond disruptions and cleavages through a chemical reaction which depends on the value of the pre-exponential factor as the thermal energy of activation is proportional to the frequency of collision between the reactant molecules in the gasifier.

Figure 5.2-5.5 shows the model free FWO plots of $\ln(\beta_i)$ versus $1000/T_{\alpha i}$ (K^{-1}) of the decomposition process for wood and wood with 10% CaO, 20% CaO and 25% CaO.MgO mixture, respectively.

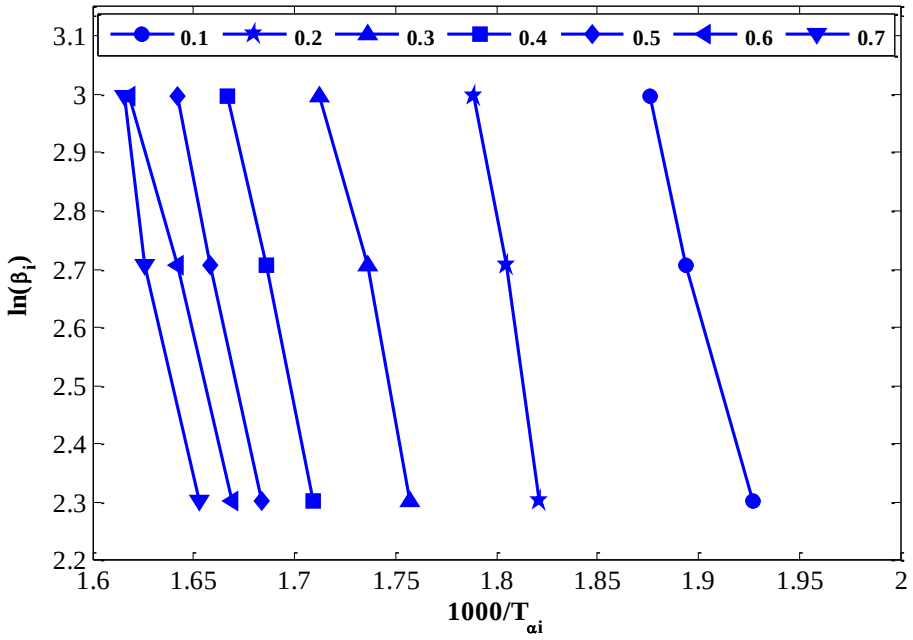

Figure 5.2: Plots of ln(β_i) versus 1000/$T_{\alpha i}$ of wood sample for the heating rates of 10 ºC/min, 15 ºC/min and 20 ºC/min and the α values ranges between 0.1-0.7.

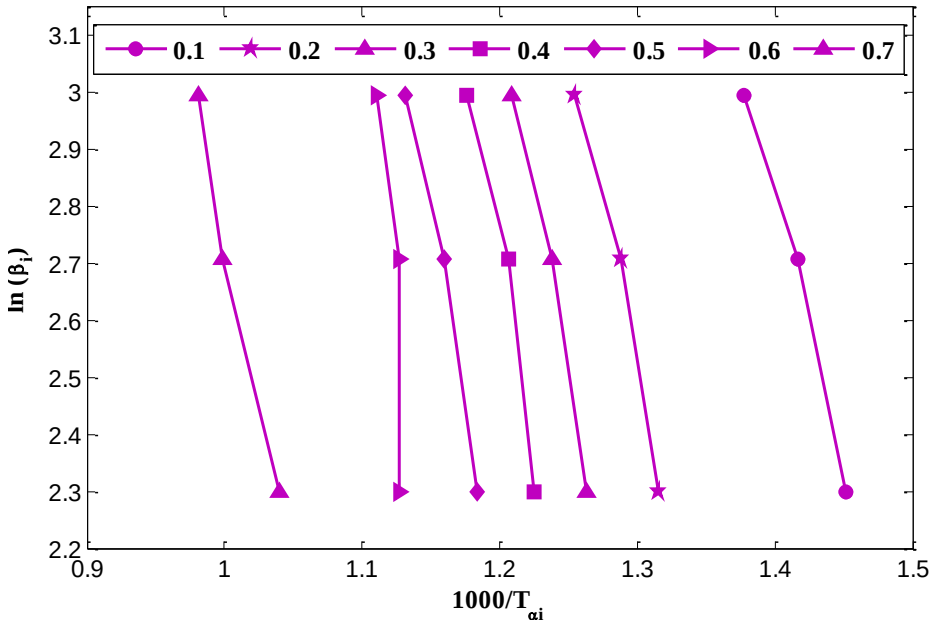

Figure 5.3: Plots of ln(β_i) versus 1000/$T_{\alpha i}$ of 10% CaO blend for the heating rates of 10 ºC/min, 15 ºC/min and 20 ºC/min and α values ranges between 0.1-0.7.

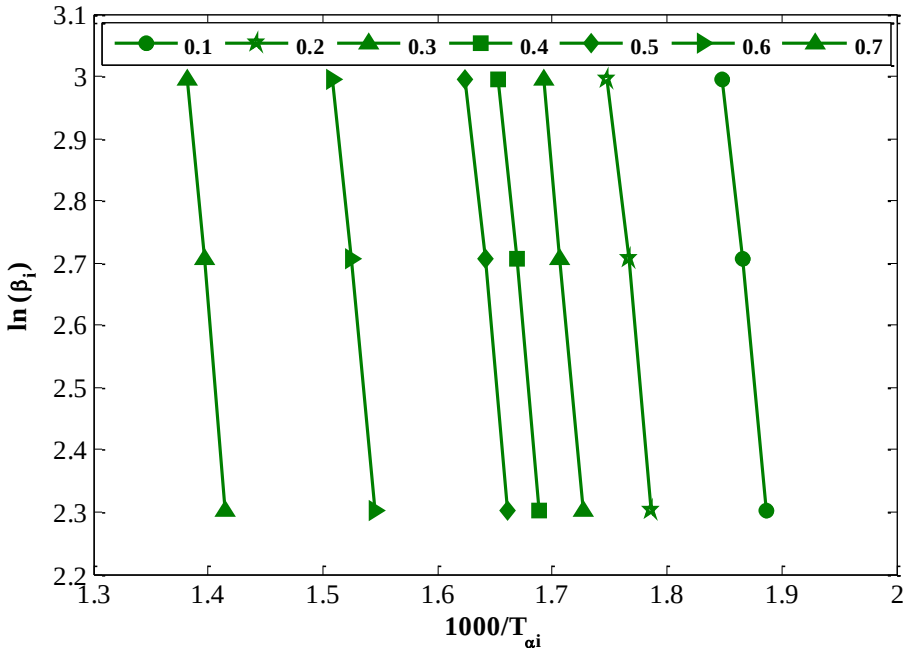

Figure 5.4: Plots of ln(β_i) versus 1000/$T_{\alpha i}$ of 20% CaO blend for the heating rates of 10 ºC/min, 15 ºC/min and 20 ºC/min and α values ranges between 0.1-0.7.

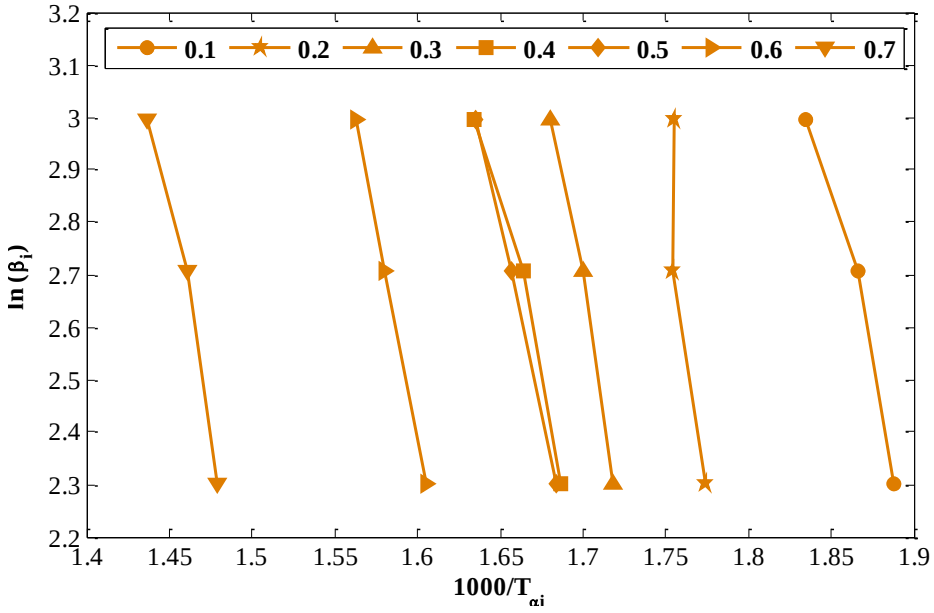

Figure 5.5: Plots of ln(β_i) versus 1000/$T_{\alpha i}$ of 25% CaO.MgO blend for the heating rates of 10 ºC/min, 15 ºC/min and 20 ºC/min and α values ranges between 0.1-0.7.

The conversion (α) was calculated from Eq. (3.28). The activation energy (E_α) and pre-exponential factor (A_α) were determined from the linear fit corresponding to each value of α using Eq. (3.43) where $T_{\alpha i}$ is a temperature which corresponds to a given value of heating rate (β_i) and a given value of conversion (α) and the g (α) is constant at given value of the conversion. The activation energy was calculated from the slope -1.052 E_α/R. It is advisable to limit the selection of the α in the range such as 0.10–0.90 or 0.05–0.95, since the experimental errors in the kinetic data are larger at lowest and highest α values [Vyazovkin *et al.*, 2011]. To determine the kinetic parameters from this method, the values of α were chosen from the range 0.1 to 0.7 for all curves at different heating rate. This assists in getting the temperature which corresponds to each of the conversion. The results of activation energy and pre-exponential factor obtained from this method are presented in Table 5.2.

Table 5.2: Kinetic parameters (E_α and A_α) obtained by FWO method.

FWO Method								
	Wood		**10%CaO**		**20%CaO**		**25%CaO.MgO**	
A	E_α **(kJ/mol)**	A_α **(min^{-1})**	E_α **(kJ/mol)**	A_α **(min^{-1})**	E_α **(kJ/mol)**	A_α **(min^{-1})**	E_α **(kJ/mol)**	A_α **(min^{-1})**
0.1	114.84	3.00×10^{10}	89.55	8.91×10^{05}	128.27	1.09×10^{14}	117.53	4.71×10^{11}
0.2	124.56	5.79×10^{11}	101.88	2.30×10^{05}	137.99	4.03×10^{13}	122.82	5.7×10^{12}
0.3	125.59	3.84×10^{08}	115.08	1.19×10^{06}	144.32	1.21×10^{14}	128.51	1.33×10^{12}
0.4	128.51	5.41×10^{11}	124.48	3.46×10^{06}	144.87	2.04×10^{13}	134.68	6.32×10^{08}
0.5	131.75	7.54×10^{12}	131.36	5.52×10^{06}	147.48	3.4×10^{12}	144.08	4.26×10^{09}
0.6	138.39	8.52×10^{11}	146.14	8.49×100^{07}	150.32	5.9×10^{11}	147.72	1.45×10^{10}
0.7	141.16	1.32×10^{11}	162.10	3.16×10^{08}	152.93	1.38×10^{12}	156.81	5.12×10^{09}
[1]Avrg	129.26	1.38×10^{12}	124.37	1.29×10^{07}	143.74	4.91×10^{13}	136.10	1.08×10^{12}

[1]Averaged E_α

It is also advantageous to use the model free method because there is no need to assume or choose a reaction model. This table represents the apparent values of kinetic parameters. These are the sum of parameters of physical processes and chemical reactions that occur simultaneously during pyrolysis [Slopiecka *et al.*, 2011]. The value of the activation energy obtained from the Kissinger method is within the range of activation energy obtained from FWO method. This implies that both the methods are reliable for the determination of kinetic parameters. The averaged activation energies were found to be 129 kJ/mol, 124 kJ/mol, 143 kJ/mol and 136 kJ/mol for wood, wood with 10%CaO, 20%CaO and 25%CaO.MgO blends, respectively. It can also be observed from the table that the activation energy for both samples increased with an increase in the conversion (α). This implies, as expected, that the mechanism is not the same in the whole decomposition process. Figure 5.6 shows the plot of activation energy (E_α) versus the conversion (α) obtained from the FWO method.

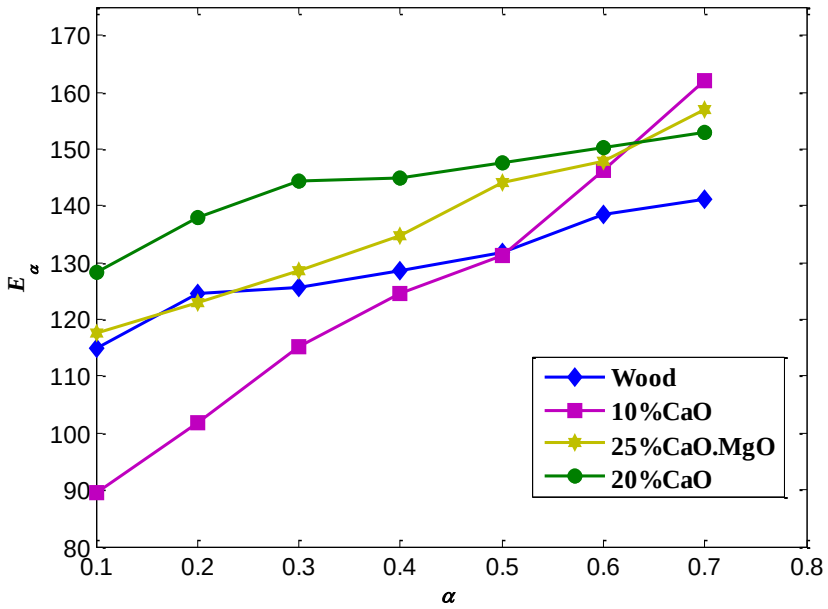

Figure 5.6: Plots of activation energy (E_α) versus the conversion (α) of wood sample (blue) and wood with 10% CaO (red), 20% CaO (green) and 25% CaO.MgO (orange) blends.

This activation energy varies for all samples. This is due to the complexity in multistep mechanism that occurs in solid state [Slopiecka *et al.,* 2011].

5.3. Model fitting kinetic analysis

The results obtained from TGA were also elaborated according to the model fitting method to calculate the kinetic parameters (*A* and *E*). Nonlinear least squares and the linear regression models were considered in this study.

5.3.1. Nonlinear model fitting kinetics results

The nonlinear model fitting results of wood, 10% CaO, 20% CaO and 25% CaO.MgO blends at 20 ºC/min are presented in Table 5.3. The Table also shows the correlation coefficients and the deviation between the experimental and calculated DTG curves.

***Table 5.3*:** Kinetic parameters (*E* and *A*) obtained from the nonlinear model fitting approach

Sample	***E* (kJ/mol)**	***A* (s^{-1})**	***n***	***Dev* (%)**	R^2
Wood	169.46	$5.6x10^7$	1.55	0.50	0.999
10%CaO	163.27	$3.1x10^7$	1.55	0.15	0.998
20%CaO	178.82	$5.4x10^7$	1.59	0.24	0.999
25%CaO.MgO	172.39	$4.4x10^8$	1.58	0.51	0.999

The initial guess values of wood sample from the literature [Nolan *et al.,* 1973] have been adopted as starting values for the fitting procedure to obtain the results in Table 5.3. First order

reaction model was first assumed. Figures 5.7 - 5.10 compare the experimental and calculated DTG curves of wood, 10% CaO, 20% CaO and 25% CaO.MgO blends at 20 ºC/min, respectively. The calculated DTG curve in all the graphs is shown in black line plot. The results show that the model calculated curves fit well to the experimental, which demonstrates that the pyrolysis zone of these samples is better described by the reaction order presented in the Table 5.3.

Figure 5.7 shows the experimental and calculated DTG curves of wood sample at 20 ºC/min.

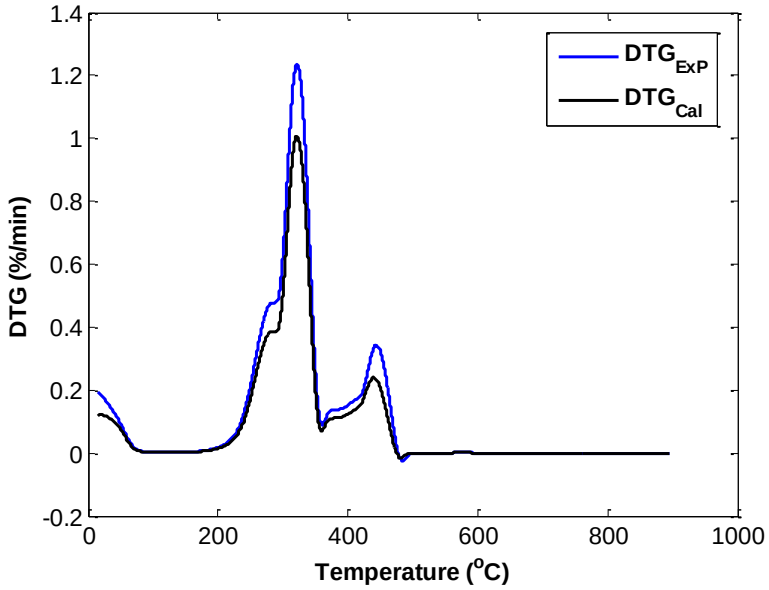

Figure 5.7: Experimental and calculated DTG curves of wood versus temperature at 20 ºC/min.

The difference between the experimental and calculated curves can be observed between 250-270 ºC, 280-320 ºC and 390 -480 ºC temperature range which is very small. The goal of this analysis is to minimize the squared residuals for the experimental and the calculated values of the parameters. This is done in order to perceive any agreement between the calculated and

experimental results. If the calculated fits well to the experimental, then we can conclude that the error from the data is acceptable and then the models can be used and developed with confidence to evaluate the kinetic parameters. Therefore, the better the fit the more accurate is the model. The average value of deviation (*DEV*) between the calculated and experimental DTG curves and quality of fit (QF_{DTG}) for 20 ºC/min rate was determined from Eq. (3.40) and (3.39), respectively. The best fit can be observed in this graph with the deviation of 0.50%. The values recorded for a wood sample (Table 5.3) are in agreement with the literature [Grønli *et al.*, 1999].

Figure 5.8 shows the experimental and calculated DTG curves of 10%CaO blend at 20 ºC/min.

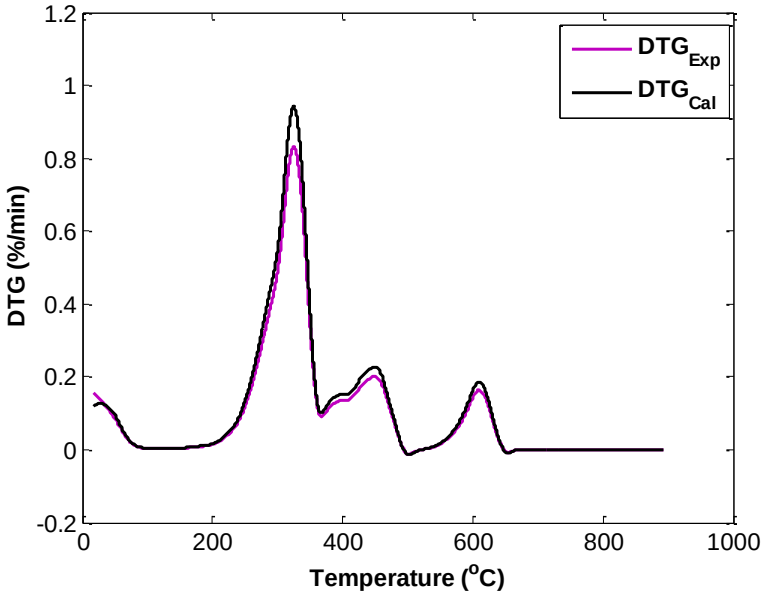

Figure 5.8: Experimental and calculated DTG curves of 10%CaO blend versus temperature at 20 ºC/ min.

From this figure we can observe that the calculated and experimental curves fit well, with the deviation of 0.15% between the temperature range of 200 ºC and 600 ºC. The deviation value for

the 10%CaO blend as recorded in Table 5.3 is lower (0.15%) compared to others due to a good quality of fit between the experimental and calculated DTG curves as shown in this figure.

Figure 5.9 shows the experimental and calculated DTG curves of 20%CaO blend at 20 ºC/min.

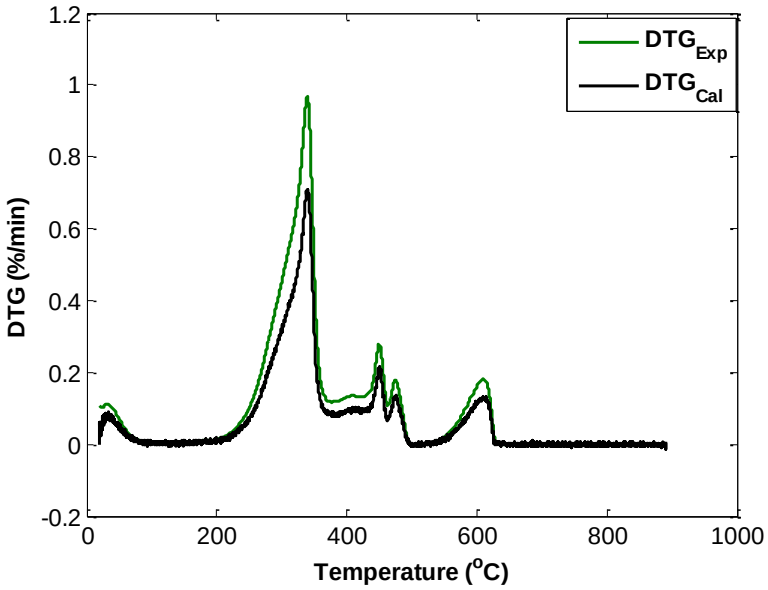

Figure 5.9: Experimental and calculated DTG curves of 20%CaO blend versus temperature at 20 ºC/min.

The deviation between the experimental and calculated curves was found to be 0.24%.

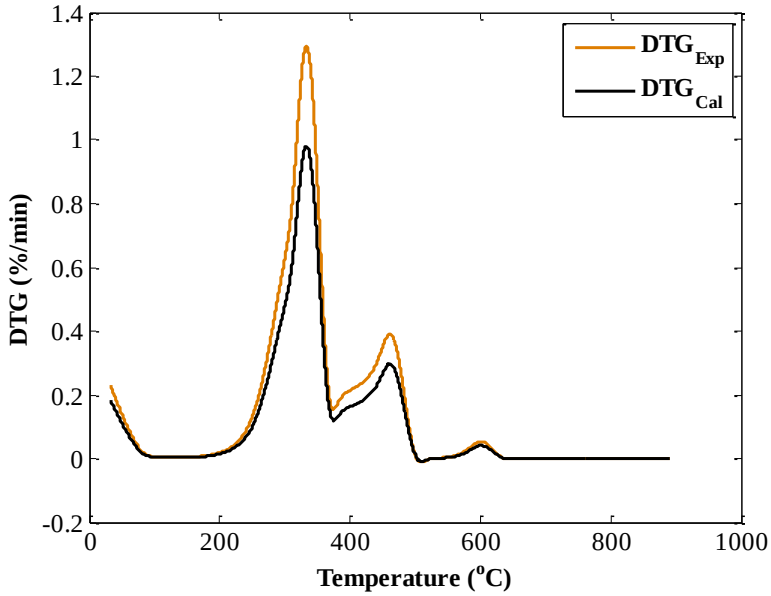

Figure 5.10: Experimental and calculated DTG curves of 25%CaO.MgO blend versus temperature at 20 ºC/min.

The disparity is between the temperature ranges of 200-500 ºC, which is the main devolatilization stage where pyrolysis is taking place. The deviation of 0.51% is observed and recorded in Table 5.3.

It can be concluded that the calculated data fit to the experimental data as discussed earlier in this section. The disparity observed between the temperature ranges of devolitalization is quite small with deviation in the range of 0.1-0.51%. The experimental error observed could be the cause of the difference and perhaps the sample heterogeneity. It is recommended that the TGA machines should be well calibrated and make sure that the blends are homogeneously mixed before conducting the experiments. Optimization of the data should be performed before estimation of the kinetic parameters and developing any desired models. The disparity between the experimental and calculated curve differed from one sample to the other, therefore, it can be

concluded that the different material behaves differently during devolatilization process and that the reactions taking place are partialy different.

5.3.2. Validation of kinetics

Mathematical modeling can be profitably applied for process design and optimization, but the validity of predictions is highly dependent upon an adequate description of chemical and physical processes, extensive model validation, and the correctness of input data [Grønli *et al.*, 2002].

The validity of kinetics for this study was performed on a wood sample at 20 ºC/min and the results were compared with the once obtained earlier (Figure 5.7) for the same sample at the same heating rate. The same value of the activation energy of 169.46 kJ/mol and the reaction order of 1.53 was achieved, which is very close to the one obtained earlier (1.55). Less than 1% of difference from earlier results was achieved for the pre-exponential factor (0.0360 s^{-1}). Figure 5.11 shows the experimental and calculated DTG curves of wood sample at 20 ºC/min.

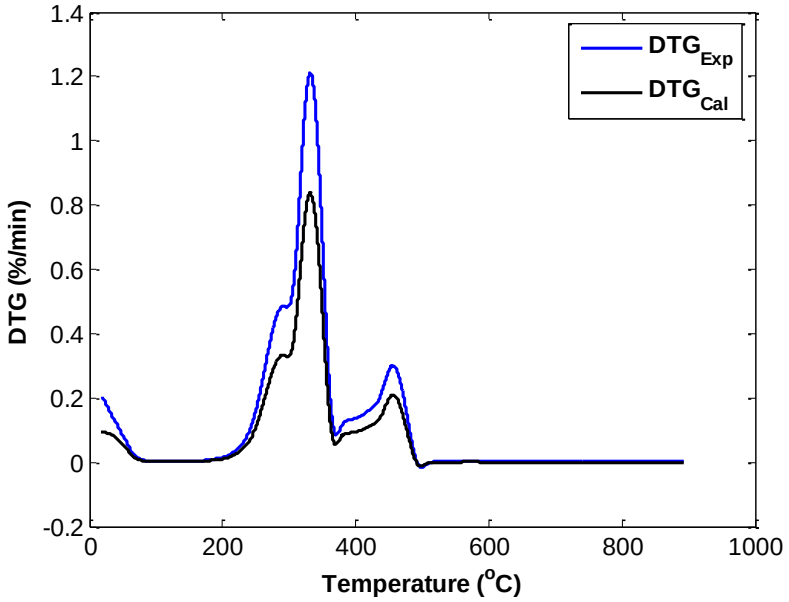

Figure 5.11: Experimental and calculated DTG curves of wood versus temperature at 20 ºC/min.

The shape and the degradation rate of this graph is the same as the one in Figure 5.7. This implies that this model is valid for the kinetic analysis. The trend of the calculated curve is the same as the experimental one. Most of the calculated points are close to the experimental points, with the deviation of 0.51%.

5.3.3. Linear model fitting kinetics results

For the estimation of kinetic parameters in the pyrolysis stage the temperature range 200–800 ºC at 20 ºC/min was considered. The Mampel first order model (Table 3.2 in section 3) was first assumed to determine the kinetic parameters of wood, 10%CaO, 20%CaO and 25%CaO.MgO samples. The results obtained by Antal *et al.*, [1998] show that a first-order model can offer a good fit to weight loss curves obtained at a single heating rate. In order to use the models, the selection of some conversion values (α) is required, which is defined in Eq. (3.28) and it should

be between 0.1-0.90 or 0.05-0.95. For this analysis the range of α values was between 0.1-0.90. The wood sample is being treated as a reference for this study since there is enough literature on the kinetics of biomass such as wood, compared to the biomass with sorbent blends.

The first order linear regression model 5 from Table 3.2, together with Eq. (3.36) enables the determination of the activation energy (E) and the pre-exponential factor (A) from the slope and the intercept, respectively. Figure 5.12-5.15 shows the linear plots from the first order model for wood, 10%CaO, 20%CaO and 25%CaO.MgO samples, respectively.

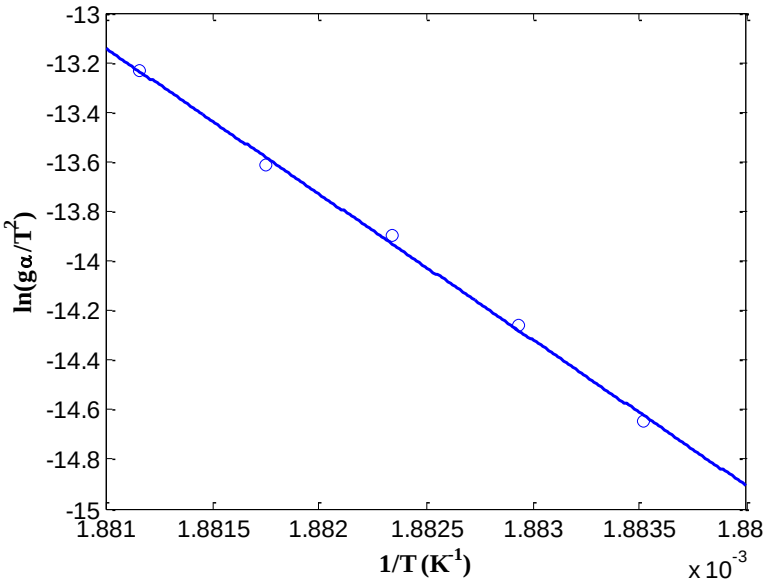

Figure 5.12: Plots of $\ln(g(\alpha)/T^2)$ versus $1/T$ of wood sample at the heating rates of 20 ºC/min.

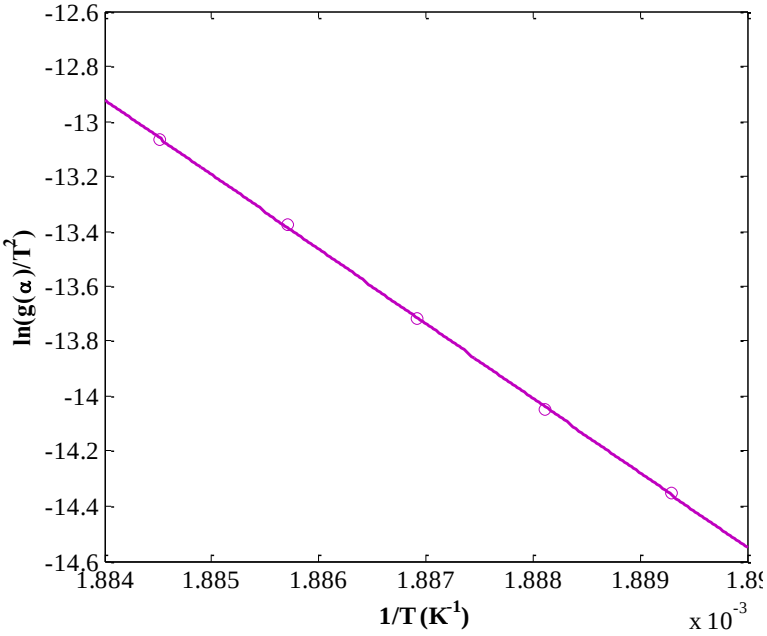

Figure 5.13: Plots of $\ln(g(\alpha)/T^2)$ versus $1/T$ of wood with 10%CaO blend at the heating rates of 20 ºC/min.

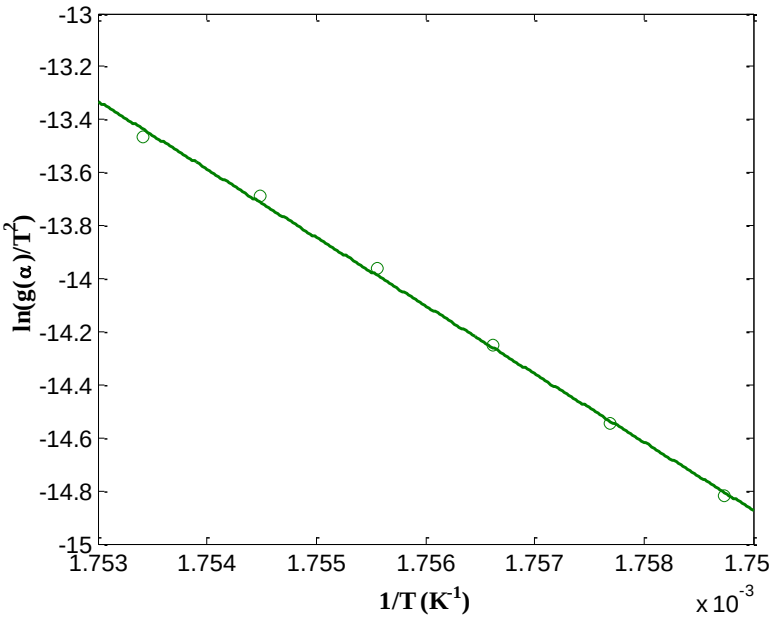

Figure 5.14: Plots of $\ln(g(\alpha)/T^2)$ versus $1/T$ of wood with 20%CaO blend at the heating rates of 20 ºC/min.

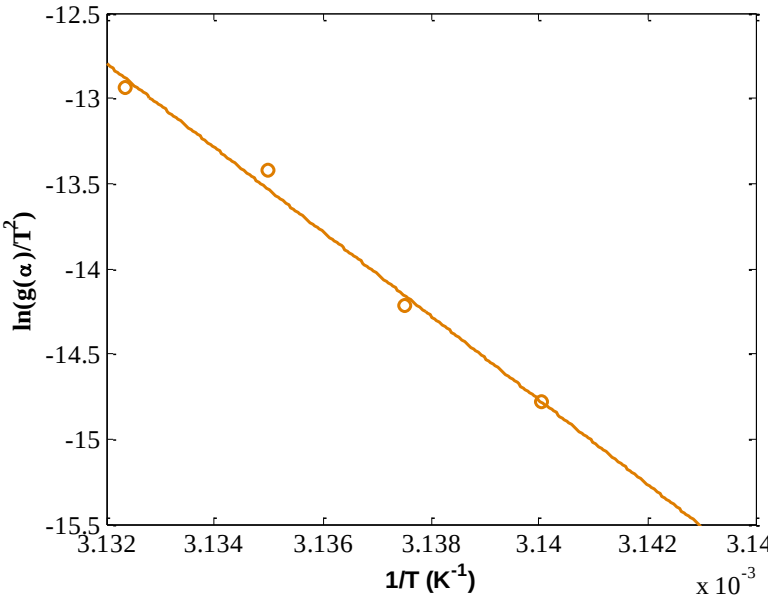

Figure 5.15: Plots of ln($g(\alpha)/T^2$) versus 1/T of wood with 25%CaO.MgO blend at the heating rates of 20 ºC/min.

The kinetic values for E and A were obtained from the first order linear plots above at 20 ºC/min. The first sets of kinetic values were obtained from the actual data. Before the estimation of kinetic parameters from this model, the constraint linear optimization was performed to the actual experimental data. Basically, this is done by maximizing the desired values from the experimental data and minimizing the undesired ones in order to achieve the highest performance within certain limits. The data were optimized for better output of the kinetic parameters and the results were compared with the actual values. This also assisted in the accurate model prediction. The kinetic values of E and A are presented in Table 5.4, where E_1, E_2 and E_3 are the activation energy values from the actual data, optimized data and predicted model, respectively, and A_1, A_2 and A_3 are their corresponding pre-exponential values. Their corresponding correlation coefficient values (R) are also presented in the table.

***Table 5.4*:** Kinetic parameters (*E* and *A*) obtained by Coats and Redfern method

	Wood	10%CaO	20%CaO	25%CaO.MgO
E_1 **(kJ/mol)**	62.60	52.32	57.20	71.26
A_1 **(min^{-1})**	2.4×10^{10}	7.5×10^{9}	8.2×10^{9}	2.8×10^{10}
R_1	0.989	0.999	0.998	0.998
E_2 **(kJ/mol)**	125.71	123.05	139.69	133.04
A_2 **(min^{-1})**	4.9×10^{10}	1.8×10^{10}	5.4×10^{10}	1.9×10^{10}
R_2	0.997	0.993	0.999	0.995
E_3 **(kJ/mol)**	191.32	187.89	216.41	210.03
A_3 **(min^{-1})**	7.5×10^{10}	2.7×10^{10}	8.4×10^{10}	3.0×10^{10}
R_3	0.999	0.999	0.999	0.999

The kinetic values of E_1 from the actual data are lower than the values obtained from the optimized data (E_2) and the predicted model (E_3). During devolatilization or pyrolysis process, many complex reactions take place and the knowledge of this is very important during gasification. Therefore, these values for *E* are the energy needed for the reaction to take place. The optimized and predicted model values are too high when compared to the actual values. This sounds to be overestimated, but the E_2 and E_3 are in good agreement with the literature in the case of wood [Nolan *et al.,* 1973, Di Blasi, 2009]. The reason could be that the actual data is suspected to have errors. The source of the errors is not clear, but could be due to limitations by heat and mass transfers. This error was minimized by means of optimization of the experimental data. The predicted model values are higher compared to both actual and optimized for all the

samples due to the fact that the data was first optimized and we expect it to fit well to the model. The values of the pre-exponential factor (A) obtained from actual data are lower compared to optimized and predicted values, thus, $A_1<A_2<A_3$.

Therefore, we can conclude that optimization was essential for this study since it led to better output. Well established models may not properly fit to specific data, because they are mostly developed from certain data and the data treatment and conditions is not always the same. Errors from the sample preparation may have not been eliminated before building up a model. It is also crucial to develop a model which can suit specific data perfectly.

5.4. Pre-exponential factor comparison

The pre-exponential factors were also determined from Eq. (3.36) and their results were compared with Eq. (3.35) (Table 5.6). White *et al.*, [2011] assumed that the second right hand part of Eq. (3.35) is far less than one; hence it was neglected when calculating the pre-exponential factor, i.e $2RT'/E << 1$. The purpose of this comparison is to confirm this assumption and how significant is the difference in the A values. The results of the pre-exponential factor from the actual data, optimized data and predicted model are presented in Table 5.5.

***Table 5.5*:** Comparison of *A* values obtained from Eq. 3.35 and 3.36.

	A (s^{-1})	Wood	10%CaO	20%CaO	25%CaO.MgO
Eq. (3.36)	A_1	$2.4x10^{10}$	$8.2x10^{9}$	$7.5x10^{9}$	$2.8x10^{10}$
	A_2	$4.9x10^{10}$	$1.8x10^{10}$	$1.9x10^{10}$	$5.4x10^{10}$
	A_3	$7.5x10^{10}$	$2.7x10^{10}$	$3.0x10^{10}$	$8.4x10^{10}$
Eq. (3.35)	A_1	$2.8x10^{10}$	$1.0x10^{10}$	$9.3x10^{9}$	$3.3x10^{10}$
	A_2	$5.8x10^{10}$	$2.2x10^{10}$	$2.4x10^{10}$	$6.4x10^{10}$
	A_3	$7.8x10^{10}$	$2.8x10^{10}$	$3.1x10^{10}$	$8.8x10^{10}$

From the table, we can observe that the values of *A* obtained from Eq. (3.35) and (3.36) are close to each other with no significant difference between the values from both actual, optimized and predicted model. This implies that the data that was fitted in these models is in agreement with the literature, because it fits well to the model.

CHAPTER 6

COMPUTER SIMULATIONS

6.1. Introduction

The gasification efficiency and the hydrogen content of biomass/sorbent blends were estimated through computer simulation software developed by Jayah *et al.* [2003]. Some parameters such as throat angle and diameter of a downdraft gasifier (Figure 6.1) were varied in order to investigate their impact on the conversion efficiency.

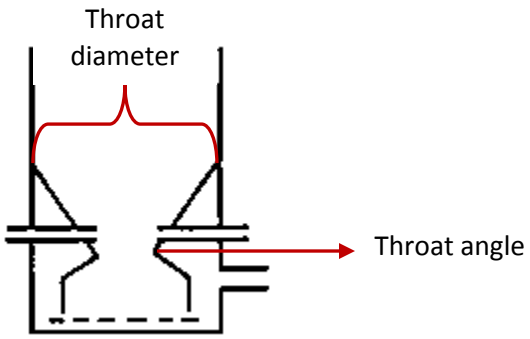

Figure 6.1: Downdraft gasifier throat angle and diameter.

6.2. Gasification efficiency

The conversion efficiency is one of the important parameters that determine the actual technical operation and the economic feasibility of a gasifier system. Most of the commercial scale gasification systems have a cold gas efficiency of at least 65% and some exceed 80% [Rajvanshi, 1986]. Elemental composition presented in Table 4.1 was used as input parameters together with parameters in Table 6.

Table 6: Gasification simulation parameters: the bulk densities for both wood and blends were in the range 0.39-0.4 g/cm^3.

Parameters	**Values**
Bulk density (g/cm^3)	0.4
Diameter of wood particle (cm)	2.5
Throat angle (Degrees)	30
Insulation thickness (cm)	17.5
Thermal conductivity of heat (W/cm.K)	2.8
Temperature of air input (K)	900
Feed input (kg/hr)	50
Air input (kg/hr)	44.5
Heat loss (%)	12.8

Heat loss is the transfer of heat from inside to outside of the gasifier.

The parameters in Table 6 were varied until the optimum efficiency was achieved. The conversion efficiency was then calculated from Eq. (2.6). The parameters in Table 4.1 and 6 have resulted in optimum conversion efficiency. Figure 6.3 shows the conversion efficiency of wood, wood with 10%CaO, 20%CaO, and 25%CaO.MgO blends as a function of time.

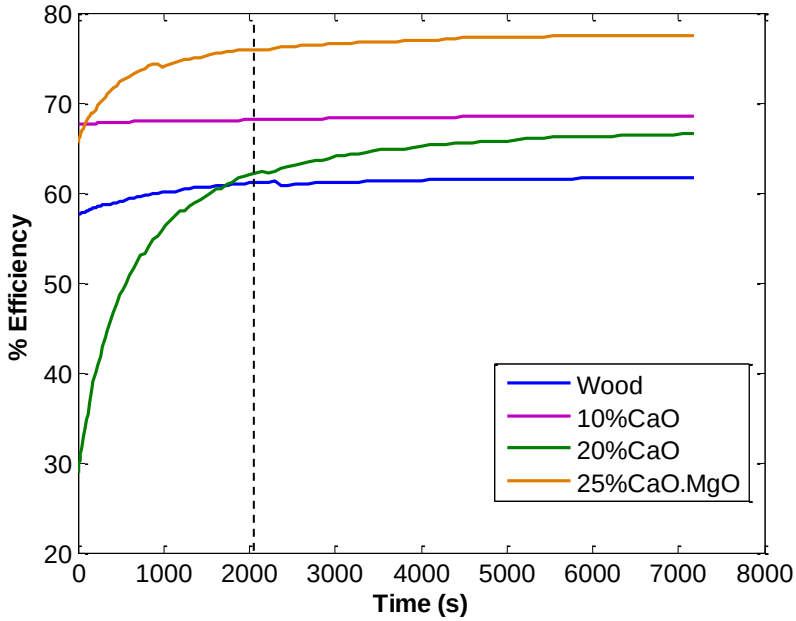

Figure 6.2: The simulated possible efficiency achieved when gasifying wood, wood with 10%CaO, 20%CaO, and 25%CaO.MgO blends versus time.

It can be observed from this figure that wood with 25%CaO.MgO mixture resulted in higher conversion efficiency of 78%, followed by the blend of 10%CaO. Dolomite (CaO.MgO) is known for cracking tars in the gasifier at high temperature, which leads to high production of syngas. Thus, the sorbent material in the gasifier captures carbon dioxide, thereby releases heat, which then increases the temperature, resulted in an increase in cracking of tar and conversion of the char present [Hanaoka *et al.*, 2005b]. By so doing, it means producer gas in the gasifier is increased, hence an increase in conversion efficiency. The difference of 21% was observed between pine wood and 25% CaO.MgO blend which means that the sorbent has an effect of increasing the conversion efficiency of the gasifier system. This will in the end help with the selection and prediction of the performance of the material. This information can also assist in the design of a gasification system.

There is much difference before all the materials stabilize after 2000 s. Compared to other blends, 25% CaO. MgO material was found to be suitable to perform better during gasification.

6.2.1. The Effect of throat diameter and angle on gasification

The effect of throat angle and diameter on gasification efficiency was performed on the sample which resulted in the highest efficiency (25%CaO. MgO). Figure 6.3 shows the conversion efficiency (%) when varying the throat angle (a) diameter (b) versus time (s). The throat diameter and angle were varied in the following manner: 10 cm, 30 cm and 60 cm while fixing the angle (30º) and 30º, 60º and 90º while fixing the diameter (10 cm) respectively, in order to observe their effect on gasification efficiency.

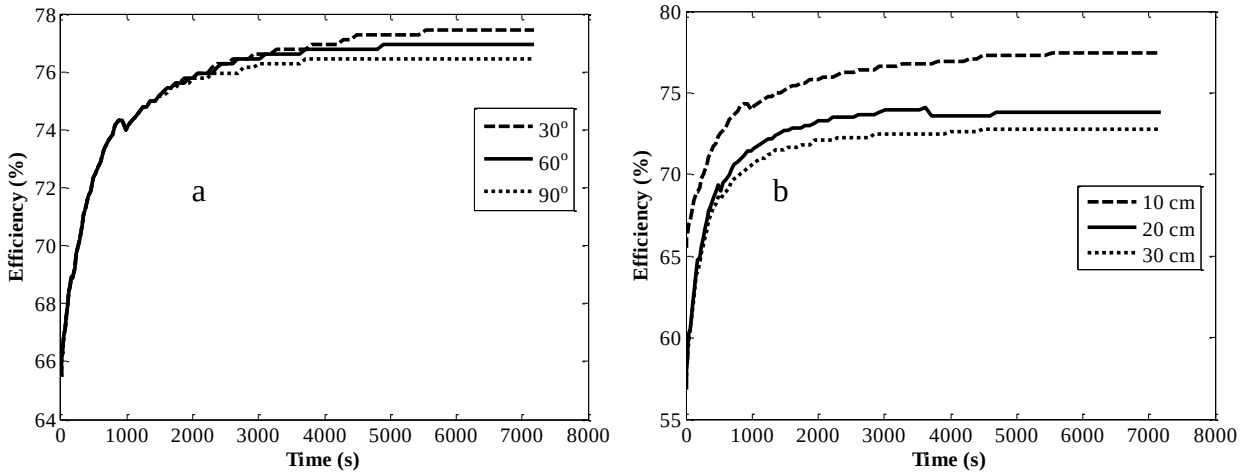

Figure 6.3: Conversion efficiency of 25%CaO.MgO blend for different (a) throat diameters and fixed angle 30º and (b) throat angles and fixed diameter (10 cm).

The effect of throat angle on conversion efficiency is one of the important features of downdraft gasifiers [Jayah *et al.,* 2003]. From Figure 6.3 (a) it can be observed that increasing the throat angle decreases the conversion efficiency, but the difference was not significant, below 10%.

Jayah *et al.,* [2003] reported that the conversion efficiency decreases as the throat angle increases, because the divergent effect of the throat decreases the temperature and hence the reaction rate. The authors also mentioned that the smaller angles need a longer gasification zone length to reach their optimum efficiency. The same applies to the throat diameter, where the small diameter tends to increase the conversion efficiency as compared to the larger diameter (Figure 6.3 (b)). The effect of throat angle and diameter of the reduction zone was investigated by Kumar *et al.,* [2008]. Their results also show that the smaller throat diameter (10 cm) tends to increase the conversion efficiency, whereas larger throat diameters (30 cm) decrease the cumulative conversion efficiency. This is because the larger throat diameter decreases the temperature due to the divergent effect and hence the reaction rate. The same applies to the throat angles; the smaller angles (45º) tend to increase the conversion efficiency, whereas larger angles (90º) decrease the conversion efficiency. Although smaller diameter or angles increase the conversion efficiency, a longer reduction zone length is needed to reach a higher efficiency [Kumar *et al.,* 2008]. Figure 6.3 confirmed that the results obtained in this study are consistent with the literature as discussed earlier.

6.2.2. Hydrogen content

The goal of simulating hydrogen content from the blends was to observe if the hydrogen produced from an air-blown fixed bed downdraft gasifier can be enhanced without using steam as a gasification agent. It demonstrated the possibility of taking advantage of the steam produced during the drying of the feedstock and converts it to useful hydrogen through the water-gas-shift reaction enhanced by the addition of sorbents in the process. The simulated hydrogen content of wood, 10%CaO, 20%CaO and 25%CaO.MgO blend is shown in Figure 6.4.

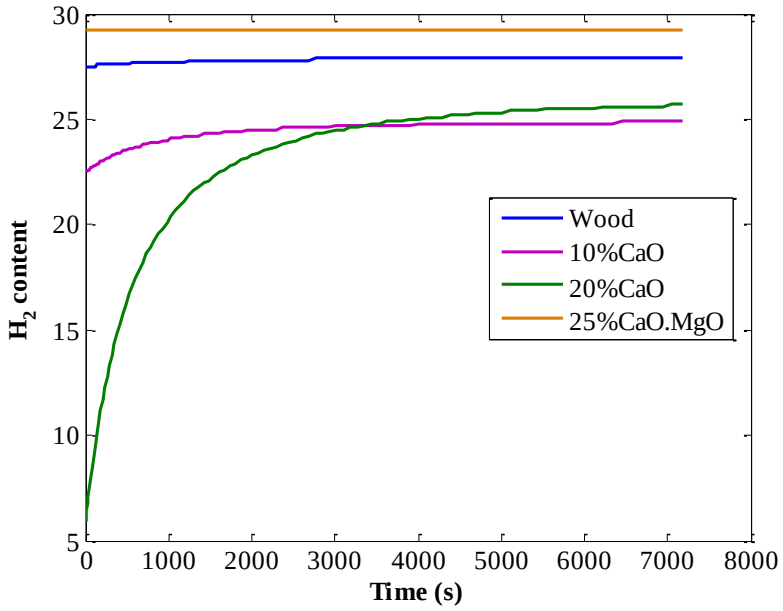

Figure 6.4: The hydrogen gas volume obtained during computer simulation.

It can be observed that the highest hydrogen (29%) content was obtained from a blend with 25% CaO.MgO followed by wood biomass (28%). The percentage difference between these samples is not significant. The mixture of biomass with CaO sorbent loaded to the gasifier absorb the released CO_2 to enhance the water-gas shift reaction towards hydrogen production, which

provides the necessary energy for the endothermic gasification through the carbonation reaction releasing heat. The same blend has also resulted in the highest gasifier conversion efficiency. This is because of the higher hydrogen content produced by the two blends respectively as indicated in Figure 6.4. The efficiency of the gasifier is dependent on the volume of combustible gases, which are hydrogen, methane and carbon monoxide.

With this less increment of hydrogen, we cannot confidently recommend the use of the blend of wood with sorbents for hydrogen production from the air-blown gasifier but is can be used for the purpose of tar cracking. The computer simulation results suggested that a blend of 25%CaO.MgO results in the highest hydrogen content produced during gasification and enhanced gasification efficiency, but the difference is insignificant.

CHAPTER 7

SUMMARY, CONCLUSION AND RECOMMENDATIONS

7.1. Summary of the findings

7.1.1. Physical and chemical composition of biomass and biomass/sorbent blends

The pine-wood was used as biomass material and calcium oxide and magnesium oxide as sorbents. The blends of these materials were homogeneously mixed before conducting the experiments. Pine-wood was crushed to a powder form (250 μm). The proximate and ultimate analysis was carried out through the Thermogravimetric analyzer (TGA) and Carbon, Hydrogen, Nitrogen and Sulfur (CHNS) analyzer, respectively. The oxygen was obtained by the difference method. The pine-wood was higher in carbon content as compared to biomass/sorbent blends since pine-wood is a carbonaceous material. The hydrogen content, however, remained fairly constant in both pure wood and the blends. The nitrogen was present in minimal quantities in all the samples; however the small quantities do not have a significant impact on gasification.

The moisture content of the samples was between 4 and 9%, which is within the moisture levels for gasification in a downdraft gasifier. The volatile matter was higher in pine-wood (69%) than in the blends (47-65.5%). This is due to the fact that biomasses in general have higher volatile matter than the sorbents. Very low quantity of ash was observed in pine-wood samples (0.4%), and this was in agreement with the literature (0.1-5.0%) [Ragland and Aerts, 1991]. However, the biomass/sorbent blends had between 5 and 20% of the remaining carbonates. This is because biomass is high in volatile matter compared to sorbents, which implies that the addition of oxides

to biomass decreases the volatile content of the blends. The fixed carbon (FC) was high in 25%CaO, 10%CaO.MgO, 15%CaO.MgO and 25%CaO.MgO mixtures (26-32%) compared to wood (23.8%) which implies that these blends can produce more energy from the remaining carbon (FC).

7.1.2. Thermal stability of the materials

The thermal stability of the biomass/sorbent blends was determined from TGA and the differential thermogravimetric (DTG) curves at different heating rates of 10 ºC/min, 15 ºC/min and 20 ºC/min under nitrogen atmosphere. The goal of this analysis was to determine the most thermally stable material between wood and wood blended with CaO and/or MgO sorbents. The thermal decomposition process during gasification can be influenced by operating parameters such as temperature and heating rate. The behavior of the conversion curve is mainly affected by the heating rate. The increase of heating rates results in slight changes in the TGA curve position towards higher temperatures. The heating rate also affects the position of the DTG peaks. The temperature of maximum mass loss rate, the initial decomposition temperature and the final decomposition temperature were determined from DTG curves. Biomass properties, such as the size and shape of particles, composition, and moisture content can also influence the decomposition process of gasification system. Less than 10% of moisture content was obtained from the DTG curves of the samples around 120 ºC, which is acceptable for gasification operation. The blends of 20%CaO and 25% CaO. MgO have resulted in higher thermal stability compared to others. There was a significant difference (95%) in weight loss between the wood

and wood with a sorbent mixture (25% CaO.MgO) at higher temperatures (600-900 ºC), which implies that the wood with sorbents have better thermal stability compared to pure wood.

The statistical analysis was also performed with a one way analysis of variance (ANOVA) test to determine the significant mean difference between the rates of degradation of the samples. The sample with a higher mean value was found to be 25%MgO (51.29%) which is not very different from 25%CaO (51.17%). ANOVA one way test does not show which sample has the significant mean difference from the other samples, therefore a multicomparison test was performed to determine which sample has the significant mean difference from the other. A significant difference in the mean of wood, 10%CaO, 25%CaO.MgO with 25%CaO sample was observed, for $F(4, 324) = 4.37$ $p = 0.0019$. No significant mean difference was observed between 20%CaO and 25%CaO blends. Since there was an insignificant difference of the mean between these samples kinetics was performed for wood, 10%CaO, 25%CaO.MgO, 20%CaO samples. It was concluded that the mean of 25%MgO can as well differ significantly with other samples, which have very low mean values.

7.1.3. The kinetic parameters of the materials

The main aim of this study was to determine the kinetic parameters (activation energy (E), pre-exponential factor (A) and the reaction order (n)) of biomass and biomass/sorbent blends. The knowledge of the kinetic parameters in the pyrolysis zone is very important in the designing of the gasification system, since pyrolysis is an important step of gasification and combustion. The

model free and model fitting approaches were employed to estimate these parameters. In order to estimate these parameters experimental data from TGA was used.

The model free Kissinger and Flyn-Wall-Ozawa (FWO) methods as well as the regression models were used to estimate the kinetic parameters. The kinetic parameters determined by the model free Kissinger method shows the activation energy of 131.11, 126.06, 139.63 and 134.72 kJ/mol for wood and wood with 10% CaO, 20% CaO and 25% CaO.MgO blend, respectively. These values are consistent within the range of average values obtained by the FWO method (129 kJ/mol, 124 kJ/mol, 143 kJ/mol and 136 kJ/mol for wood, wood with 10%CaO, 20%CaO and 25%CaO.MgO blends, respectively). The activation energy of 25%CaO.MgO blend obtained from Kissinger and averaged FWO method is 6.1% and 5.8% higher than the biomass, respectively. This implies that the blend requires more energy to start the reaction and would thus gasify at higher temperatures and release more energy than pure biomass materials. The released energy is due to the exothermic reaction whereby CaO absorbs CO_2 during the water-gas shift reaction in the gasifier. The resultant energy can be used by other endothermic reactions in the gasifier and for external use. The values of the kinetic parameters obtained from both the model free methods are reliable for the determination of kinetic parameters.

The activation energy values of the nonlinear least square model were 169.46, 163.27, 178.82, 172.39 for wood, 10% CaO, 20% CaO and 25% CaO.MgO blend, respectively. The linear regression model was also conducted from the actual data and optimized data. The optimized data were fitted to the predicted model to obtain the kinetic parameters. The results from the actual data has resulted in lower values of E_1 (62, 52, 71, and 57 kJ/mol) compared to the

activation energy values of optimized data, E_2 (125.7, 123, 139.7 and 133 kJ/mol) and predicted model, E_3 (191, 187.9, 216 and 210 kJ/mol) for wood, 10% CaO, 20% CaO and 25% CaO.MgO blend, respectively. The values of the nonlinear least squares model are within the range of the predicted model. Hence we can conclude that optimization is necessary before fitting the data to any models. Both regression models are effective when estimating the kinetic parameters. The values obtained from the predicted model results were higher than both the model free methods and the nonlinear regression model. For this reason it can be concluded that predicted model is the most effective since it produces high values for the activation energy and can therefore be recommended for future analysis of the same kind of study.

7.1.4. The conversion efficiency

A computer simulation was performed to estimate the conversion efficiency and hydrogen content of the syngas for the different samples under study. The results show that the blend of wood with 25%CaO.MgO sample resulted in higher conversion efficiency (78%) compared to others. The difference of 21% was observed between pine-wood and 25% CaO.MgO blend. The hydrogen content remained low from all the samples (23-29%). Amongst the samples analyzed in this study, it was concluded that wood with 25%CaO.MgO sorbent results in the highest gasification efficiency.

7.2. Summary of the contributions

Determination of kinetics during the decomposition process is one of the key problems in large scale processes of biomass conversion to valuable products via thermal treatment [Gašparovič *et*

al., 2009]. Pyrolysis as part of the gasification process involves many complex reactions, which cannot be exactly described. Therefore, it is difficult to take into consideration all the necessary reactions taking place when conducting the kinetics study of the material. Relying on the information from other researchers may lead to incorrect selection of the blend that will ultimately best perform during gasification. The kinetics of biomass/coal blends have been investigated by many authors as previously stated, however little has been done in the biomass/sorbent mixture. This study contributed to the information on the kinetics and the conversion efficiency of biomass/sorbent blends, which are part of the important parameters of operating thermochemical conversion systems such as gasification. The kinetics of biomass can be elaborated by model free or model fitting methods. Many studies only used one of these methods, but this study managed to use both methods and identified the most effective and suitable method for the material employed in this study.

7.3. Conclusion

The kinetics of biomass with sorbent blends were performed, which was the main aim of this study. In order to achieve this, the physical and chemical analysis as well as the thermal stability of the materials was determined from TGA curves at different heating rates. The most thermally stable material between wood and wood blended with sorbents was determined. The significant mean difference between the wood and wood with a sorbent mixture during devolitilization was achieved by one way ANOVA test. The blend of wood with 25% CaO. MgO has resulted in the highest thermal stability compared to others, which implies that the wood with sorbents have better thermal stability compared to wood.

The chemical kinetics was investigated by the model free, Kissinger and FWO methods as well as regression modelling. It can be concluded that both model free methods are reliable for the determination of kinetic parameters. The fitting methods actual and optimized data were used. The actual data have resulted in lower values of kinetic parameters compared to the values obtained after optimization and predicted model. The values of the nonlinear least squares model are within the range of the predicted model. It was then concluded that optimization is necessary before fitting the data to any models. Both regression models are effective when estimating the kinetic parameters. Models are developed for specific purposes, and fitting other scholars' models can give uncertain results. Therefore, it is advisable to develop your own model to obtain accurate results from your data.

The computer simulation results show that the blend of wood with 25%CaO. MgO sample shows higher conversion efficiency (78%) compared to others, with the percentage difference of 21% between pine-wood and 25% CaO.MgO blend. The hydrogen content was consistently low in all the samples (23-29%). Amongst all the samples considered in this study, the mixture of wood with 25%CaO.MgO sorbent has shown to be the most suitable for gasification.

7.4. Recommendations

The kinetics of biomass/sorbent mixtures were successfully determined from TGA data using both the model free and regression models. The conversion efficiency and the hydrogen content were performed by computer simulation software. The gasification test in the gasifier was not determined to determine these parameters. Therefore, it is necessary and recommended to

perform the actual gasification of biomass/sorbent blends and compare the results obtained with the simulated results. Experimental data can be treated differently before performing any kinetic analysis. Hence, optimization of any data can be more useful before any analysis for better estimations. When performing kinetics of material by model fitting approach, the modelling equations may fit well or not to the experimental data, but it is advisable to develop your own model for accurate results. If hydrogen will be produced from a fixed bed downdraft gasifier, the use of steam in the adsorbent bed is recommended.

Appendix A

Effect of the heating rate on TGA and DTG curves

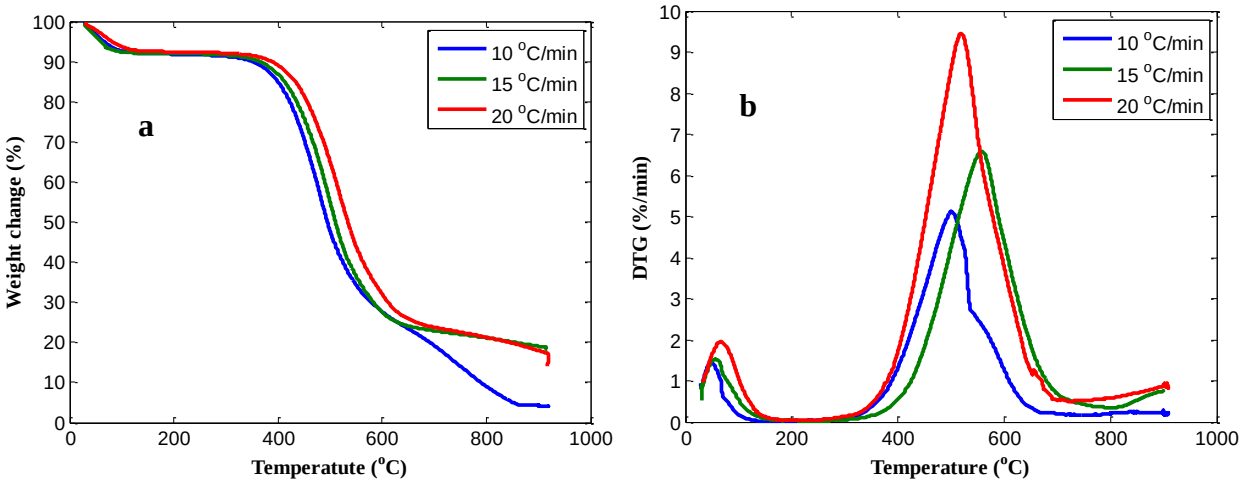

Figure 1: TGA (a) and DTG (b) of 5%CaO blend at various heating rates of 10, 15 and 20 ºC/min, respectively.

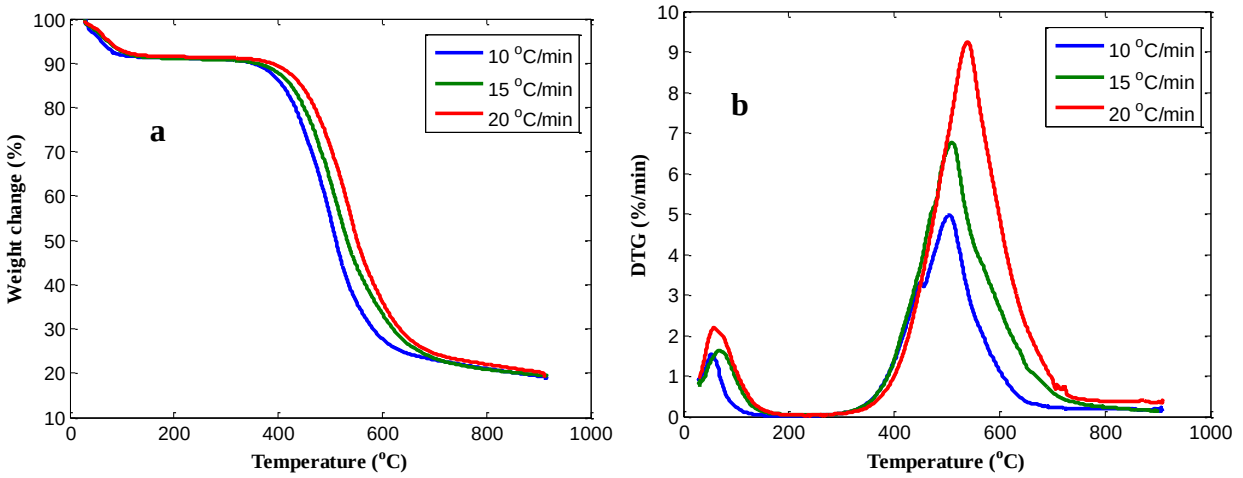

Figure 2: TGA (a) and DTG (b) of 5%MgO blend at various heating rates of 10, 15 and 20 ºC/min, respectively.

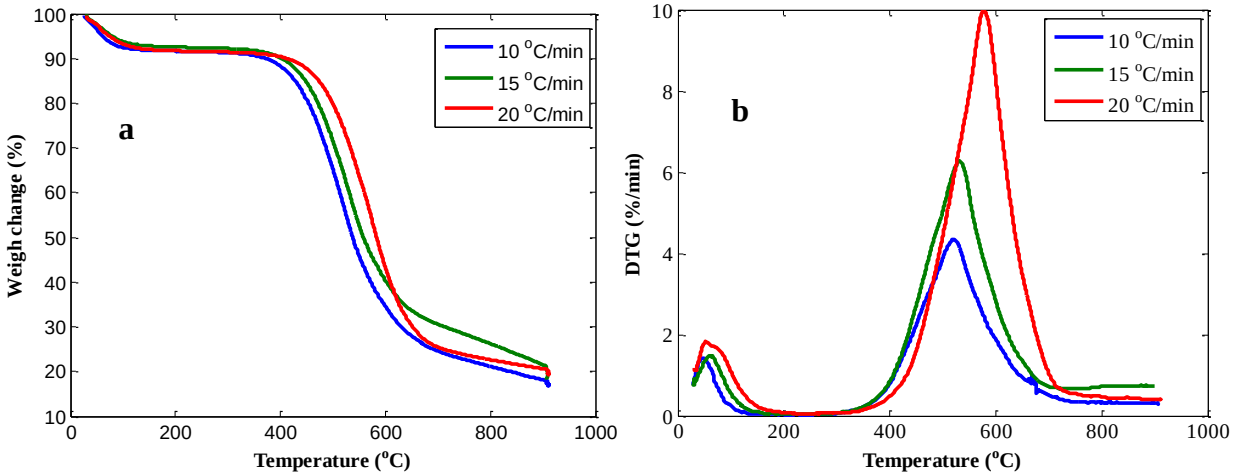

Figure 3: TGA (a) and DTG (b) of 10%MgO blend at various heating rates of 10, 15 and 20 ºC/min, respectively.

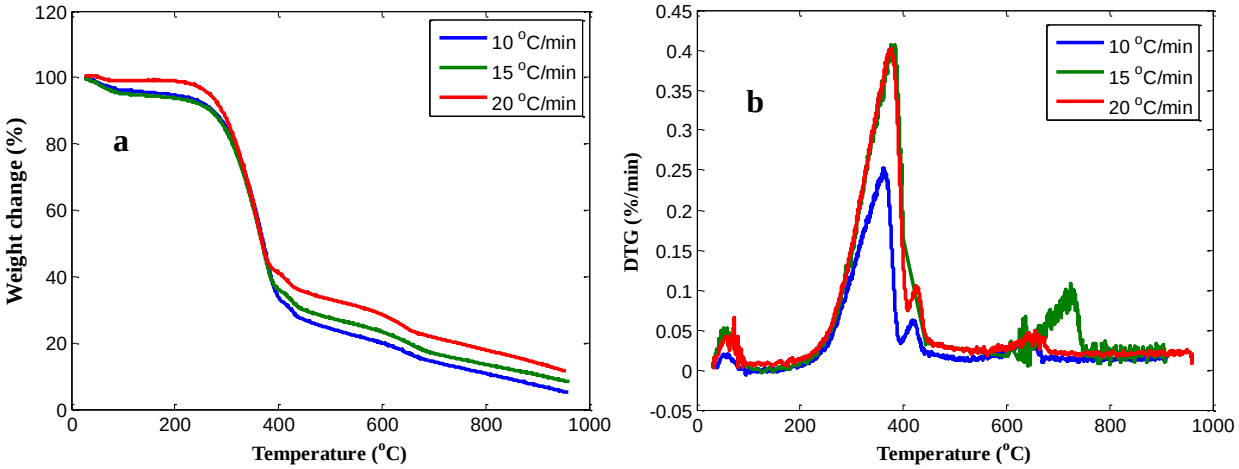

Figure 4: TGA (a) and DTG (b) of 15%CaO blend at various heating rates of 10, 15 and 20 ºC/min, respectively.

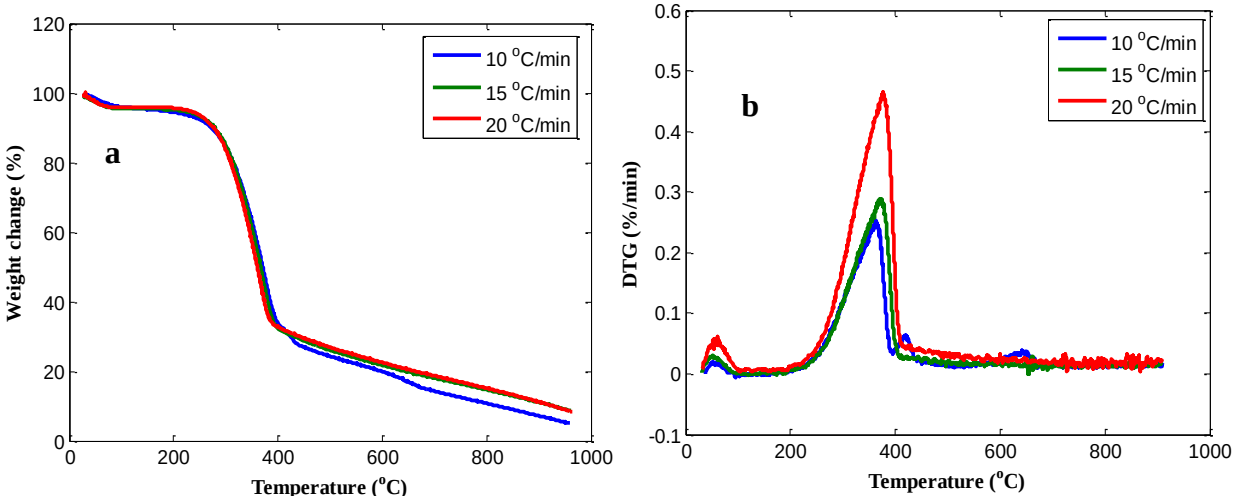

Figure 5: TGA (a) and DTG (b) of 15%MgO blend at various heating rates of 10, 15 and 20 ºC/min, respectively.

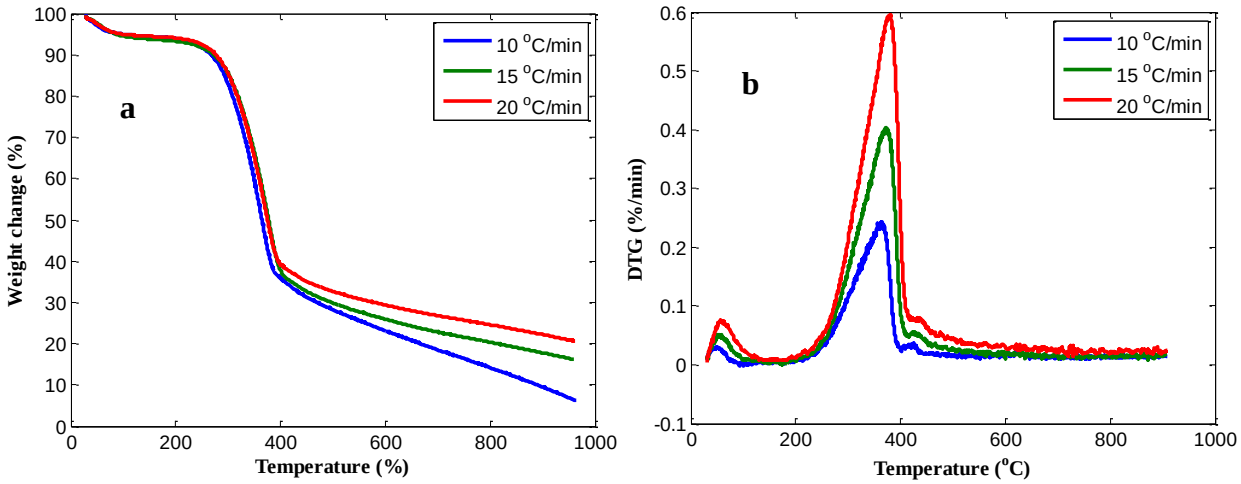

Figure 6: TGA (a) and DTG (b) of 25%MgO blend at various heating rates of 10, 15 and 20 ºC/min, respectively.

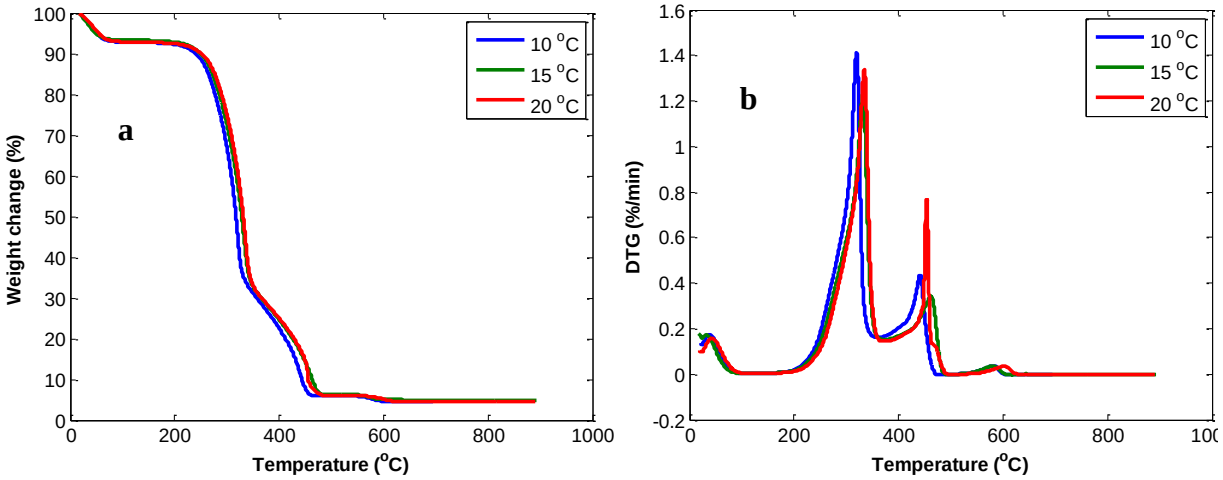

Figure 7: TGA (a) and DTG (b) of 15%CaO.MgO blend at various heating rates of 10, 15 and 20 ºC/min, respectively.

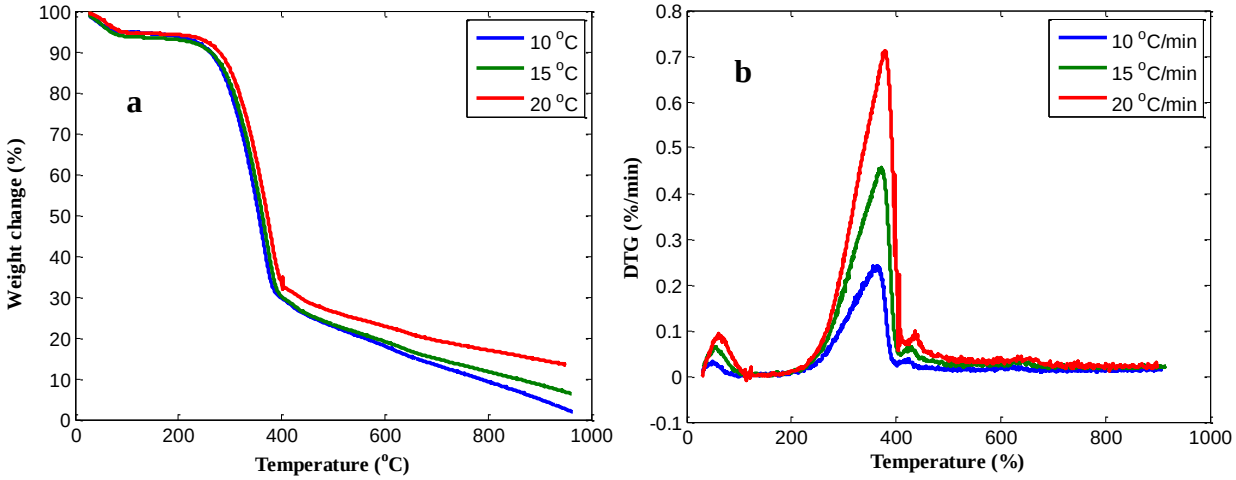

Figure 8: TGA (a) and DTG (b) of 20%CaO.MgO blend at various heating rates of 10, 15 and 20 ºC/min, respectively.

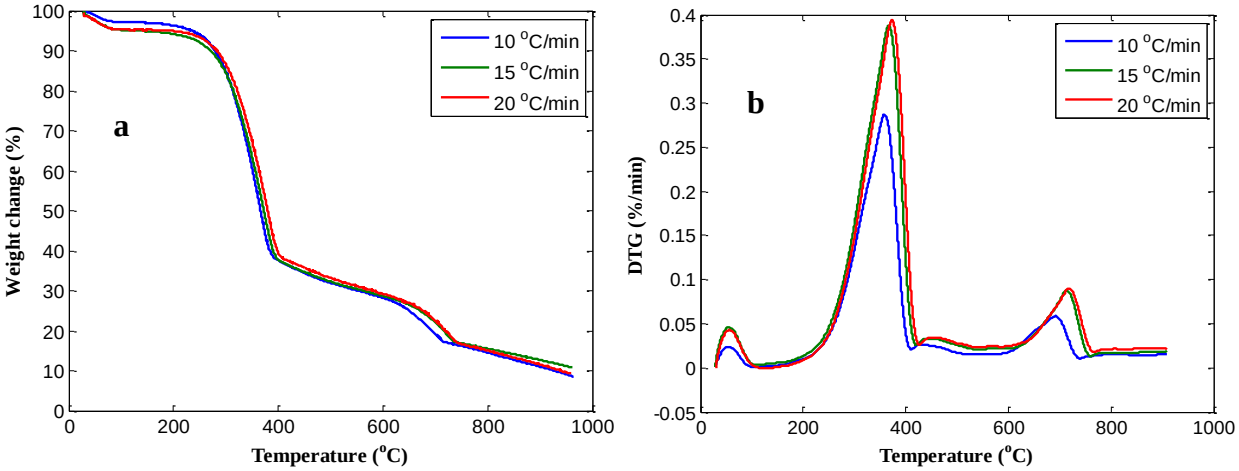

Figure 9: TGA (a) and DTG (b) of 25%CaO blend at various heating rates of 10, 15 and 20 ºC/min, respectively.

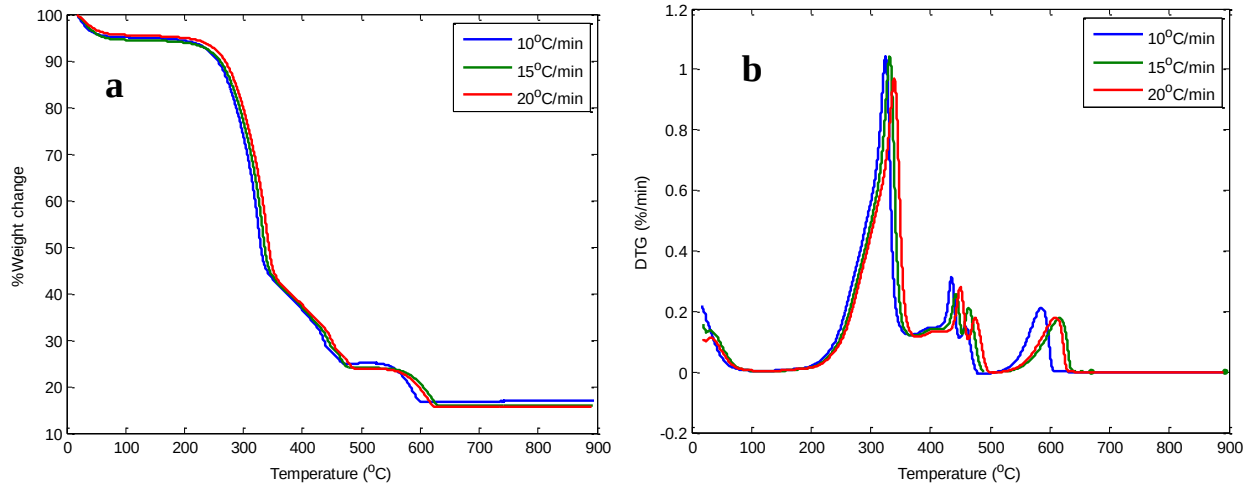

Figure 10: TGA (a) and DTG (b) curves of 20%CaO at various heating rates of 10, 15 and 20 ºC/min.

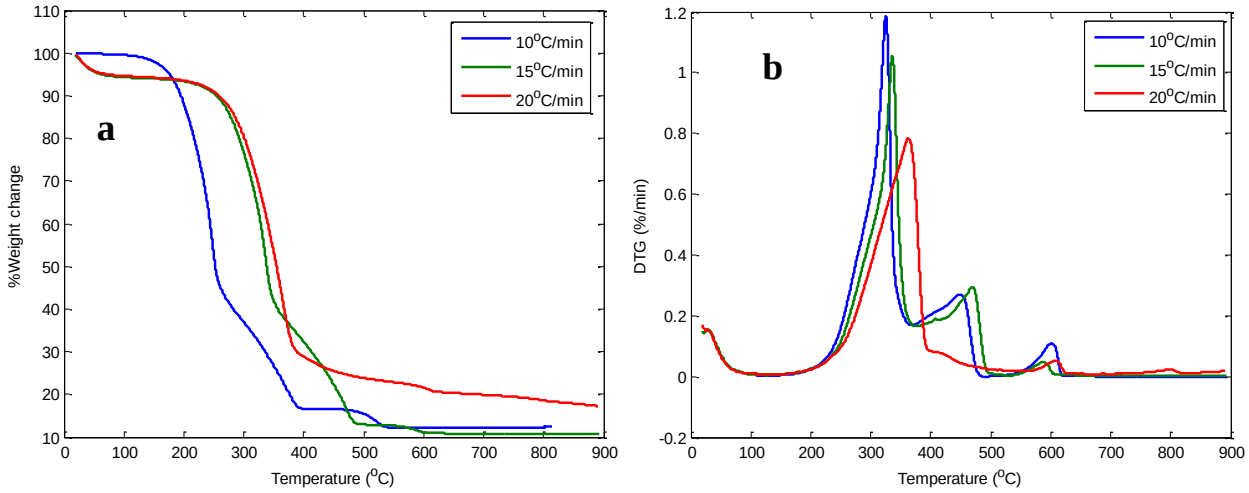

Figure 11: TGA curves of wood with 25%CaO.MgO blend at various heating rates of 10, 15 and 20 ºC/min.

Table A: Mean values for all the samples.

Samples	**Mean value (%)**
Wood	36.43
5%CaO	30.30
5%MgO	30.84
10%CaO	37.39
10%MgO	31.99
10%CaO.MgO	40.37
15%CaO	46.76
15%MgO	47.95
15%CaO.MgO	39.19
20%CaO	48.50
20%MgO	45.32
20%CaO.MgO	49.39
25%CaO	51.16
25%MgO	51.29
25%CaO.MgO	48.79

Appendix B

List of papers presented and published

1. A.I. Mabuda, N. S. Mamphweli and E. L. Meyer."Enhancement of hydrogen production using a biomass gasification process". pp. 689 - 693. ISBN: 978-1-86888-688-3. Available online at http:\\www.saip.org.za.
2. A.I Mabuda, N. S. Mamphweli and E. L. Meyer, in the Journal of Pollution Effects & Control, "Thermal analysis and computer simulation of biomass and biomass/sorbent blends for gasification purposes", in press.
3. A.I Mabuda, N. S. Mamphweli and E. L. Meyer, "Kinetic Analysis of Biomass/Sorbent blends for Gasification purposes", in Proceedings of SAIP2012: the 57th Annual Conference of the South African Institute of Physics, edited by Johan Janse van Rensburg (2014), pp. 499 - 504. ISBN: 978-1-77592-070-0. Available online at http://events.saip.org.za
4. A.I Mabuda, N. S. Mamphweli and E. L. Meyer, in Renewable & Sustainable Energy Reviews, "Chemical kinetic Analysis of Biomass/Sorbent blends in the devolatilization zone", paper in press.
5. A.I Mabuda, N. S. Mamphweli and E. L. Meyer, in Energy journal in the Southern Africa, "Thermal analysis of Biomass with Sorbent blends for gasification purposes", paper under review.

REFERENCES:

Aboyade Akinwale O., Görgens Johann F., Marion Carrier, Meyer Edson L., Johannes H. Knoetze, (2013). Thermogravimetric study of the pyrolysis characteristics and kinetics of coal blends with corn and sugarcane residues. *Fuel Processing Technology* 106 (2013) 310–320.

Aznar Maria P., Miguel A. Caballero, Jose' Corella, Gregorio Molina, and Jose´ MToledo. (2006). Hydrogen Production by Biomass Gasification with Steam-O2 Mixtures Followed by a Catalytic Steam Reformer and a CO-Shift System. *Energy & Fuels*, 20, 1305-1309.

Abanades, J.C., Alvarez, D., Anthony, E.J., Lu, D.,. (2003.). In situ capture of CO2 in a fluidized bed combustor. *17th International Fluidized Bed Combustion Conference,* May 18–21,. Jacksonville, FL, USA: Proceedings of FBC.

Adams, T. N. (1980). A simple fuel bed model for predicting particulate emissions from a wood waste boiler. *Combustion and Flame,* vol. 39, pp. 225-239.

Ajay Kumar , David D. Jones and Milford A. Hanna. (2009). Thermochemical Biomass Gasification: A Review of the Current Status of the Technology. *Energies*, 2: 556-581.

Alarcón N, García X., Centeno M.A, Ruiz P, Gordon A. (2004). *Applied Catalysis A*: General, 267 251–265.

Anderso, M. J. (2001). A new method for non-parametric multivariate analysis of variance. *Austral Ecology*, 26, 32–46.

Antal, M. J.; Varhegyi, G.; Jakab, E. (1998). Cellulose Pyrolysis Kinetics: Revisited. *Ind. Eng. Chem.* Res., 37, 1267-1275.

Asadullah M, Ito S, Kunimori K, Yamada M, Tomishige K. (2002). Biomass gasification to hydrogen and syngas at low temperature: novel catalytic system using fluidized bed reactor. *J Catal*., 208:255–9.

Athanasios N. Fatsikostas, Dimitris. I. Kondarides, Xenophon E. (2002). Verykios Production of hydrogen for fuel cells by reformation of biomass-derived ethanol. *Catalysis Today*, 75 , 145–155.

Babu B.V., Chaurasia A.S., (2004). Pyrolysis of biomass: improved models for simultaneous kinetics and transport of heat, mass and momentum. *Energy Conversion and Management*, 45, 1297-1327.

Babu B.V., Chaurasia A.S. (2003). Modeling, simulation and estimation of optimum parameters in pyrolysis of biomass. *Energy Conversion and Management*, 44, 2135–2158.

Beruto D., Botter R., Alan W. Searcy. (1987). Thermodynamics of two, two-dimensional phases formed by carbon dioxide chemisorption on magnesium oxide. *J. Phys. Chem*, 91 (13), 3578–3581.

Baxter L. (2005). Biomass-Coal Co-Combustion: Opportunity for Affordable Renewable Energy. *Fuel*, 84 (10), 1295-1302.

Baykara, S.Z., Bilgen, E. (1981.). A Feasibility Study on Solar Gasification of Albertan Coal. New York: Alternative Energy Sources IV, Ann Arbor Science.

Beenakers A.A.C.M. (1999). Biomass gasification in moving beds, a review of European Technologies. *Renewable Energy*, 16, 186.

Belgiorno V., De Feo G., Della Rocca C, Napoli R.M.A. (2003). Energy from gasification of solid wastes. *Waste Management*, 23, 1–15.

Bhattacharya, S.; Abdul, S.; Runqing, H.; Somashekar, H.; Racelis, D.; Rathnasiri, P.; Rungrawee, Y. (2005). An assessment of the potential for non-plantation biomass resources in selected Asian countries for 2010. *Biomass Bioenergy*, 29, 153–166.

Bhoi P.R, Singh R.N., Sharma A.M., Patel S.R. (2006). Performance evaluation of open core gasifier on multi-fuels. *Biomass and Bioenergy*, 30, 575–579.

Biagini E., Fantei A., Tognotti L. (2008). Effect of the heating rate on the devolatilization of biomass residues. *Thermochimica Acta*, 472 (2008) 55–63.

Biagini Enrico, Barontini Federica, and Tognotti Leonardo. (2006). Devolatilization of Biomass Fuels and Biomass Components Studied by TG/FTIR Technique. *Ind. Eng. Chem. Res*, 45, 4486-4493.

Bishnu Acharya, Animesh Dutta, Prabir Basu. (2010). An investigation into steam gasification of biomass for hydrogen enriched gas production in the presence of CaO. *International journal of hydrogen energy*, 35, 1582- 589.

Bose P.K, Maji D. (2009). An experimental investigation on engine performance and emissions of a single cylinder diesel engine using hydrogen as inducted fuel and diesel as injected fuel with exhaust gas recirculation. *International journal of hydrogen energy*, 34, 4847-4854.

Bradbury A.G.W. Sakai Y. and Shafizadeh F. (1979). A Kinetic Model for Pyrolysis of Cellulose. J. Appl. *Polymer Sci.* , 23: 3271-3280.

Bridgwater A., (2003). Renewable fuels and chemicals by thermal processing of biomass. *Chemical Engineering Journal*, 91; 87–102.

Bridgwater, A. (1994). Catalysis in thermal biomass conversion. Applied Catalysis A: *General*, 116, 5–47.

Bridgwater A.V. and Evans G.D. (1993). An assessment of thermochemical conversion systems for processing biomass refuse. ETSU Report ETSU/T1/00207/REP.

Brown M.E., Maciejewski M., Vyazovkin S., Nomen R., Sempere J., Burnham A., Opfermann J., R. Strey, H.L. Anderson, A., R. Keuleers, J. Janssens, H.O.Desseyn, C.-R. Li, T.B. Tang, B. Roduit, J. Malek, T. Mitsuhashi. (2000). Computational aspects of kinetic analysis. Part A: the ICTAC kinetics project—data, methods, and results. *Thermochimica Acta*, 355 , 125–143.

Caballero Jose´ A., Conesa Juan A. (2005). Mathematical considerations for nonisothermal kinetics in thermal decomposition. J. Anal. Appl. Pyrolysis, 73 , 85–100.

Cai J., Chen S., Liu R. (2009). Weibull mixture model for isoconversional kinetic analysis analysis of biomass oxidative pyrolysis. Journal of the Energy Institute, 82, 238–241.

Caputo, A.C.; Palumbo, M.; Pelagagge, P.M.; Scacchia, F. (2005). Economics of biomass energy utilization in combustion and gasification plants: Effects of logistic variables. Biomass Bioenergy, 28, 35–51.

Chan, R. W. (1983). Analysis of chemical and physical process during the pyrolysis of large biomass pellets, Ph.D. Thesis. Seattle, WA: Department of chemical engineering, University of Washington.

Channiwala, S. A. (1992). Thermal Data for Natural and Synthetic Fuels. Marcel Dekker Inc, NY: quoted in Gaur, S. & Reed, T. B. (1998).

Chen H.X., Liu N.A., Fan W.C., (2006). Two-step consecutive reaction model and kineticparameters relevant to the decomposition of Chinese forest fuels. Journal of Applied Polymer Science, 102, 571–576.

Chen J. S. and Gunkel W. W. (1987). Modeling & simulation of co-current moving bed gasification reactors-part I, a non-isothermal particle model. Biomass, 14 (1),51–72.

Choi S., Jeffrey H. Drese, and Christopher W. Jones. (2009). Adsorbent Materials for Carbon Dioxide Capture from Large Anthropogenic Point Sources. DOI: 10.1002/cssc.200900036.

Christina S. Martavaltzi. Eleftheria P. Pampaka, Emmanuela S. Korkakaki, and Angeliki A. Lemonidou. (2010). Hydrogen Production via Steam Reforming of Methane with Simultaneous CO2 Capture over CaO-Ca12Al14O33. Energy Fuels, 24, 2589–2595.

Coats A.W, R. J. (1964). Kinetic parameters from thermogravimetric data. Nature, 201, 68–69.

Coats A.W., Redfern J.P. (1965). Kinetic parameters from thermogravimetric data. II. Journal of Polymer Science Part B: Nature, 3, 917–920.

Conesa Juan A., Domene A. (2011). Biomasses pyrolysis and combustion kinetics through n-th order parallel reactions. Thermochimica Acta, 523, 176– 181

Corella, J.; Aznar, M. P.; Gil, J.; Caballero, M. A. (1999). Energy Fuels, 13, 1122-1127.

Corella, J.; Aznar, M. P.; Gil, J.; Caballero, M. A.; France´s, E.; Martín, J. A. (1998). Proceedings of 10th European Conference and Technology Exhibition on Biomass for Energy and Industry (pp. 1794-1797). Germany: CARMEN: Rimpar.

Cormos, C.-C. (2009). Assessment of hydrogen and electricity co-production schemes based on gasification process with carbon capture and storage. International journal of hydrogen energy, 34, 6055-6077.

Criado M., Ortega A., Gotor F. (1990). Correlation between the shape of controlledratethermal analysis curves and the kinetics of solid-state reactions. Thermochimica Acta, 157 , 171–179.

Çulcuoğlu E., Ünay E., Karaosmanoğlu F. (2001). Thermogravimetric Analysis of the Rapeseed Cake. Energy Sources, 23:889 -895.

Dayton D.C., Ratcliff M. and Bain R. (2001). Fuel Cell Integration: A Study of the Impacts of Gas Quality and Impurities. Colorado: Milestone Completion Report.

Delgado Jesu's, Mar'a P. Aznar and Jose´ Corella. (1997). Biomass Gasification with Steam in Fluidized Bed: Effectiveness of CaO, MgO, and CaO-MgO for Hot Raw Gas Cleaning. Ind. Eng. Chem. Res. , 36,1535-1543.

Demirbas, A. (2004). Combustion characteristics of different biomass fuels. Progress in Energy and Combustion Science, 30, 219–230.

Demirbas A., (2001). Biomass resource facilities and biomass conversion processing for fuels and chemicals. Energy Convers Manage, 42, 1357–1378.

Demirbas M. and Balat M. (2006). Recent advances on the production and utilization trends of bio-fuels: A global perspective. Energ. Convers. Manag. 47, 2371–2381.

Devi T.G. and Kannan M. P. . (1998.). Calcium catalysis in air gasification of cellulosic chars. Fuel, Vol. 77, No. 15, pp. 1825–1830.

Di Blasi C., Gabriella Signorelli, and Giuseppe Portoricco (1999). Countercurrent Fixed-Bed Gasification of Biomass at Laboratory Scale. Ind. Eng. Chem. Res. 38, 2571-2581.

Di Blasi C. (2000). Dynamic behaviour of stratified downdraft gasifier. Chemical Engineering Science, 55, 2931–2944.

Di Blasi C, Buoranno F, Branca C. (1999). Reactivities of some biomass chars in air. Carbon; 37:1227.

Digital data system, Bomb calorimeter system, http://cal2k.lambda-med.hu/katalogus/CAL2k-ECO-kalorimeter.pdf, last accessed September 2013.

Ewan, B.C.R., Allen, R.W.K. (2005). A figure of merit assessment of the routes to hydrogen. International Journal of Hydrogen Energy, 30, 809–819.

European commission. (2010). Cement, Lime and Magnesium Oxide Manufacturing Industries.

Feng, B., An H., Tan, E. (2007). Screening of CO2 adsorbing materials for zero emission power generation systems. Energy and Fuels, 21, 426–434.

Fernández-Berridi M.J., Gonz´alez N., Mugica A., Bernicot C. (2006). Pyrolysis-FTIR and TGA techniques as tools in the characterization of blends of natural rubber and SBR. Thermochimica Acta, 444, 65–70.

Fisher, R. (1925). Statistical Methods for Research Workers. Edinburgh, United. Edinburgh, United: Oliver & Boyd.

Florin Nicholas H., Harris Andrew T., (2008). Enhanced hydrogen production from biomass with in situ carbon dioxide capture using calcium oxide sorbents. Chemical Engineering Science, 63: 287–316.

Florin Nicholas H., Harris Andrew T. (2007). Hydrogen production from biomass coupled with carbon dioxide capture:The implications of thermodynamic equilibrium. International Journal of Hydrogen Energy, 32: 4119 – 4134.

Francis S. Lau, David A. Bowen, Remon Dihu, Shain Doong, Evan E. Hughes, Robert Remick, Rachid Slimane, Scott Q. Turn, Robert Zabransky. (2002). Techno-Economic Analysis of Hydrogen Production by Gasification of Biomass. Springfield: Gas Technology Institute.

Galwey A.K., Brown M.E., (2002). Application of Arrhenius Equation to Solid State Kinetics: Can this be Justified. Thermochimica Acta, 386, 91–98.

Gašparovič L., Koreňová Z., Jelemenský L. (2009). Kinetic study of wood chips decomposition by TGA. 36th International Conference of SSCHE, May 25–29. Tatransk´e Matliare, Slovakia.

Gašparovič Lukáš, Zuzana Koreňová, Ľudovít Jelemenský. (2010). Kinetic study of wood chips decomposition by TGA. Chemical Papers, 64 (2) 174–181.

Géraldine Villain, Mickaël Thiery, Gérard Platret. (2007). Measurement methods of carbonation profiles in concrete: Thermogravimetry, chemical analysis and gamma densimetry. Cement and Concrete Research, 37, 1182–1192.

Gil J., Caballero M.A., Martin J.A., Aznar M.P, and Corella J. (1999). Biomass Gasification with Air in a Fluidized Bed: Effect of the In-Bed Use of Dolomite under Different Operation Conditions. Ind. Eng. Chem. Res., 38, 4226-4235.

Gonzalez-Perez J.A., Gonzalez-Vila F.J., Almendros G., Knicker H. (2004). The effect of fire on soil organic matter—a review. Environment International, 30, 855–870.

Greenfield et. al. (2006). Evaluation of analytical instrumentation: Part XIX CHNS elemental analysers. London: Royal Society of Chemistry.

Groeneveld M. J. and Van Swaaji W. P. M. (1979). Gasification of solid waste-potential and application of co-current moving bed gasifiers. Applied Energy, 165-178.

Gumz. W. G. (1950). Gas Producers and Blast Furnaces, Theory and Method of Calculation,. New York. John Wiley and Sons.

Gupta, H.; Fan, L.S. (2002). Carbonation-Calcination cycle using high reactivity calcium. Ind. Eng. Chem. Res., 41, 4035–4042.

Han L., Wang Q., Ma Q., Yu C., Luo Z., Cen K. (2010). Influence of CaO additives on wheat-straw pyrolysis as determined by TG-FTIR analysis. Journal of Analytical and Applied Pyrolysis, 88,199–206.

Hanaoka T., Yoshida T., Fujimoto S., Kamei K., Harada M., Suzuki Y., Hatano H., Yokoyama S., Minowa T. (2005b). Hydrogen production from woody biomass by steam gasification using a CO2 sorbent. Biomass and Bioenergy, 28, 63–68.

Hanaoka, T., Inoue, S., Uno, S., Ogi, T., Minowa, T. (2005a). Effect of woody biomass components on air-steam gasification. Biomass and Bioenergy, 28, 69–76.

Harun N.Y, M.T. Afzal and M.T. Azizan. (2008). TGA Analysis of Rubber Seed Kernel. International Journal of Engineering, Volume (3): Issue (6) 639.

Herguido, J., Corella, J., Gonzalez-Saiz, J. (1992). Steam gasification of lignocellulosic residues in a fluidized bed at small pilot scale. Effect of type of feedstock. Industrial and Engineering Chemistry Research, 31, 1274–1282.

Hauserman, W.B., Giordano, N., Lagana` , M., Recupero, V. (1997). Biomass gasifiers for fuel cells systems. La Chimica & L' Industria 2, 199–206.

Howell, D. (2002). Statistical Methods for Psychology. Duxbury, pp. 324–325. ISBN 0-534-37770-X.

Huang C.H., Chang K.P., Yu C.T, Chiang P.C., Wang C.F. (2010). Development of high-temperature CO2 sorbents made of CaO-based mesoporous silica. Chemical Engineering Journal, 161, 129–135.

Huang Jiu, Gerhard Klaus Schmidt and Zhengfu Bian. (2011). Removal and Conversion of Tar in Syngas from Woody Biomass Gasification for Power Utilization Using Catalytic Hydrocracking. Energies, doi:10.3390/en4081163, 4, 1163-1177.

Iyer, M. V.; Gupta, H.; Sakadjian, B. B.; Fan, L.S. (2004). Multicyclic Study on the Simultaneous Carbonation and Sulfation of High-Reactivity CaO. Ind. Eng. Chem. Res, 43, 3939–394.

Jayah T.H. (2002). Evaluation of a downdraft wood gasifier. Thesis.

Jayah, T. H. Lu, A. Fuller, R. J and Stewart, D.F. (2003). Computer simulation of a downdraft wood gasifier for tea drying. Biomass and Bioenergy, 25, 459-469.

Jenkins B.M., Baxter L.L., Miles R.T. Jr., Miles R.T. (1998). Combustion properties of biomass. Fuel Processing Technology, 54, 17–46.

Juniper. (2000). Pyrolysis & Gasification of Waste. Worldwide Technology & Business Review. Juniper Consultancy Services Ltd.

Kastanaki Eleni, Vamvuka Despina. (2006). A comparative reactivity and kinetic study on the combustion of coal–biomass char blends. Fuel, 85, 1186–1193.

Kastanaki E., Vamvuka D., Grammelis P., Kakaras E. (2002). Thermogravimetric studies of the behavior of lignite–biomass blends during devolatilization. Fuel Processing Technology, 77–78, 159– 166.

Kemmler A., Brown M.E., Maciejewski M., Vyazovkin S., Nomen R., Sempere J., et al., (2000). Computational aspects of kinetic analysis. Part A: The ICTAC kinetics project-data, methods and results, Thermochim. Acta 355 125–143.

Khan, M. R.; Hshieh, F. Y., (1989). Influence of Steam on Coal Devolatilization and on the Reactivity of the Resulting Char. Abstr. Pap. Am. Chem. Soc. Fuel. 198, 76.

Kissinger, H. (1956). Variation of Peak Temperature with Heating Rate in Differential Thermal Analysis. Journal of Research of the National Bureau of Standards, Vol.57, No 4, pp. , 217-221.

Koufopanos C.A., Papayannakos N., Maschio G. and Lucchesi A. (1991). Modelling of the Pyrolysis of Biomass Particles. Studies on Kinetics, Thermal and Heat Transfer Effects. The Canadian Journal of Chemical Engineering, 69 : 907-915.

Kumar S.S, Pitchandi A, Natarajan E. (2008). Modeling and Simulation of Down Draft Wood Gasifier. Journal of Applied Science, 8 (2): 271 – 279.

Laihong Shen, Yang Gao, Jun Xiao. (2008). Simulation of hydrogen production from biomass gasification in interconnected fluidized beds. Biomass and bioenergy, 32, 120 – 127.

Larson, M. G. (2008). Analysis of Variance. Dallas: American Heart Association.

Leiby S.M. (1994). Options for Refinery Hydrogen. Menlo Park, CA.: SRI Report No. 212.

Leroy V., Cancellieri D., Leoni E., Rossi J. (2010). Kinetic study of forest fuels by TGA: model-free kinetic approach for the prediction of phenomena. Thermochimica Acta, 497, 1–6.

Lester Edward, Gong Mei, Thompson Alan. (2007). A method for source apportionment in biomass/coal blends using thermogravimetric analysis. J. Anal. Appl. Pyrolysis, 80, 111–117.

Lettner F., Timmerer H., Haselbacher P. (2007). Biomass gasification – State of the art description, deliverable of Gasification Guide. Europe: Intelligent Energy.

Lewellen P.C., Peters W.A. and Howard J.B. (1969). Cellulose Pyrolysis, Kinetics and Char Formation Mechanism. 12th Symposium on Combustion (pp. 1471-1480). Pitts: The Combustion Institute.

Li X.T., Grace J.R., Lim C.J., Watkinson A.P., Chen H.P., Kim J.R. (2004). Biomass gasification in a circulating fluidized bed. Biomass and Bioenergy, 26, 171 – 193.

Lin SY, Suzuki Y, Hatano H, Harada M. (2002). Developing an innovative method HyPr-RING to produce hydrogen from hydrocarbons. Energy Convers Manage, 43, 1283–90.

Lin Shiying, Michiaki Harada, Yoshizo Suzuki, and Hiroyuki Hatano, (2004). Gasification of Organic Material/CaO Pellets with High-Pressure Steam. Energy & Fuels, 18, 1014-1020.

Lin, Y.; Tanaka, S. (2006). Ethanol fermentation from biomass resources: Current state and prospects. Appl. Microbiol. Biot. 69, 627–642.

Liu N.A., Weicheng Fan, Ritsu Dobashi, Liusheng Huang. (2002). Kinetic modeling of thermal decomposition of natural cellulosic materials in air atmosphere, Journal of Analytical and Applied Pyrolysis. 63,303–325.

Lv P., Chang J., Wang T., Fu Y., and Chen Y. (2004). Hydrogen-Rich Gas Production from Biomass Catalytic Gasification. Energy & Fuels, 18, 228-233.

Madhukar R. Mahishi, D.Y. Goswami. (2007). Madhukar R. Mahishi, D.Y. Goswami. An experimental study of hydrogen production by gasification of biomass in the presence of a CO2 sorbent. International Journal of Hydrogen Energy, 32: 2803 – 2808.

Mahishi M.R., Goswami D.Y. (2007). An experimental study of hydrogen production by gasification of biomass in the presence of a CO2 sorbent. International Journal of Hydrogen Energy. 32, 2803 – 2808.

Malek J., . (1992). The kinetic analysis of non-isothermal data. Thermochimica Acta, 200, 257–269.

Mamphweli S. (2009). Implementation of a 150KVA biomass gasifier system for community economic empowerment in South Africa. PhD thesis, University of Fort Hare

Manya` Joan J., Enrique Velo, and Luis Puigjaner. (2003). Kinetics of Biomass Pyrolysis: a Reformulated Three-Parallel-Reactions Model. Ind. Eng. Chem. Res. , 42, 434-441.

Mansaray K.G. , Ghaly A.E. (1999). Determination of kinetic parameters of rice husks in oxygen using thermogravimetric analysis. Biomass and Bioenergy, 17, 19-31.

Maria Puig-Arnavat, Joan Carles Bruno, Alberto Coronas. (2010). Review and analysis of biomass gasification model. Renewable and Sustainable Energy Reviews, 14, 2841–2851.

Mayoral M.C., Izquierdo M.T., AndreÂs J.M., Rubio B. (2001). Different approaches to proximate analysis by thermogravimetry analysis. Thermochimica Acta, 370, 91-97.

McKendry, P., M. (2002). Energy production from biomass (part 1): conversion technologies. Bioresource Technology, 83, pp 37–46.

Meng Ni, Dennis Y.C. Leung, Michael K.H. Leung, K. Sumathy. (2006). An overview of hydrogen production from biomass. Fuel Processing Technology, 87; 461 – 472.

Michele R. Derrick E. F. Doehne A.E., Parker & Stulik. D.C. (1994). Some new analytical techniques for use in conservation. Journal of the American Institute for Conservation, Volume 33, Number 2, Article 8 (pp. 171 to 184).

Miller G.Q., Stoecker J. (1989). Selection of a hydrogen separation process. San Francisco, CA: National Petrochemical and Refiners Association.

Morten Grønli, Michael Jerry Antal, Jr, Ga´bor Va´rhegyi. (1999). A Round-Robin Study of Cellulose Pyrolysis Kinetics by Thermogravimetry. Ind. Eng. Chem. Res. , 38, 2238-2244.

Motulsky H.J, Ransnas LA. (1987). Fitting curves to data using nonlinear regression: a practical and nonmathematical review. FASEB J., Nov 1 (5): 365-74.

Narváez, I.; Orío, A.; Aznar, M.P.; Corella, J. (1996). Biomass gasification with air in an atmospheric bubbling fluidized bed. Effects of six operational variables on the quality of the produced raw gas. Ind. Eng. Chem. Res., 35: 2110–2120.

Nolan P.F., Brown D.J. and Rothwell E. (1973). 14th Symposium (Intl.) on Combustion (p. 1143). Pitts: The Combustion Institute.

Osorio E., Gomez M. L. I., Vilela A. C. F., Kalkreuth W., Almeida M. A. A., Borrego A. G. et al. (2006). Evaluation of petrology and reactivity of coal blends for use in pulverized coal injection (PCI). International Journal of Coal Geology, vol. 68, pp.14-29.

Ozawa, T. (1965). A New Method of Analyzing Thermogravimetric Data. Bull Chem Soc Jpn, 1881–6.

Padró C. E. G., Putsche V. (1999). Survey of the Economics of Hydrogen Technologies. National Renewable Energy Laboratory.

Parikh J., Channiwala S.A., Ghosal G.K. A correlation for calculating HHV from proximate analysis of solid fuels. Fuel 84 (2005) 487–494

Pasangulapati, V., Ramachandriya, D. K., Kumar, A., Wilkins, R. M., Jones, L.C., Huhnke, L.R. (2012) Effects of cellulose, hemicellulose and lignin on thermochemical conversion characteristics of the selected biomass, Bioresource Technology, 114, pp.663–669

Pena MA, Gome JP, Pierro JLG. (1996). New catalytic routes for syngas and hydrogen production. Appl Catal A General, 144, 7–57.

Perez J., Monoz-Dorado J. (2002). Biodegradation and biological treatment of celluloe, hemicellulose and lignin: An overview. Inter. Microbiol, 5, 53-63.

Perez-Maqueda L.A., CriadoJ.M., Sanchez-Jimenez P.E. (2006). Combined kinetic analysis of solid-state reactions: a powerful tool for the simultaneous determination of kinetic parameters and the kinetic model without previous assumptions of the reaction mechanism. J. Phys. Chem. A, 110 , 12456–12462.

Puig Arnavat, Maria; Bruno, Joan Carles; Coronas, Alberto, (2010). Review and analysis of biomass gasification models. J*ournal of Renewable & Sustainable Energy Reviews*, 14, (9): 2841-2851.

Quaak, P., Knoef, H., Stassen, H. (1999). Energy from biomass. World Bank technical paper no. 422. Energy series.

Quan C., Li A., Gao N. (2009). Thermogravimetric analysis and kinetic study on large particles of printed circuit board wastes. *Waste Management*, Vol.29, No 8, 2353-236.

Ragland K. W., Aerts D. J. (1991). Properties of Wood for Combustion Analysis. *Bioresource Technology,* 37, 161-168.

Rajvanshi A. K. (1986). Biomass gasification. In ed. D. Y. Goswami (Ed.), Alternative energy in agriculture Vol. II (pp. 83-102.). CRC Press.

Rampling, T., Gill, P., (1993). Fundamental research on the thermal treatment of wastes and biomass: thermal treatment characteristics of biomass. ETSU B/T1/00208/Rep/2.

Rapagná, S.; J and, N.; Foscolo, P. U. (1998). Catalytic gasification of biomass to produce hydrogen rich gas. *Int. J. of Hydrogen Energy*, 7, 551-557.

Raveendran, K.; Ganesh, A.; Khilar, K. C. (1996). Pyrolysis characteristics of biomass and biomass components. *Fuel*, 75, 987-998.

Reed, T. B. & Das, A. (1988), Handbook of Biomass Downdraft Gasifier Engine System, SERI, Golden, Colorado.

Rensfelt, E.; Ekstro¨m, C. (1989). Fuel Gas from Municipal Waste in a Integrated Circulating Fluid-Bed Gasification/Gas-Cleaning Process. *Energy Biomass Wastes*, 12, 891-906.

Roberts, A. (1971). Problems Associated with the Theoretical Analysis of the Burning of Wood. *16th Int. Symposium on Combusion* (pp. 893-903). Pitts: The Combustion Institute.

Sami M., Annamalai K., Wooldridge M. (2001). Co-firing of coal and biomass fuel blends. *Progress in Energy and Combustion Science* 27, 171–214.

Segurola, J,. Allen, N.S., Edge, M., & Mahon, A.M. (1999). Design of eutectic photo initiator blends for UV/visible curable acrylated printing inks and coatings. *Prog. Org.Coat*, 37, 23-37.

Shafizadeh, F. (1982). Introduction to pyrolysis of biomass. *Journal of Analytical and Applied Pyrolysis*, 3: 283-305.

Sheffe, H. (1999). The analysis of variance. New York: Wiley-Interscience Publication.

Sheng C., Azevedo J.L.T. (2005). Estimating the higher heating value of biomass fuels from basic analysis data. *Biomass and Bioenergy*, 28, 499–507.

Shoko E., McLellan B., Dicks A.L., Diniz da Costa J.C. (2006). Hydrogen from coal: Production and utilisation technologies. *International Journal of Coal Geology*, 65, 213– 222.

Simell P.A., LeppClahti J.K. and J. B-son Bredenberg. (1992). Catalytic purification of tarry fuel gas with carbonate rocks and ferrous materials. *Fuel*, 71, 211–218.

Šimon, P. (2004). Isoconversional methods: Fundamentals, meaning and application. *Journal of Thermal Analysis and Calorimetry*. 76, 123-132. DOI: 10.1023/B:JTAN.0000027811. 80036.6c.

Sinha, S., Jhalani, A., Ravi, M.R., and Ray, A. (2000). Modeling of pyrolysis in wood: a review. *Journal of Solar Energy Society of India*, 2000 , 10 (1) 41-62.

Sipilä, K. (1993). New power production technologies: various options for biomass and cogeneration. Bioresour. Technol, 46: 5-12.

Sivakumar S., Pitchandi K., Natarajan E. (2006). Design and Analysis of down Draft Biomass Gasifier using Computational Fluid Dynamics. 2nd International Conference on Computational Mechanics and Simulation.

Sjöström Eero, (1993). Wood Chemistry: Fundamentals and Applications. Nature - 293 pages

Skodras George, Panagiotis Grammelis, Panagiotis Basinas, Emmanuel Kakaras, and George Sakellaropoulos, (2006). Pyrolysis and Combustion Characteristics of Biomass and Waste-Derived Feedstock. *Ind. Eng. Chem*. Res. , 45, 3791-3799.

Skov Niels A and Papworth, Mark L. (1974). The Pegasus Unit: The LostArt of Driving Without Gasoline, Pegasus, 1974; now available from H. LaFontaine, Biomass Energy Foundation, Inc., 1995 Keystone Blvd., Miami, Fla., 33181.

Slopiecka K., Bartocci P., Fantozzi F. (2011). Thermogravimetric analysis and Kinetic study of poplar wood pyrolysis. *3rd International Conference on Applied Energy*-16-18 (pp. pages 1687-1698). Perugia, Italy: International Conference on Applied Energy.

Soltes E.J. and Elder T.J. (1981). Organic Chemicals from Biomass. Pyrolysis, CRC Press , 63-95.

Soltes, E. (1983). Thermochemical routes to chemicals, fuels and energy from forestry and agricultural residues. Biomass utilization, NATO ASI Series A67 (p. 537). New York: Plenum: In: CoÃteÂ WA, editor.

Stahl R., Henrich E, Gehrmann H.J., Vodegel S., Koch M.. (2003). Renewable fuels for advanced power trains Integrated Project Sustainable energy systems. SES6-CT 502705.

Sugar Milling Research Institute (2008). Sugarcane bagasse. Proc S Afr Sug Technol Ass. 81, 266 – 273.

Thompson M. (2008). CHNS Elemental Analysers. amc technical briefs,. Analytical Methods Committee AMCTB No 29, © The Royal Society of Chemistry.

Turn S, Kinoshita C, Zhang Z, Ishimura D, Zhou J. (1998). An experimental investigation of hydrogen production from biomass gasification. *Int J Hydrogen Energy*. 23, 641–8.

Várhegyi G, Szabo´ P, Jakab E, Till F. (1996). Mathematical modeling of char reactivity in Ar–O_2 and CO_2–O_2 mixtures. *Energy Fuels*; 10 (6): 1208–14.

Varhegyi G, A. J. (1997). Kinetic modeling of biomass pyrolysis. *J Anal Appl Pyrolysis*, 42, 73-87.

Vyazovkin S. (2000). Computational aspects of kinetic analysis. Part C. The ICTAC Kinetics Project of the light at the end of the tunnel. *Thermochimica Acta*, 355, 155-163.

Vyazovkin S., Wight C.A., (1998). Isothermal and non-isothermal kinetics of thermallystimulated reactions of solids. *International Reviews in Physical Chemistry*, 17, 407–433.

Vyazovkin S., Alan K. Burnham, José M. Criado, Luis A. Pérez-Maqueda,. (2011). ICTAC Kinetics Committee recommendations for performing kinetic computations on thermal analysis data. *Thermochimica Acta*, 520, 1–19.

Vyazovkin S., Charles A. Wight. (1999). Sergey Vyazovkin, Charles A. Wight. Model-free and model-fitting approaches to kinetic analysis of isothermal and nonisothermal data. *Thermochimica Acta*, 340-341, 53-68.

Walawender, W.P., Hoveland, D.A., Fan, L.T. (1985.). Steam Gasification of Pure Cellulose. 1. Uniform temperature profile. *Industrial and Engineering Chemistry Process Design and Development*, 24, 813–817.

Wang D., Xiao R, Zhang H., He G. (2010). Comparison of catalytic pyrolysis of biomass with MCM-41 and CaO catalysts by using TGA–FTIR analysis. *Journal of Analytical and Applied Pyrolysis*, 89, 171–177.

Wang, C.; Du, Z.; Pan, J.; Li, J.; Yang, Z. (n.d.). (2007). Direct conversion of biomass to bio-petroleum at low temperature. *J. Anal. Appl. Pyrol.*, 78, 438–444.

White J.E, W. James Catallob,1, Benjamin L. Legendre. (n.d.). John E. Whitea,W. James Catallob,1, Benjamin L. Legendrea, (2011). Biomass pyrolysis kinetics: A comparative critical review with relevant agricultural residue case studies. *Journal of Analytical and Applied Pyrolysis*, 91, 1–33.

Xu Jian and Qiao Li. (2012). Mathematical Modeling of Coal Gasification Processes in a Well Stirred Reactor: Effects of Devolatilization and Moisture Content. *Energy Fuels*, 26, 5759−5768.

Yildiz Kalinci, Arif Hepbasli, Ibrahim Dincer. (2009). Biomass-based hydrogen production: A review and analysis. *International journal of hydrogen energy*, 34, 8799-8817.

Živorad R Lazić. (2004). Design of experiments in chemical engineering: a practical guide. Weinheim, Germany: Wiley-VCH.

http://www.mathworks.com/products/matlab/. (n.d.). Retrieved 07 17, 2013, from http://www.mathworks.com/.